2020

Evaluation of patient doses from 177lu-PSMA in metastases prostate cancer treatment at King Chulalongkorn Memorial hospital

Kotchakorn Chatachot
Faculty of Medicine

Evaluation of patient doses from ^{177}Lu-PSMA in metastases prostate cancer treatment at King Chulalongkorn Memorial Hospital

Miss Kotchakorn Chatachot

A Thesis Submitted in Partial Fulfillment of the Requirements
for the Degree of Master of Science in Medical Physics
Department of Radiology
FACULTY OF MEDICINE
Chulalongkorn University
Academic Year 2020

การศึกษาปริมาณรังสีที่ผู้ป่วยได้รับจากการรักษามะเร็งต่อมลูกหมาก ด้วยสารเภสัชรังสีลูทีเชียม-177 พีเอสเอ็มเอ ณ โรงพยาบาลจุฬาลงกรณ์ สภากาชาดไทย

น.ส.กชกร ชาตะโชติ

วิทยานิพนธ์นี้เป็นส่วนหนึ่งของการศึกษาตามหลักสูตรปริญญาวิทยาศาสตรมหาบัณฑิต
สาขาวิชาฟิสิกส์การแพทย์ ภาควิชารังสีวิทยา
คณะแพทยศาสตร์ จุฬาลงกรณ์มหาวิทยาลัย
ปีการศึกษา 2563

Thesis Title	Evaluation of patient doses from ^{177}Lu-PSMA in metastases prostate cancer treatment at King Chulalongkorn Memorial Hospital
By	Miss Kotchakorn Chatachot
Field of Study	Medical Physics
Thesis Advisor	Assistant Professor KITIWAT KHAMWAN, Ph.D.

Accepted by the FACULTY OF MEDICINE, Chulalongkorn University in Partial Fulfillment of the Requirement for the Master of Science

..... Dean of the FACULTY OF MEDICINE
(Professor SUTTIPONG WACHARASINDHU, M.D.)

THESIS COMMITTEE

..... Chairman
(Assistant Professor YOTHIN RAKVONGTHAI, Ph.D.)
..... Thesis Advisor
(Assistant Professor KITIWAT KHAMWAN, Ph.D.)
..... External Examiner
(Professor Kosuke Matsubara, Ph.D.)

กชกร ชาตะโชติ : การศึกษาปริมาณรังสีที่ผู้ป่วยได้รับจากการรักษามะเร็งต่อมลูกหมากด้วยสารเภสัชรังสีลูทีเชียม-177 พีเอสเอ็มเอ ณ โรงพยาบาลจุฬาลงกรณ์ สภากาชาดไทย. (Evaluation of patient doses from ^{177}Lu-PSMA in metastases prostate cancer treatment at King Chulalongkorn Memorial Hospital) อ.ที่ปรึกษาหลัก : ผศ. ดร.กิติวัฒน์ คำวัน

ปัจจุบันมีการนำลูทีเชียม-177 พีเอสเอ็มเอ มาใช้ในทางการแพทย์เพิ่มขึ้นอย่างแพร่หลายสำหรับใช้ในการรักษามะเร็งต่อมลูกหมากด้วยสารกัมมันตรังสีตามหลักการของเทอราโนสติกส์ ดังนั้นการคำนวณปริมาณรังสีที่เหมาะสมโดยปราศจากผลข้างเคียงเป็นประเด็นที่สำคัญ งานวิจัยนี้มีวัตถุประสงค์เพื่อต้องการคำนวณหาค่าปริมาณรังสีดูดกลืนในอวัยวะต่างๆของผู้ป่วยมะเร็งต่อมลูกหมากระยะลุกลามที่ได้รับการรักษาด้วยลูทีเชียม-177 พีเอสเอ็มเอ ณ โรงพยาบาลจุฬาลงกรณ์ สภากาชาดไทย โดยหาค่าปริมาณรังสีดูดกลืนต่อความแรงรังสีใน 8 อวัยวะเป้าหมายที่สนใจ จากข้อมูลการรักษาของผู้ป่วย 8 ราย 12 รอบการรักษาด้วยลูทีเชียม-177 พีเอสเอ็มเอ การศึกษานี้ได้วิเคราะห์ข้อมูลจากภาพถ่ายแบบทั่วทั้งตัว (whole-body) ทางเวชศาสตร์นิวเคลียร์ ซึ่งเก็บข้อมูลที่เวลาทันทีหลังจากฉีดยา, 4 ชั่วโมง, และ 24 ชั่วโมง หลังจากได้รับการรักษาด้วยลูทีเชียม-177 พีเอสเอ็มเอ ทำการวาดขอบเขต 8 อวัยวะต้นกำเนิดรังสีเพื่อคำนวณหาค่านับวัด ได้แก่ ไต, ตับ, ม้าม, ไขกระดูก, กระเพาะปัสสาวะ, ต่อมน้ำตา, ต่อมน้ำลายหน้ากกหู และต่อมน้ำลายใต้ขากรรไกรล่าง โดยนำข้อมูลที่ได้มาสร้างกราฟแสดงความสัมพันธ์ระหว่างเวลาและค่าความแรงรังสี ทำการอินทิเกรตพื้นที่ใต้กราฟเพื่อคำนวณหาค่าปริมาณรังสีสะสมในอวัยวะต้นกำเนิดรังสี โดยงานวิจัยนี้ใช้ค่า S-values ที่คำนวณด้วยหุ่นจำลองคอมพิวเตอร์ NURBS computational phantoms จากโปรแกรม OLINDA/EXM เวอร์ชั่น 2.0 และคำนวณหาค่าปริมาณรังสีดูดกลืนของแต่ละอวัยวะเป้าหมายโดยใช้สมการของ Medical Internal Radiation Dose (MIRD) ปริมาณรังสีดูดกลืนในส่วนไขกระดูกทำการคำนวณด้วยวิธีการ planar two-compartment โดยแยกบริเวณส่วนที่เป็น high-uptake กับ low-uptake ตามงานวิจัยของ Svensson et al และใช้วิธีคำนวณโดยอาศัยแบบจำลองทรงกลม (spherical model) ในส่วนของการคำนวณหาค่าปริมาณรังสีดูดกลืนในต่อมน้ำตา

ผลจากงานวิจัยนี้พบว่าค่าเฉลี่ยปริมาณรังสีดูดกลืนต่อค่าความแรงรังสีของ ไต, ไขกระดูก, ตับ, ม้าม, กระเพาะปัสสาวะ, ต่อมน้ำตา, ต่อมน้ำลายหน้ากกหู และต่อมน้ำลายใต้ขากรรไกรล่าง มีค่าเท่ากับ 0.81±0.24, 0.02±0.01, 0.13±0.10, 0.27±0.25, 0.16±0.07, 3.62±1.78, 0.21±0.14, และ 0.09±0.07 เกรย์ต่อกิกะเบ็คเคอเรล ตามลำดับ โดยไม่มีผู้ป่วยรายใดที่มีปริมาณรังสีดูดกลืนสะสมเกินกว่า 23 เกรย์ และ 2 เกรย์ ที่ไตและไขกระดูก งานวิจัยนี้สรุปได้ว่ามีความเป็นไปได้ที่จะสามารถเพิ่มปริมาณความแรงรังสีต่อรอบการรักษาหรือเพิ่มรอบการรักษาได้โดยไม่ก่อให้เกิดอันตรายต่ออวัยวะสำคัญจากการรักษาด้วยลูทีเชียม-177 พีเอสเอ็มเอ ในผู้ป่วยมะเร็งต่อมลูกหมากระยะลุกลาม

สาขาวิชา ฟิสิกส์การแพทย์ ลายมือชื่อนิสิต .....

ปีการศึกษา 2563 ลายมือชื่อ อ.ที่ปรึกษาหลัก .....

6270002530 : MAJOR MEDICAL PHYSICS
KEYWORD: 177Lu-PSMA, radiopharmaceutical therapy, theranostics, MIRDscheme

Kotchakorn Chatachot : Evaluation of patient doses from ^{177}Lu-PSMA in metastases prostate cancer treatment at King Chulalongkorn Memorial Hospital. Advisor: Asst. Prof. KITIWAT KHAMWAN, Ph.D.

^{177}Lu-PSMA I&T has increasingly used for targeted radionuclide therapy of metastatic castration-resistant prostate cancer (mCRPC). Dosimetric calculation, therefore, is critical to achieve the optimal therapeutic activity while sparing side effects to the normal tissues. The purpose of this study was to determine the radiation dosimetry for metastases prostate cancer patients treated by ^{177}Lu-PSMA I&T at King Chulalongkorn Memorial Hospital (KCMH). Whole-body planar images were acquired in eight patients (12 treatment cycles) at immediately, 4 and 24 h after ^{177}Lu-PSMA I&T injection (range 4.36 to 8.58 GBq). Region of interests (ROIs) were manually contoured on the whole-body, liver, spleen, urinary bladder, lacrimal glands, and salivary glands (parotid and submandibular glands) in order to determine the time-integrated activity (TIA) in source organs and fitted the time-activity curves with the mono-exponential function. The S-values were extracted from the OLINDA/EXM version 2.0 calculated by the NURBS computational phantoms. These S-values were used to calculate the absorbed dose coefficient in target organs according to the Medical Internal Radiation Dose (MIRD) scheme. The absorbed doses to the red bone marrow were estimated using the planar two-compartment method described by Svensson et al by separating the high-uptake and low-uptake compartment. The spherical model was used to calculate the absorbed doses in the lacrimal glands.

The results showed that mean absorbed dose coefficients to the kidneys, bone marrow, liver, urinary bladder, spleen, lacrimal glands, parotid and submandibular glands were 0.81±0.24, 0.02±0.01, 0.13±0.10, 0.27±0.25, 0.16±0.07, 3.62±1.78, 0.21±0.14, 0.09±0.07 Gy/GBq, respectively. The dose constraints for the kidneys of 23 Gy, and 2 Gy for the bone marrow were not reached in any patients. The dosimetry results in this study suggest that ^{177}Lu-PSMA I&T treatment with higher activities and more cycles is possible without the risk of damaging the organ-at-risk in prostate cancer patients.

Field of Study:	Medical Physics	Student's Signature .....
Academic Year:	2020	Advisor's Signature .....

ACKNOWLEDGEMENTS

The success of this thesis depends on the contribution of many people. I cannot express enough thanks all of them for continued support and encouragement. First and foremost, I would like to express my deepest and sincere gratitude to my advisor, Asst. Prof. Kitiwat Khmawan, Ph.D. Division of Nuclear Medicine, Department of Radiology, Faculty of Medicine, Chulalongkorn University, Bangkok, Thailand for his trusting and giving me an opportunity to do this research and providing invaluable guidance, patience, motivation and enthusiasm thorough this research. His guidance helped me in all the time of writing of the thesis. Without him this thesis would have been at this point.

I profoundly and profusely thank my thesis committee: Assistant Professor Yothin Rakvongthai, Chulalongkorn University Biomedical Imaging Group, Department of Radiology, Faculty of Medicine, Chulalongkorn University, Chairman of my thesis committee and Professor Kosuke Matsubara, Ph.D., Kanazawa University, Japan external examiner of thesis defense for their encouragement and insightful comments which incented me to widen my research from various perspectives.

In addition, thanks you for Support for Tuition Fee for study leave, Division of Nuclear Medicine, Department of Radiology, Buddhachinaraj Hospital, Phitsanulok, Thailand and Stipend Scholarship for Graduate Student, Faculty of Medicine, Chulalongkorn University for lighten my load of expense throughout my master degree.

I am extreme grateful to my research group members in Chulalongkorn University Biomedical Imaging Group (CUBIG) for their energy, understanding, and help throughout my work for all two years.

Last but not the least, I would like to thank my family for their support and encouragement during the compilation of this dissertation. They kept me going on and this work would not have been possible without their input.

Kotchakorn Chatachot

TABLE OF CONTENTS

Page

LIST OF TABLES

Page

LIST OF FIGURES

Page

CHAPTER 1
INTRODUCTION

1.1 Background and rationale

In 2018, 9.5 million cases of estimate 18 million cancer cases worldwide were found in men as well as the report on global cancer incidence from the American Institute for Cancer Research, prostate cancer ranked the second most common cancer in men, and most of them presented with localized or indolent disease (1). Approximately 30% of men experience biochemical recurrences are often followed by progression to metastatic castration-resistant prostate cancer (mCRPC). Treatment choices in prostate cancer are begun with hormonal therapy, then followed by surgery, chemotherapy, external radiation therapy, and radionuclides therapy (2). For external radiation therapy, just only part of the body is irradiated by sending a beam of high-energy photons to the major parts. Radionuclides therapy in different circumstances is like chemotherapy, which is a systemic treatment that captures reaching cells throughout the body by getting through the blood-flow. On the other hand, unlike chemotherapy, such disease sites are specifically targeted by these radioactive substances, which are administered to patients. Therefore, reducing potential side effects with the use of internal radiation dosimetry concept to optimize the injected activity (3).

Radionuclide therapy uses radiopharmaceuticals specifically targeting and validating for tumor types such as lymphomas, thyroid, or bone metastases, including prostate gland delivering radiation to tumorous lesions as part of a therapeutic treatment. With the exclusivity of radionuclides with various emissions properties, the choice of radionuclide depends on the target of interest. The biological action of a radiopharmaceutical is established by the ionizing radiation emitted with a comparatively short path length, into the tissue for therapy such as alpha or beta emitters, which release their energy close to their targets by the radionuclide (3). In some ways, various emitters are used to allow both imaging and therapy with the same radionuclide. The pharmaceuticals should particularly localize prefer the targeted tumor sites that are interested (4).

Currently, appearing as a targeted, safe, and efficient radionuclide is the perception of theranostics, which focuses on specific tumors. The treatment of metastases cancer using radionuclide therapy according to the theranostic concept. The term ‘Theranostics’ starts to earn interest in the treatment which consists of therapy and diagnosis, concentrates on developing new structures that can perform efficient target therapy. Specifically, theranostic was created to be applied for a variety of imaging approaches including single-photon computed tomography (SPECT) and positron emission tomography (PET), this is an advantage that allows the patient to clearly monitor the outcome of treatment with radiographs.

With the availability of radionuclides possessing various emission properties, the choice of radionuclide depends on the target of interest. Lutetium-177 (^{177}Lu) has been widely used as a radioisotope of choice for targeted radionuclide therapy in theranostics, with a half-life of 6.65 days. The simultaneous emission of gamma photons imaging with the energy of 208 keV (11%) and 113 keV (6.4%) also particulates beta emission maximum energy 498 keV [Ref]. The daughter of the isotope is Halfnium-177 (^{177}Hf). The decay scheme of ^{177}Lu is shown in Figure 1.1.

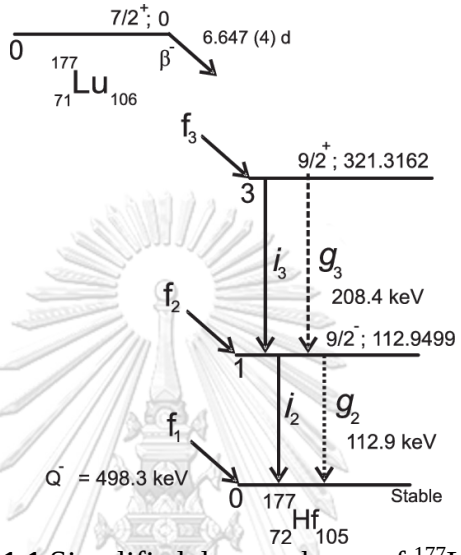

Figure 1.1 Simplified decay scheme of ^{177}Lu (5).

Prostate-specific membrane antigen (PSMA) is the small-molecule radiotherapeutics targeting receptors, that are currently becoming a lot of attention in the treatment of prostate cancer. Prostate-specific membrane antigen (PSMA) is a type of protein located on the surface of a cell and is naturally found on the prostate gland. In prostate cancer patients, an increased amount of PSMA cell surface receptor is obviously presented. If the prostate cancer spreads to other parts of the body, the PSMA will also appear in those areas. Thus, PSMA is a pharmaceutical that suitable for use with PCa patients (6).

Lutetium-177 PSMA therapy uses a molecule that attaches itself to the PSMA receptors on the cancer cells. Before it is administered, the PSMA molecule is labeled with ^{177}Lu, which emits beta radiation and it can be with the direct delivery of the radioactive element itself, a destructive type of radiation that damages the cancer cells when it is in close proximity to them. Over time, it destroys the prostate cancer cells. The PSMA molecule acts as a means of transporting the radiation to the tumor site so that the whole body does not get exposed to the radiation.

The biological effects of radioactive sources in the human body can be assessed through the physical quantity of the absorbed dose. For this reason, measuring the dose of various normal organs in the human body is essential to make a judgment on the benefits of the radiopharmaceutical being used against the hazards of radiation for patients. In general, activity data is placed into mathematical models describing radionuclide distribution in tissue, and then the energy deposited can be estimated in different parts of the body. In order to calculate the absorbed dose in nuclear medicine, the time-activity kinetics of a radiopharmaceutical must be

determined in the target organs. Dose distribution varies according to the choice of radiopharmaceutical and radiation specifications. Therefore, examining internal dosimetry for each patient is the great importance of this method (7).

As the radiation absorbed into entire target organs, the expression of PSMA in normal organs such as the small intestine, central nervous system, proximal renal tubules, prostate, and especially the critical organs such as red bone marrow, kidneys, and lacrimal glands can be a cause of serious side effects, which may greatly affect the well-being of the treated patients. Moreover, the patients who did not respond to PSMA-targeted radionuclide therapy (TRT), the absorbed doses to normal organs treated by the radionuclide therapy should be concerned. This is the fundamental challenge for PSMA because these organs indicate high uptake of nearly all PSMA-targeting radiotracers (8). However, it is difficult to directly measure the absorbed dose to humans from nuclear medicine procedures. Hence, the formalism of the Medical Internal Radiation Dose (MIRD) according to the Committee of the Society of Nuclear Medicine and Molecular Imaging (SNMMI) has been adopted as the accepted calculation method for estimating radiation doses to organs from radionuclide distributed in the body. Current evidence indicates that the kidneys can tolerate mean absorbed doses above the general dose limit of 23 Gy, and 2 Gy to the red bone marrow, based on treatments with ^{131}I and blood-based dosimetry (9). Although the utility of ^{177}Lu-PSMA I&T has become increasingly popular for prostate cancer treatment in theranostic, the radiation doses delivered to the organs for the patient receiving ^{177}Lu-PSMA I&T in Thai patients are not yet available. As such, it is of great interest to study the dose received and biokinetic of ^{177}Lu-PSMA I&T in the normal organs as well as organs-at-risk to provide the preliminary data as a baseline in Thai patients and the Asian population.

1.2 Research objective

To estimate the absorbed doses in the target organs for metastasis prostate cancer patients who were treated by ^{177}Lu-PSMA I&T at King Chulalongkorn Memorial Hospital.

1.3 Definition (10)

Absorbed dose	The amount of energy deposited by ionizing radiation in a unit mass of tissue. It is expressed in units of joule per kilogram (J/kg) called “Gray” (Gy).
Activity (radioactivity)	The property of certain nuclides of emitting radiation by spontaneous transformation of their nuclei. Various units of (radio)activity have been used including curie (1 Ci = 3.7 x 10^{10} disintegrations per second) and becquerel (1 Bq = 1 disintegration per second).

Activity concentration	The ratio of the amount of a specific substance in a given volume or mass of solution to the mass or volume of solvent.
Becquerel (Bq)	The SI unit of activity. The amount of a radioactive material that will undergo one decay (disintegration) per second.
Beta particles	Electrons ejected from the nucleus of a decaying atom. Although they can be stopped by a thin sheet of aluminum, beta particles can penetrate the dead skin layer, potentially causing burns. They can pose a serious direct or external radiation threat and can be lethal depending on the amount received. They also pose a serious internal radiation threat if beta-emitting atoms are ingested or inhaled.
Biological half-life	The time required for one half of the amount of a substance, such as a radionuclide, to be expelled from the body by natural metabolic processes, not counting radioactive decay, once it has been taken in through inhalation, ingestion, or absorption.
Clearance time	The net effect of the biological processes by which radionuclides are removed from a tissue, organ or area of the body.
Critical organ:	Relating to the highest doses or risks attributable to a specified source organ.
Curie (Ci):	The traditional measure of radioactivity based on the observed decay rate of 1 gram of radium. One curie of radioactive material will have 37 billion disintegrations in 1 second.
Effective half-life	The time required for the amount of a radionuclide deposited in a living organism to be diminished by 50% as a result of the combined action of radioactive decay and biological elimination.
Internal exposure:	Exposure to radioactive material taken into the body.

Radioactive decay	The spontaneous disintegration of the nucleus of an atom.
Radioactive half-life	The time required for a quantity of a radioisotope to decay by half.
Reference man	An idealized adult Caucasian human male defined by the International Commission on Radiological Protection for the purpose of radiation protection assessment.
Theranostic	The general concept of using a radionuclide-labelled agent that may be imaged to guide radiopharmaceutical therapy; a radionuclide that may be used for both imaging and therapy.
Time-activity curve	The amount of radioactivity in a particular region of the body as a function of time. Time-versus-activity curves are used in absorbed dose calculations; they may be obtained from imaging or direct sampling.

CHAPTER 2
REVIEW OF RELATED LITERATURE

2.1 Theory

2.1.1 Radioactivity

Radioactivity is the phenomenon of the spontaneous disintegration of unstable atomic nuclei to atomic nuclei to form more energetically stable atomic nuclei. Radioactive decay is a highly exoergic, statistically random, first-order process that occurs with a small amount of mass being converted to energy. Since it is a first-order process, each radioactive species is characterized by its own half-life, the length of time in which an initially very large number of such nuclei will have decayed to only half the original number. In radioactive decay, a relatively large amount of energy is liberated in each disintegration—typically about 1 million times more than the amount of energy liberated in an exothermic chemical reaction, that is, a few million electron volts (MeV) of energy per nucleus, compared to only a few electron volts (eV) of energy per atom or molecule. Since radioactive decay is a nuclear rather than an electronic phenomenon, its rate for a given radioactive species (radioisotope or radionuclide) is not altered measurably by changes in temperature or pressure; the only exception to this is the production of very slight changes in half-life by the use of great pressures on a few radionuclides that decay by the process of orbital electron capture (EC) (11).

2.1.2 Decay of Radioactivity

- The Decay Constant

  The decay constant has a characteristic value for each radionuclide. It is the fraction of the atoms in a sample of that radionuclide undergoing radioactive decay per unit of time during a period that is so short that only a small fraction decay during that interval. Alternatively, it is the probability that any individual atom will undergo decay during the same period.

  The fundamental law of radioactive decay is based on the fact that the decay, i.e. the transition of a parent nucleus to a daughter nucleus is a purely statistical process. The disintegration (decay) probability is a fundamental property of an atomic nucleus and remains equal in time. Mathematically this law is expressed as:

$$\Delta N = \lambda N \Delta t \qquad \text{Eq.2.1}$$

  where N is the number of radioactive nuclei

  λ is the probability of decay per nucleus per unit of time. This decay constant λ is specific for each decay mode of each nuclide.

- Activity

The strength of a radioactive source is called its activity which is defined as the rate at which the isotope decays. Specifically, it is the number of atoms that decay and emit radiation in one second. Radioactivity may be thought of as the volume of radiation produced in a given amount of time. It is similar to the current control on an X-ray generator. The International System (SI) unit for activity is the becquerel (Bq), which is that quantity of radioactive material in which one atom transforms per second. A becquerel is a small unit. In practical situations, radioactivity is often quantified in kilobecqerels (kBq) or megabecquerels (MBq). The curie (Ci) is also commonly used as the unit for activity of particular source material. The curie is a quantity of radioactive material in which 3.7×10^{10} atoms disintegrate per second. This is approximately the amount of radioactivity emitted by one gram (1 g) of Radium-226. One curie equals approximately 37,037 MBq. New sources of cobalt will have an activity of 20 to over 100 curies, and new sources of iridium will have an activity of similar amounts. The radioactivity or decay rate is the activity of the sample. It is essentially a measure of "how radioactive" the sample is

$$A(Bq) = \Delta N / \Delta t = \lambda N \qquad \text{Eq.2.2}$$

where A is activity in becquerel (Bq)
N is the number of undecayed nuclei
λ is decay constant (s^{-1})

- The Decay Factor

With the passage of time, the number N of radioactive atoms in a sample decrease. Therefore, activity A of the sample also decreases. Figure 2.1 is used to illustrate radioactive decay with the passage of time. The following equation gives the quantitative relationship between the original number of nuclei present at time zero (N_0) and the number (N) at a later time:

$$N = N_0 e^{-\lambda t} \qquad \text{Eq.2.3}$$

where N_0 is number of undecayed nuclei at t = 0
t is time after t = 0 in seconds
N is the number of undecayed nuclei at time t
λ is decay constant (s^{-1})

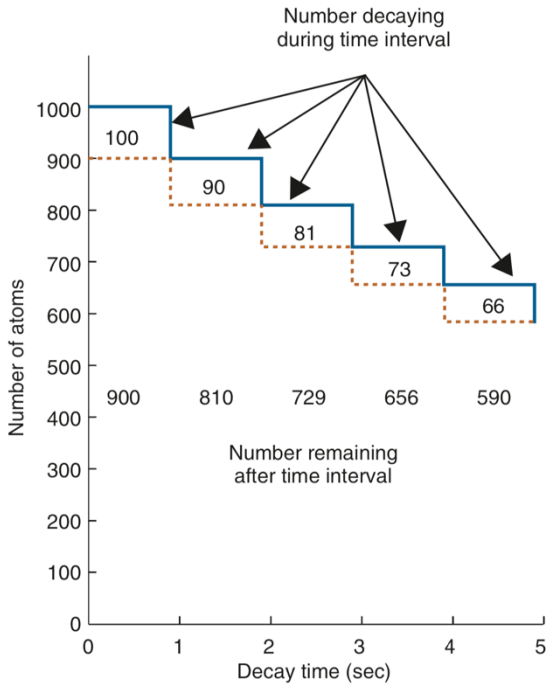

Figure 2.1 Decay of a radioactive sample during successive 1-sec increments of time, starting with 1000 atoms, for λ = 0.1 sec^{-1}. Both the number of atoms remaining, and activity (decay rate) decrease with time. Note that the values shown are approximations, because they do not account precisely for the changing number of atoms present during the decay intervals (12).

- Half-Life

  As indicated in the preceding section, radioactive decay is characterized by the disappearance of a constant fraction of the activity present in the sample during a given time interval. The half-life ($T_{1/2}$) of a radionuclide is the time required for it to decay to 50% of its initial activity level. The half-life and decay constant of a radionuclide are related as:

$$T_{1/2} = \ln 2 / \lambda \qquad \text{Eq.2.4}$$

where ln 2 ≈ 0.693

2.1.3 Radiopharmaceutical therapy

Rapidly proliferating cells are very sensitive to ionizing radiation and this phenomenon is harnessed in the use of radiation to control growth or eliminate fast-dividing cancer cells. Radiotherapy can be external and internal. During internal radiotherapy, the radiation source can be either sealed and implanted (brachytherapy) or administered intravenously for in vivo molecular interaction.

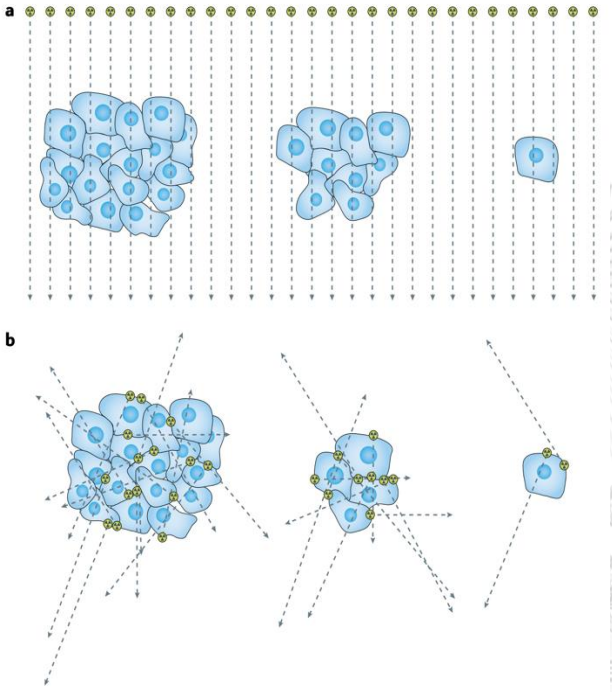

Figure 2.2 Tumor cell irradiation: radiotherapy versus radiopharmaceutical therapy. a | An external beam delivers the same absorbed dose per cell regardless of the number of cells. b | In radionuclide therapy, the absorbed dose delivered per cell by emissions originating from cells is influenced by the range of the emissions, the number of cells that are clustered together and the number of cells that have been targeted. A single cell is very difficult to sterilize with radionuclide therapy. If the range of the emitted particle is much longer than the dimension of the cell nucleus, a smaller fraction of the total emitted energy will be absorbed in the nucleus (13).

This topic focuses on internal radiotherapy on a molecular level. In oncology, it considers deposition of radiation energy of alpha (α), beta (β^-), or Auger/conversion electrons inside or in the vicinity of cancer cells with the aim of damaging or destroying them. This occurs due to the interaction of radiation energy with water molecules with the formation of free radicals that induce single and/or double-strand breaks in DNA. However, most radiotherapeutic procedures are palliative (14). Therapeutic radiopharmaceuticals are usually administered intravenously and distributed by blood circulation to various organs. The inherent advantage of internal targeted radiotherapy is that the radiation is delivered to both the primary tumor and distant metastases. In the design of radiotherapeutic agents, it is essential to ensure a high degree of radioactivity accumulation in the lesions and fast elimination from healthy tissue, especially from radiation-sensitive organs such as bone marrow. Important parameters in the choice of therapeutic nuclides are the path length (range, μm) and linear energy transfer (LET, keV/μm) that define the distance between the emission site and the energy deposition location (Table 2.1).

Table 2.1 Range and Kinetic Energy of the Three Groups of Particulate Radiation for Radiotherapy.

Emission	**Range**	**Kinetic Energy**
β^- particles	0.2–12 mm	0.1–2.5 MeV
α particles	40–100 μm	4–9 MeV
Auger electrons	1–10 nm	2–50 keV

The high-energy beta (^{131}I, ^{90}Y, ^{186}Re, ^{188}Re) has a relatively long range of several millimeters and thus energy might be accumulated outside the tumor causing toxicity to the healthy adjacent tissue. However, the advantage of these characteristics is that such radionuclides (e.g., ^{90}Y, ^{188}Re) can be used for treating poorly perfused, bulky tumors as well as inducing a "crossfire" effect on the adjacent cell with low expression of the target. In comparison, ^{177}Lu emits lower-energy β-particles and spares the healthy tissue. Moreover, it has been demonstrated that ^{177}Lu can be useful in the treatment of small as well as large tumors despite lower energy transfer. Thus, radionuclides vary in the type of radiation and its radiobiological effectiveness and range of action, which provides selection possibility for a particular tumor type. Radionuclide therapy is an essential and growing part of nuclear medicine and has found application or demonstrated potential in the management of bone pain palliation and thyroid, lymphoma, colon, lung, breast, prostate, and brain cancer types.

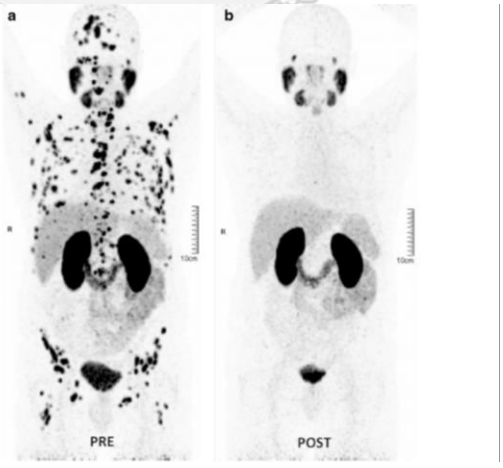

Figure 2.3 Radionuclide therapy in oncology with PSMA. ^{177}Lu-PSMA I&T radioligand therapy in a 67-year-old man with metastatic castration-resistant prostate cancer. a Pretherapy. PET image evidenced a diffuse metastatic involvement. b 4 months following the treatment with ^{177}Lu-PSMA I&T radioligand therapy, PET showed a complete metabolic response (15).

2.1.4 From Radionuclide Therapy to Theranostics

The high value of molecular imaging diagnostics in assisting cancer therapy in terms of early detection, staging, therapy selection, and planning, as well as follow-up, is recognized. It has been used for over 30 years, considerably improving patient management. The in vivo visualization and quantification of the biological processes underlying the disease are the characteristics of nuclear imaging that provide information for the staging, lesion delineation for external and internal radiotherapy, response prediction, and monitoring. The molecular characterization of an individual tumor guides the choice of the therapeutic strategy for a specific patient. Early assessment of the response to the treatment allows termination and substitution of ineffective therapy. The clinical value of molecular imaging diagnostics is greatly elevated by its improved accuracy and safety as compared to biopsy with regard to discrimination of the heterogeneity of a primary tumor and between a primary tumor and metastases. Specifically, theranostics in nuclear medicine usually corresponds to a combination of imaging and RNT for oncological applications. The use of the same or similar compounds both for imaging and RNT, which are labeled with photon-emitters for imaging and with beta or alpha emitters for RNT, has been one of the main streams in nuclear oncology. Such application of radiopharmaceuticals through imaging to therapy for enhancing the efficacy and safety of practices should be a typical example of theranostic approaches (16).

The concept of theranostics unifies diagnosis and therapy, providing a basis for individualized patient treatment whereby the presence and extent of a molecular target for a specific therapeutic modality are first determined by diagnostic means. Therapeutic agents are becoming more refined and target specific. Treatment outcome depends on the quantitative assessment of the target presence and changes in metabolism, which can be accomplished by imaging. In the context of nuclear medicine, the respective technology considers the use of radioactive diagnostic and therapeutic agents. The prime requirement of the agents that comprise radionuclides is that they have similar chemical, physicochemical, and biological properties. Such a diagnostic agent is used as a surrogate for the potential therapeutic agent to 1.) localize and stage the disease; 2.) investigate the biodistribution and dosimetry for the optimization of the therapeutic dose; 3.) monitor the response to the treatment. Some radionuclides (so-called dual radionuclides) emit several types of radiation that can be used for both diagnosis and therapy, thus allowing the use of the same agent in one administration occasion. Another possibility is the use of various isotopes of the same element, allowing for the design of diagnostic and therapeutic agents differing from each other only by the radionuclide isotope. However, it is the properties of the agents as a whole that play a crucial role, and even radionuclides of different chemical elements can be used if the agents demonstrate similar biodistribution.

Dual radionuclides can be divided into three groups by the combination of gamma emission for imaging and the therapeutic emission type, such as electrons

(^{47}Sc, ^{67}Cu, ^{117m}Sn, ^{131}I, ^{153}Sm, ^{177}Lu, ^{213}Bi), Auger electrons (^{67}Ga, ^{111}In, ^{123}I), and alpha particles (^{211}At). It might seem ideal to use these radionuclides, however, there are several factors that until now have prevented the wide use. The production and availability of those radionuclides might be limited. High gamma energy in combination with a longer half-life resulted in undesired additional radiation dose to healthy organs during the therapy. Moreover, the imaging and quantification characteristics of gamma emitters are less attractive than those of positron emitters. The combination of relatively low energy gamma and beta emission of ^{177}Lu provides the possibility for dosimetry measurements during radiotherapy.

Different radionuclides may demonstrate similar chemical properties and result in agents of similar biological activity and biodistribution. For example, ^{89}Zr- and ^{111}In-labeled compounds might be used as surrogates to perform biodistribution studies to estimate the dosimetry and toxicity before radiotherapy with ^{90}Y- or ^{177}Lu-comprising analogs. Other possible combinations are $^{123/124}$I and ^{211}At, or ^{99m}Tc and $^{188/186}$Re. To utilize the imaging advantages of PET over SPECT, ^{89}Zr and ^{68}Ga may serve as surrogates for ^{111}In. However, it should always be considered that even minor changes in the structure of an imaging agent such as a radionuclide may result in considerable variation in pharmacokinetic properties. Thus, for example, in addition to the benefits that ^{68}Ga/PET-CT as an imaging technology provides over ^{99m}Tc/SPECT, the similarity of the coordination chemistry of ^{68}Ga and that of therapeutic radionuclides such as ^{90}Y and ^{177}Lu provides the possibility for theranostics where in pretherapeutic imaging and radiotherapy is conducted with the same vector molecule exchanging the imaging and therapeutic radionuclides (Figure 2.4). However, the difference in half-lives of, for example, short-lived ^{68}Ga and long-lived ^{177}Lu may complicate the pretherapeutic dosimetry.

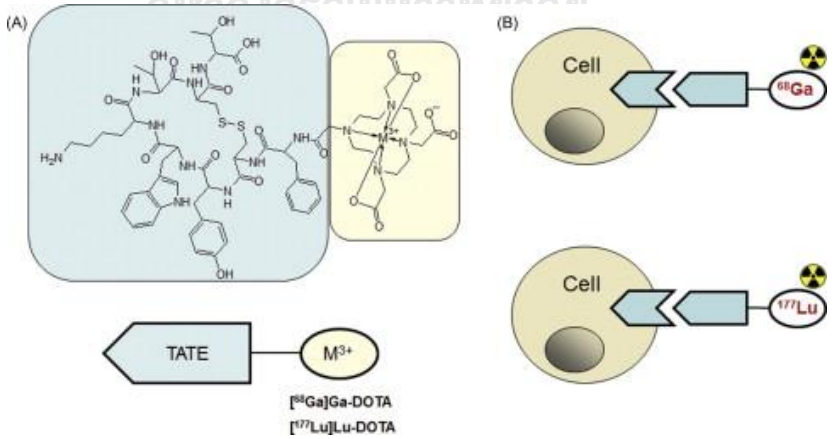

Figure 2.4 (a) Structure (top) and respective schematic presentation (bottom) of a vector (somatostatin analog, DOTA-TATE) labeled with a radiometal cation designated as M3+. (b) Drawing of the interaction of the agent, either imaging if labeled with ^{68}Ga (top) or radiotherapetic if labeled with ^{177}Lu (bottom), with the cell receptor (14).

Radionuclide therapy uses radiopharmaceuticals targeting specific and validated for a tumor type. A radiopharmaceutical is an unsealed source of radioactivity in liquid, gaseous, or particulate form, which has to be removed from its container before administration. Most, but not all, radioisotopes require a carrier molecule (ligand) to be transported around the body and localize into the tissue or organ of interest. The applicability of a particular radiopharmaceutical depends on both the radioisotope and the ligand. Radiopharmaceuticals based on vectors with specific binding capability to, for example, receptors, antigens, and enzymes upregulated in a particular disease can be designed for both diagnostic imaging and subsequent internal radiotherapy. There should be selective concentration in the target organ with fast clearance from surrounding tissues (e.g., blood) giving a high target-to-background ratio (17). The most pronounced example is the selection of oncological patients for peptide receptor radionuclide therapy (PRRT) where image-guided minimally invasive targeted radiotherapy is the major aim. For example, Prostate-specific membrane antigen (PSMA) (Figure 2.5) is currently under approval for treatment of metastatic castration resistant prostate cancer (mCRPC) patients with late stage disease. Radioimmunotherapy (RIT) and PRRT are very promising alternatives to chemotherapy. One of the advantages is that radiotherapeutic agents are used in very low mass amounts, consequently reducing the side effects. Both RIT and PRRT target specific binding sites on the diseased cells and employ, respectively, antibody- and peptide-based vectors. Improved clinical outcomes of molecular imaging-guided radiotherapy have already been demonstrated.

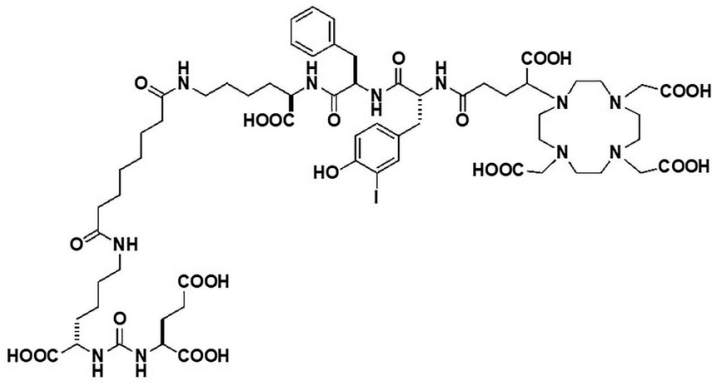

PSMA-I&T

Figure 2.5 Chemical structure of PSMA-I&T. ^{68}Ga and ^{177}Lu (18).

2.1.5 SPECT Data acquisition

Planar imaging and single photon emission computed tomography (SPECT) detect gamma particles and thus, require radiopharmaceuticals comprising gamma-emitting radionuclides. Both technologies utilize gamma cameras for detection (Figure 17.1(a), top), where emitted gamma particles are registered by collimated detector. The collimators direct gamma particles into an array of scintillation crystals that convert the gamma photons into optical photons that are in turn detected by photomultiplier tubes (PMT). These signals are then reconstructed into a two-dimensional image (scintigram) of planar projection reflecting radioactivity distribution. Planar scintigraphy demonstrates high sensitivity but poor signal-to-noise ratio and low spatial resolution (5–10 mm). In SPECT, the gamma camera is rotated around the subject obtaining a number of projections from incremented angles (Figure 2.6 (a), right).

The reconstructed two-dimensional images are combined to generate cross-sectional images of the radioactivity distribution. A full rotation of 360° is required for the optimal reconstruction of images. Dual- and triple-headed cameras shorten the acquisition time because the data are acquired simultaneously from various angles. The advantage of SPECT is three-dimensional imaging (tomography) resulting in more accurate radioactivity distribution detection and physiological and functional information. The hybrid SPECT/CT adds detailed anatomy information and improved attenuation correction of gamma rays (19).

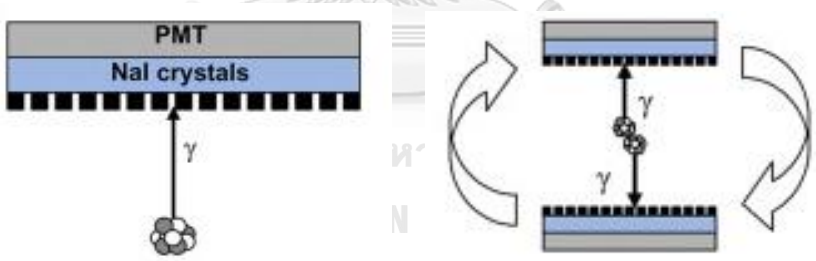

Figure 2.6 Schematic representation of the gamma camera (left) and SPECT (right). Gamma rays selectively pass the lead collimator and enter the scintillator and ionize iodine atoms with subsequent production of light photons that are converted into an electrical signal by PMT. Planar scintigraphy utilizes one gamma camera (left), and SPECT has two or three rotating cameras (right) (14).

Radionuclides used in gamma scintigraphy have K-shell electron vacancy filled by an electron in the M-shell, and thus they decay by electron capture or isomeric transition emitting gamma particles with a common energy range of 90 to 300 keV, which is sufficient for escape from the body. Gamma-emitting radionuclides have the advantage of a longer half-life to match vectors with slower pharmacokinetics such as, for example, antibodies that might circulate in the blood for

several days. On the other hand, the half-life should be short enough to fade away as soon as possible after imaging to avoid unnecessary irradiation.

Table 2.2 Therapeutic Radionuclides, Their Physical Characteristics and Production Mode.

Radionuclide	Half-life	E_{max} (keV)	Radiation	Production
^{32}P	14.3 d	1710	β^-	Reactor
^{47}Sc	3.34 d	441, 600	β^-	Reactor
^{67}Cu	62 h	392, 484, 577	β^-	Accelerator
^{77}Br	57 h	11	Auger electrons	Accelerator
^{89}Sr	52.7 d	1463	β^-	Reactor
^{90}Y	64.0 h	2270	β^-	Generator
^{117m}Sn	14 d	159 (149)	γ (CE)	Reactor
^{125}I	60 d	350	Auger electrons	Reactor
^{131}I	8.0 d	1810	β^-	Fission
^{153}Sm	1.95 d	103 (280)	γ (β^-)	Reactor
^{177}Lu	6.71 d	113, 208.4 (598)	γ (β^-)	Reactor
^{188}Re	16.98 h	2116	β^-	Reactor
^{211}At	7.2 h	5870	α	Accelerator
^{212}Pb	10.64 h	159, 335, 574	β^-	Naturally occurring
^{213}Bi	45.7 m	5800, 8400	α	Generator

2.2. Radiation dosimetry

Fifty-five years after discovery of x-ray by Wilhelm Conrad Roentgen in 1895, International Commission on Radiological Protection (ICRP) established a committee on permission internal exposure. Natural and man-made radionuclides can enter human body, cause damage effect and lead to health risk; on the other hand, radionuclides can cure cancers and other noncancer diseases by irradiating the malignant cells and tissues. The radiation doses delivered to the tissues and organs are inevitable to assess risk or to judge the benefit of application of radiation on humans. In this basic methodology for dose assessment of internally deposited radionuclides is reviewed. After brief introduction of interactions and effects of radiation, the biokinetic models developed by ICRP for incorporation of radionuclides in humans are described. One of the important things to focus on is therapeutic dosimetry.

Therapeutic individual dosimetry is important so as to avoid radiotoxicity to essential radiosensitive organs such as bone marrow and organs with physiological uptake of the radiopharmaceutical, as well as healthy tissue surrounding lesions and excretory organs. Undesired irradiation of healthy organs may lead to side effects. The major purpose of dosimetry is evaluation of the distribution and kinetics of the administered radiopharmaceutical. In the case of PRRT with small peptides, the kidney is the major excretory organ and thus, the maximal tolerated absorbed dose must be determined for each individual patient to optimize the radiotherapeutic dose and avoid both undertreatment and nephrotoxicity. The response to the treatment of different types of tumors varies, and thus, dosimetry may provide essential information for the optimization of the risk-to-benefit ratio for slow- and fast-proliferating tumors. Dosimetry on an individual basis might become a routine tool for therapy planning, estimation of the effects of radiotherapy, and improvement of the treatment outcome.

As mentioned earlier, some therapeutic radionuclides (e.g., ^{177}Lu) also emit gamma particles that can be detected by SPECT, and assessment of the dosimetry in individual patients can be accomplished by serial SPECT and whole-body scintigraphy measurements. However, the absolute measurement of radioactivity concentrations with SPECT is still a major challenge. The spatial resolution of ^{177}Lu/SPECT images is around 2 cm and leads to underestimation of absorbed doses in lesions smaller than 4 to 5 cm. The number of scans is limited and thus, the data sampling is scarce, resulting in large inaccuracies due to oversimplification of the underlying kinetics. Moreover, the long half-life of gamma-emitting radionuclides precludes the measurement at early time points where the kinetic changes are more pronounced and drastic. The main aim of dosimetry is accurate determination of radioactivity distribution, kinetics, and so the quantification accuracy.

2.2.1 Biokinetic models

Radionuclides can accidentally and intentionally enter human body through various incorporation routes, e.g., inhalation, ingestion, injection, transdermal resorption, wound, instillation and other part of the body, especially with intentional application of radioactive medicaments in nuclear medical diagnostics and therapy. The uptake of radionuclides in the blood through respiratory tract or alimentary tract can further be continuously transferred and distributed, like the radionuclides directly injected into blood, to other organs and tissues. Incorporated radionuclides can be eliminated or excreted through kidneys by urine, through alimentary tract by faces through exhalation and through skin by sweat, excretion in nails and hair. The intake and uptake and transfer and distribution, elimination and excretion are generally described as biokinetics of incorporated radionuclides in human body.

The concept of biokinetics was derived from Greek words bio (life) and kinetics (transport). In the earlier publications of ICRP, the concept of metabolism is

used which is more about the chemical and physical changes of the substances. The biokinetic model was used by ICRP from its publication 56 and can be described in a form of compartmental model. Basically, the biokinetic model can be mathematically described in a system of coupled differential equations with first-order or higher-order. To quantitatively calculate the internal doses, the biokinetic information of incorporated radionuclides must be determined first. Directly quantifying the distribution and retention of radionuclides in human body is experimentally unpractical and challenging. However, these data are basis for setup of biokinetic model and calculating the cumulated radioactivity in human body for dose estimation.

The physiologic biodistribution of radiolabeled PSMA, at present mainly using ^{177}Lu, includes the salivary and lacrimal glands, the small intestine, liver, spleen, and blood. It can also be taken up, to a lesser extent, in normal prostate tissue (19).

2.2.2 Internal Dosimetry

Internal Dosimetry is the scientific methodology used to measure, calculate, estimate, assay, predict and otherwise quantify the radioactive energy absorbed by the ionization and excitation of atoms in human tissues as a result of the emission of energetic radiation by internally deposited radio nuclides. Internal Dosimetry deals with the determination of the amount and the spatial and temporal distribution of radiation energy deposited in tissue by radionuclides within the body. Internal dose is calculated from external measurements of activity in the patient. Methods for acquiring quantitative data on radionuclide biodistribution and or calculation of the radiation absorbed dose using standard anthropomorphic models were developed by the Medical Internal Radiation Dose (MIRD) committee of the Society of Nuclear Medicine. This system of mathematical equations for calculating the internal dosimetry of administered radiopharmaceuticals is referred to as the MIRD schema. Which has been recommended in the Society of Nuclear Medicine and Molecular Imaging (SNMMI).

2.2.3 Medical Internal Radiation Dose (MIRD)

Absorption of energy from ionizing radiation can cause damage to living tissues. This is used to advantage in radionuclide therapy, but it is a limitation for diagnostic applications because it is a potential hazard for the patient. In either case, it is necessary to analyze the energy distribution in body tissues quantitatively to ensure an accurate therapeutic prescription or to assess potential risks.

One of the most important factors to be evaluated in the assessment of radiation effects on an organ is the amount of radiation energy deposited in that organ. Calculation of radiation energy deposited by internal radionuclides is the subject of internal radiation dosimetry. There are two general methods by which these calculations may be performed: the classic method and the absorbed fraction method.

Although the classic method is somewhat simpler, and the results by the two methods are not greatly different, the absorbed fraction method (also known generally as the MIRD method, after the Medical Internal Radiation Dose Committee of the Society of Nuclear Medicine) is more versatile and gives more accurate results. Therefore, it has gained wide acceptance as the standard method for performing internal dosimetry calculations.

2.2.3.1 Basic concepts of MIRD

A naive concept for estimating absorbed dose in human body could be preliminarily formulated as the quotient of the decay energy deposited of the incorporated radionuclides in the body and the mass of the body. However, the incorporated radionuclide transfers to different organ and tissues through blood circulation system and can be excreted through kidney in urine and alimentary tract in consequently eliminated out of the human body. Radiation can penetrate organs to outside the body, so that not all decay energies deposit inside body. Furthermore, radionuclides distribute heterogeneously in various organ and tissues and deliver different energies and organs exhibit different degree of radiosensitivity. Therefore, the concept of estimating internal dose should be developed by taking into account firstly the dynamic behavior, e.g. retention and excretion, of the incorporated radionuclides in the body, i.e. aforementioned biokinetics

The radionuclides deposited in different region will irradiate the organs and tissues around and themselves especially for alpha and beta emitters and this cross-fire radiation fraction from source regions to target regions is defined as S values, now called S coefficients. The determination of these S coefficients needs the spatial relation of anatomic organs and tissues, the human digital phantoms, and the radiation transport simulation with human phantoms applying Monte Carlo techniques. The organ absorbed dose can be then estimated by multiplying the activity in the source organ and the S coefficients from the source organ to the target organs under interest. In the following, the human computational phantoms and the generalized formula recommended by ICRP and MIRD Committee are introduced. Furthermore, the treatment of decay products in dose calculations and commonly used software in internal dosimetry are introduced (20).

The absorbed fraction dosimetry method allows one to calculate the radiation dose delivered to a target organ from radioactivity contained in one or more source organs in the body (Figure 2.7). The source and target may be the same organ, and in fact, frequently the most important contributor to radiation dose is radioactivity contained within the target organ itself. Generally, organs other than the target organ is considered to be source organs if they contain concentrations of radioactivity that exceed the average concentration in the body.

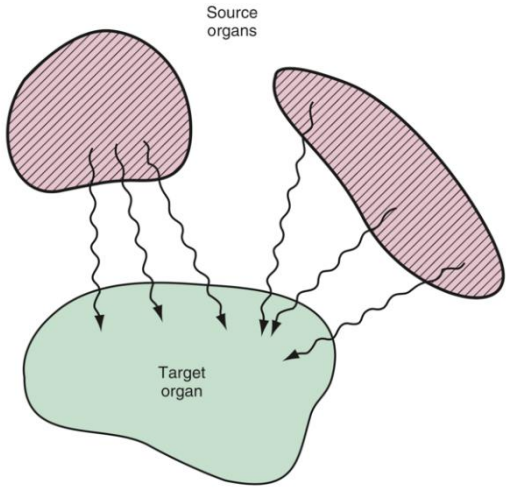

Figure 2.7 Absorbed dose delivered to a target organ from one or more source organs containing radioactivity is calculated by the absorbed fraction dosimetry method (12).

- Source region: region that holds a radiopharmaceutical for a specific amount of time related to the biological half-life of the pharmaceutical, and it is emitting ionizing radiation to other regions nearby.
- Target region: region that is exposed to the ionizing radiation from the source regions.

The absorbed dose D to a target region from activity in a source region is calculated as the product between the time-integrated activity Ã and the S value. It can be mathematically expressed as:

$$D(r_T) = \sum_{r_S} \tilde{A}(r_S) \cdot S(r_T \leftarrow r_S), \qquad \text{Eq.2.5}$$

where $D(r_T)$ is the mean absorbed dose to the target organ (mGy), $\tilde{A}(r_s)$ is the time-integrated activity; TIA (MBq.s) representing the total number of disintegration nuclear transformation in the source tissue r_s over dose-integration period, $S(r_T \leftarrow r_S)$ is the radionuclide-specific quantity representing the mean absorbed dose to target organ r_T per unit of time-integrated activity in a specified source organ r_s, (mGy/MBq.s).

- The time-integrated activity (TIA): Ã

The radiation dose delivered to a target organ depends on the amount of activity present in the source organ and on the length of time for which the activity is present. The product of these two factors is the time-integrated activity in the source organ. it is essentially a measure of the total number of radioactive disintegrations occurring during the time that radioactivity is present in the source organ. The radiation dose delivered by activity in a source organ is proportional to its time-integrated activity.

Each radiotracer has its own unique spatial and temporal distribution in the body, as determined by radiotracer delivery, uptake, metabolism, clearance, and excretion, and the physical decay of the radionuclide. The amount of activity contained in a source organ therefore generally changes with time. If the time-activity curve is known, the time-integrated for a source

organ is obtained by measuring the area under this curve (Figure 2.8). Mathematically, if the time-activity curve is described by a function A(t), then

$$\tilde{A} = \int_0^\infty A(t)\,dt \qquad \text{Ep.2.6}$$

where it is assumed that activity is administered to the patient at time t = 0 and measured to complete disappearance from the organ (t = ∞).

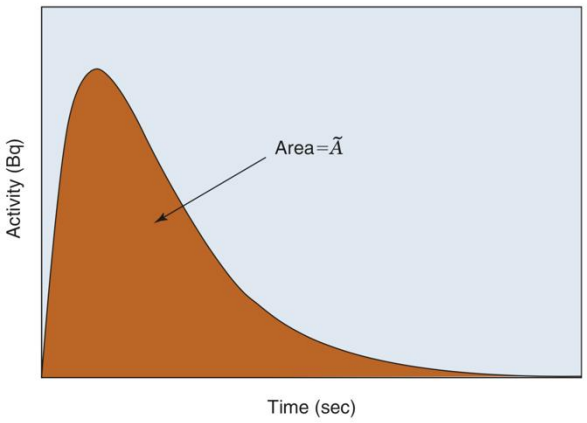

Figure 2.8 The area under the curve A(t) equals the area for the rectangle and ã, the number of decays per unit activity, can be described also as an average time that the activity spends in a source region (12).

- Absorbed dose rate per unit activity (S value), The S value is given by:

$$S(r_T \leftarrow r_S) = \frac{1}{M(r_T)} \sum_i E_i Y_i \phi(r_T \leftarrow r_S, E_i), \qquad \text{Ep.2.7}$$

where E_i is the mean energy of the i^{th} radiation, $\phi(r_T \leftarrow r_S, E_i)$ is the fraction of radiation energy E_i emitted by the source region (r_S) that is absorbed by a target region (r_T), Y_i is the yield for the i^{th} radiation per nuclear transformation, and $M(r_T)$ is the mass of the target region.

S value for a certain radionuclide and source-target combination: generated from Monte Carlo simulations in a computer model of the anatomy. It is well known that a precise representation of the human body is important for accurate internal dosimetry. The ideal situation would be to use the diagnostic image of the patient as anatomic model to estimate doses received by the diagnostic image itself or by a previous nuclear medicine treatment. Such “patient-specific” anatomic models can and are used in a research-level, where the Computed Tomography (CT) portion of Single Photon Emission Tomography/Computed Tomography) SPECT/CT or Positron Emission Tomography/ Computed Tomography (PET/CT), or even Tridimensional Magnetic Resonance (3D MRI) as shown by Berdeguez et al. could be used for radiation transport simulation and new dose planning methodologies. Problems of image-based patient-specific models include the lack of whole-

body coverage in most cases and the need to segment those images to quantify organ absorbed doses separately. Anthropomorphic phantoms exist to simulate the human body's reaction to ionizing radiation and allow whole-body or partial dosimetry in the organ of interest. First models, the stylized phantoms have the size and form of the body and its organs are described by mathematical expressions (combinations/intersections of planes, circular and elliptical cylinders, spheres, cones, etc.) (20). Several stylized phantoms exist are adult man, non-pregnant female, pregnant woman for each trimester of pregnancy, children (from the newborn and up to 15 years of age) as well as models of the brain, kidneys, and unit density spheres. Second generation of phantoms, Voxel phantoms were developed by various groups, which offers the possibility of more detailed models of the anatomy. They can be based on the segmentation of organs from tomographic image data, such as CT or MRI images. Third generation phantoms, Hybrid phantoms are the combination of both stylized and voxel phantoms. The hybrid approach to a computational phantom construction created using Non-Uniform Rational Spline (NURBS). NURBS: mathematical model used in computer graphics to represent surfaces, that represents both geometrical shapes and free forms with the same mathematical representation, and the surfaces are flexible and can easily be rotated and translated. These three generations are shown in Figure 2.9.

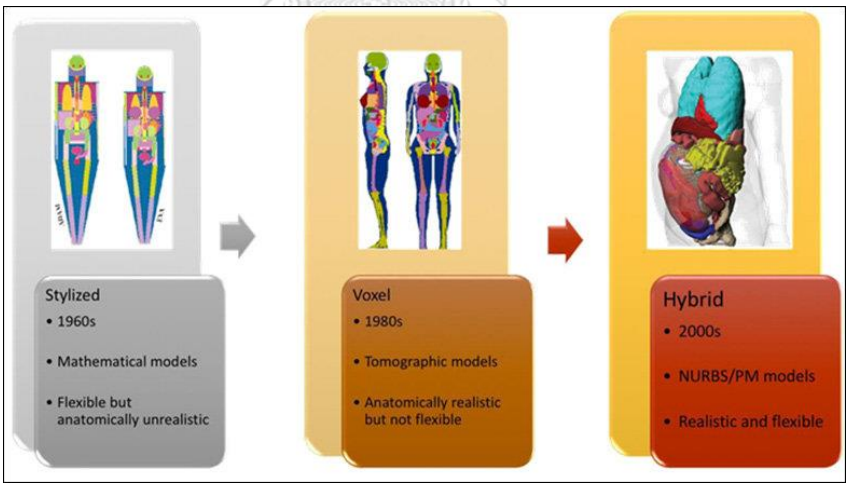

Figure 2.9 From left to right, examples and characteristics of the first, the second and the third generation of computational phantoms (20).

2.2.3.2 Software for internal dosimetry

Internal radiation doses to tissues or organs can be calculated by following above introduced methods and procedures provided the intake activity, the intake pathway and radionuclides are known. However, the procedures can be programmed in a computer code and it speeds up the calculations if the structures and parameters

of biokinetic models and computational phantoms are default of the reference person. In some cases, structures and parameters of models may be requested to it the new measured biokinetic data, or an individual phantom is needed for a personalized set of S coefficients, then a new dedicated computer program may be developed or available computer programs might be modified. In the following, several common used computer programs for biokinetic modeling and internal dose calculations are introduced.

OLINDA/EXM is commercial software for internal dose assessment in nuclear medicine. It was designed according to the MIRD methodology. It was received approval from the FDA. It is widely used by nuclear medicine department to practically estimate organ doses of patients or to provide dose report for new radiopharmaceuticals. Users can apply this program to fit the image-based dynamic activities and time-integrated activities in organs and select appropriate phantoms to calculate organ absorbed doses. Users can also put available time-integrated activities in source organs to get the absorbed dose for patient (21).

2.2.3.3 Limitation of MIRD method

There are a number of important limitations in the MIRD approach for calculating radiation dose. Although, the values of φ are currently based on simplistic models of human anatomy that assume specific relationships in the shape, size, and location of various organs (see Figure 2.10).

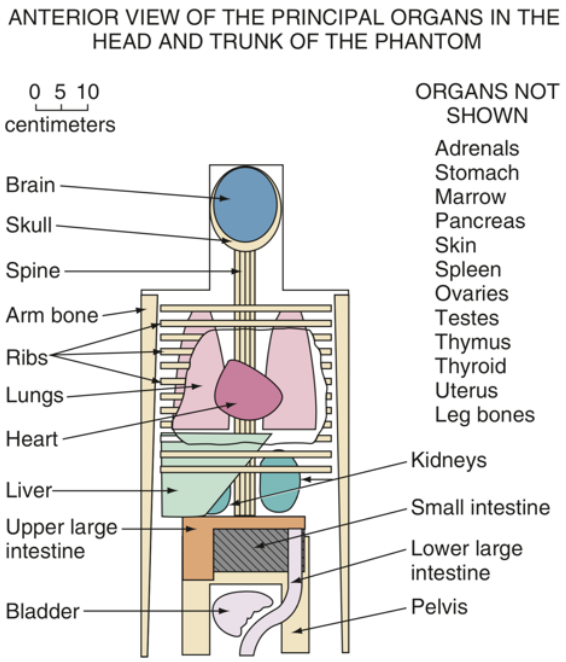

Figure 2.10 Representation of an “average man” used for MIRD dose calculations (12).

More realistic models of the human body, based on medical imaging data and advanced computer modeling, are currently under development for dosimetry purposes. The MIRD formulation also implicitly assumes that activity is distributed uniformly within each organ and that energy is uniformly deposited throughout the organ. The assumption can cause a significant error in the calculated dose from nonpenetrating radiation (e.g., Auger electrons) when the activity is taken up in specific regions or cell types within an organ. Local radionuclide concentrations and hence, the absorbed dose can be much higher than organ average calculations might suggest.

The MIRD standard anatomic models do not fit the real dimensions and morphology of each patient. The critical effect of organ morphology and sizes in dosimetry calculations has been demonstrated by several studies. In addition, the assumption of uniform activity and dose in organs does not allow considering the dosimetry effect of cold spots on the tumor and hot spots in normal organs. It is known that the non-uniform distribution of therapeutic dose significantly affects the regression/ablation in the case of tumors and the radiotoxicity of normal tissues.

2.3 Review of related literatures

Okamoto S. et al, J Nucl Med 2017 (21**)**

The authors aimed to estimate the absorbed doses for normal organs and tumor lesions using ^{177}Lu-PSMA imaging and therapy (I&T) in metastatic castration-resistant prostate cancer (mCRPC) patients. Eighteen patients were analyzed retrospectively. Whole-body scintigraphy was performed at least between 30–120 min, 24 h, and 6–8 d after administration. Regions of interest on the whole body; kidneys; liver; parotid, submandibular, and lacrimal glands; and up to 4 tumor lesions were delineated manually on the anterior and posterior whole-body images. Absorbed doses for individual cycles were calculated using OLINDA/EXM dosimetry software. Organ- and tumor-absorbed doses for ^{177}Lu-PSMA I&T for RLT are comparable to recent reports using the same ligand as well as ^{177}Lu-PSMA-DKFZ-617. They found that the kidney-absorbed dose is similar across different studies and is constant across several cycles in the same patient, and the maximum cumulative activity of ^{177}Lu-PSMA I&T that can be safely administered to a patient was found to be 40 GBq.

Hohberg M. et al, Mol Imaging Biol 2016 (22**)**

This study was to perform image-based absorbed dose calculation for critical organs during the first cycle of ^{177}Lu-DKFZ-PSMA-617 therapy in a small cohort of patients with metastatic prostate cancer. Data analysis was performed on nine patients with metastatic prostate cancer who underwent radioligand therapy with ^{177}Lu-DKFZ-PSMA-617. Whole-body scans were acquired at five time points: shortly after administration of therapeutic activity (G2 h post injection, ahead of bladder emptying)

followed by 24, 48, 72 h and 7 days post-injection. Individual patient doses for the whole body, kidneys, salivary glands, lacrimal glands, and nasal mucous membrane, regions of interest (ROIs) were drawn on the initial scan. From the organ residence times, effective doses per unit of administered activity were calculated by the OLINDA/EXM 1.1^{TM} application. Commonly applied dose constraints are 40 Gy for the lacrimal glands and the mean absorbed dose of 15 Gy for the lacrimal glands was obtained in this study. The lacrimal glands may represent the dose-limiting organs because critical exposure may result.

Hagmarker L. et al, J Nucl Med 2019 (9**)**

The authors aimed to compare different image-based methods for bone marrow dosimetry and study the dose-response relationship during treatment with ^{177}Lu-DOTATATE in patients with and without skeletal metastases. This cohort study included 46 patients diagnosed with advanced neuroendocrine tumors treated ^{177}Lu-DOTATATE. High and low-uptake compartments were automatically outlined in planar images collected at 2, 24, 48, and 168 h after injection. The bone marrow absorbed doses were calculated from the cross doses of the high- and low-uptake compartments and the self-dose, using the time–activity concentration curve for the low-uptake compartment. This time–activity concentration curve was adjusted using a fixed constant of 1.8 for the planar dosimetry method and using the activity concentrations in vertebral bodies in SPECT images at 24 h after injection of ^{177}Lu-DOTATATE in 4 hybrid methods: L4-SPECT used the activity concentration in the L4 vertebra, whereas V-SPECT, L-SPECT, and T-SPECT used the median activity concentration in all visible vertebrae, lumbar vertebrae, and thoracic vertebrae, respectively. Result in this study show that image-based dosimetry methods demonstrated that increased absorbed doses result in higher platelet toxicity and absorbed dose in bone marrow differed between patients with and without metastases.

Delker A. et al, J Nul Med Mol Imaging 2016 (23**)**

The authors purpose was to perform image-base absorbed dose calculation for the new PSMA ligand ^{177}Lu-DKFZ-PSMA-617 to support this pharmaceutical used for treatment of prostate cancer. Five patients with averages age of 68 years were studied by whole-body planar image combine with SPEC/CT images method. During two treatment cycles at approximately 1, 24, 48, and 72 h after injection of 3.6 GBq (range, 3.4 to 3.9 GBq) of ^{177}Lu-DKFZ-PSMA-617. Quantitative 3D SPECT OSEM reconstruction was performed with corrections for photon scatter, photon attenuation and detector blurring. A camera-specific calibration factor derived from phantom measurements was used for quantitation. Absorbed doses of target organs (kidneys, salivary glands, liver, spleen) were calculated by using a combination of linear approximation, exponential fit, and target specific S values, in accordance with the MIRD scheme. However, absorbed doses of bone marrow were estimated from planar

and SPECT images and with consideration of the blood sampling method according to the EANM guidelines. The authors suggest that ^{177}Lu-DKFZ-PSMA-617 is suitable for radiotherapy. From the result, it is possibility to treatment with higher activities and more cycles is without risk of damage in kidneys.

Svensson J. et al, EJNMMI Physics 2016 (24**)**

The purpose of this study was to develop a novel planar image-based method for bone marrow dosimetry and evaluate its correlation with hematological toxicity in ^{177}Lu-DOTATAE therapy. The sample size of this study is 46 advance neuroendocrine tumor patients, 7.2 GBq (range, 3.5 to 8.3 GBq) of ^{177}Lu-DOTATAE was injected to patient with two to five-fraction treatments. Planar gamma camera images were acquired at 2, 24, 48 and 168 h post-injection. Whole-body regions of interest (ROI) were created in the images, and a threshold-based segmentation algorithm was applied to separate the uptake of ^{177}Lu-DOTATATE into high and low uptake compartments. The conjugate view method was used to quantify the activity, the accumulated activity was calculated and the absorbed dose to the bone marrow was estimated according to the MIRD scheme. Parameter of hematological toxicity in this study based on hemoglobin (Hb), white blood cell (WBC), and platelet (PLT) counts weekly during the treatment period. They found that bone marrow dosimetry resulted closely to absorbed dose in bone marrow in earlier studies which used blood-based method in bone marrow dosimetry without need for blood and urine sampling.

Violet J. et al, J Nucl Med 2019 (25**)**

The authors aim to determined radiation dosimetry of ^{177}Lu-PSMA-617 and correlation to pretherapeutic imaging and outcomes. Thirty prostate cancer patients were injected ^{177}Lu-PSMA-617 is sample group in this study. Screening ^{68}Ga-PSMA-11 PET/CT demonstrated high PSMA expression in all patients. After therapy, patients underwent quantitative SPECT/CT at 4, 24, and 96 hours. Pharmacokinetic uptake and clearance at a voxel level were calculated and translated into absorbed dose of various organs (kidneys, submandibular glands, parotid glands, liver, spleen, and bone marrow) using voxel S values. Volumes of interest were drawn on normal tissues and tumor to assess radiation dose, and a whole-body tumors dose was defined. Relations between PSMA PET/CT parameters, dosimetry, and biochemical and therapeutic response were analyzed to identify correlation between absorbed dose, tumor burden, and patient physiology. They found that mean whole-tumor dose relative with biochemical response and appear superior to conventional index-lesion dosimetry. Whole-tumor parameters correlated to screening ^{68}Ga-PSMA PET scan. Absorbed dose in normal organ (kidneys and salivary glands) depend on individual patient condition such as body mass, body surface area and other.

Table 2.3 Summary of the dosimetry in critical organ from literature reviews.

Organs	Absorbed dose coefficient (Gy/GBq)					
	Okamoto et al. (21)	Hohberg et al. (22)	Hagmaker et al. (9)	Delker et al. (23)	Svensson et al. (24)	Violet et al. (25)
Kidneys	0.72±0.21	0.53±0.17	--	0.60±0.18	--	0.39
Liver	0.12±0.06	--	--	0.10±0.06	--	0.10
Spleen	--	--	--	0.10±0.03	--	0.08
Lacrimal glands	3.80±1.40	2.82±0.76	--	--	--	3.78
Bone marrow	--	--	0.03	0.01±0.01	0.03±0.01	0.11
Parotid glands	0.55±0.14	--	--	--	--	0.58
Submandibular glands	0.64±0.40	--	--	--	--	0.44

CHAPTER 3
RESEARCH METHODOLOGY

3.1 Research design

This study was designed as a prospective descriptive study. The steps of the procedure are shown as the following Figure 3.1.

3.2 Research design model

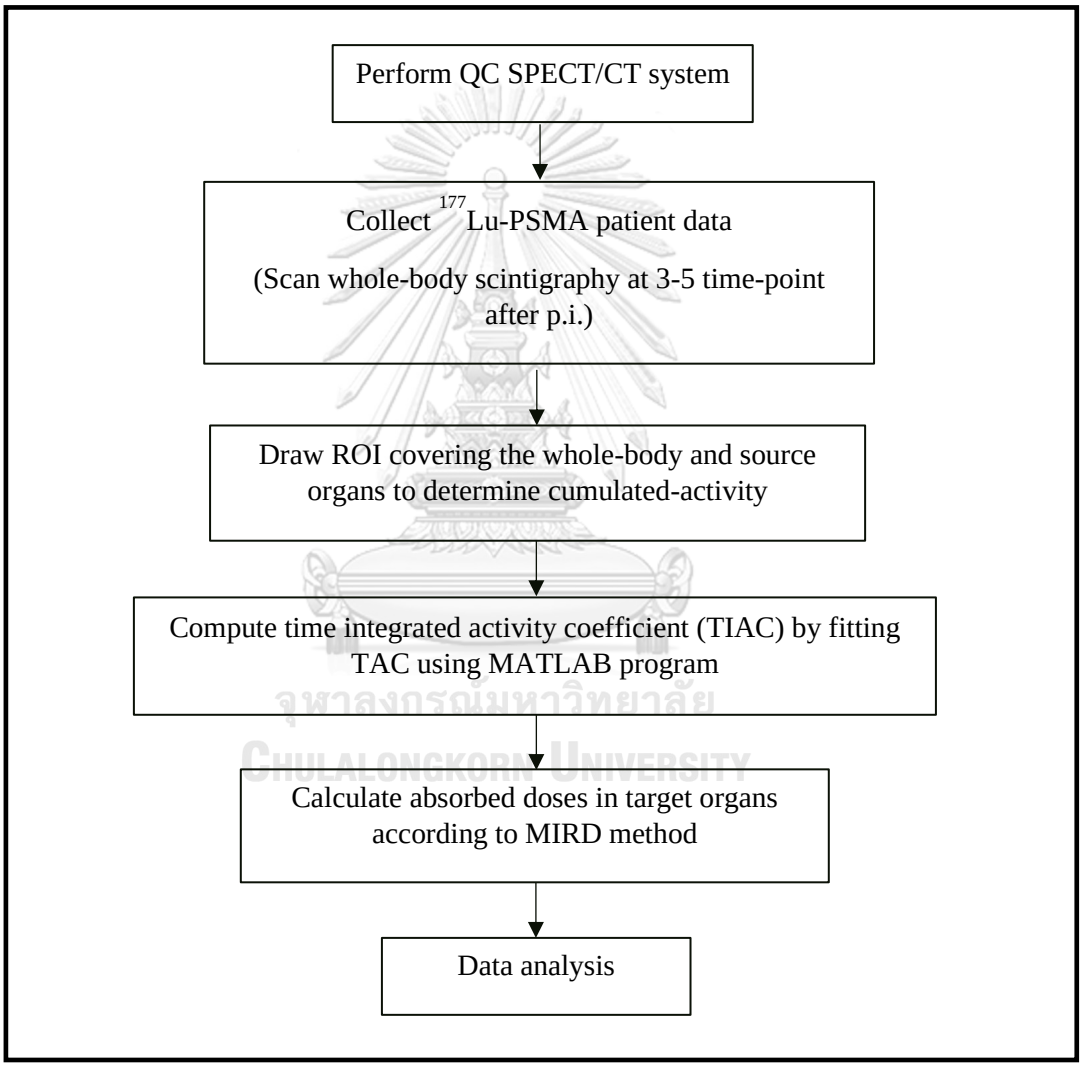

Figure 3.1 Research design model.

3.3 Conceptual framework

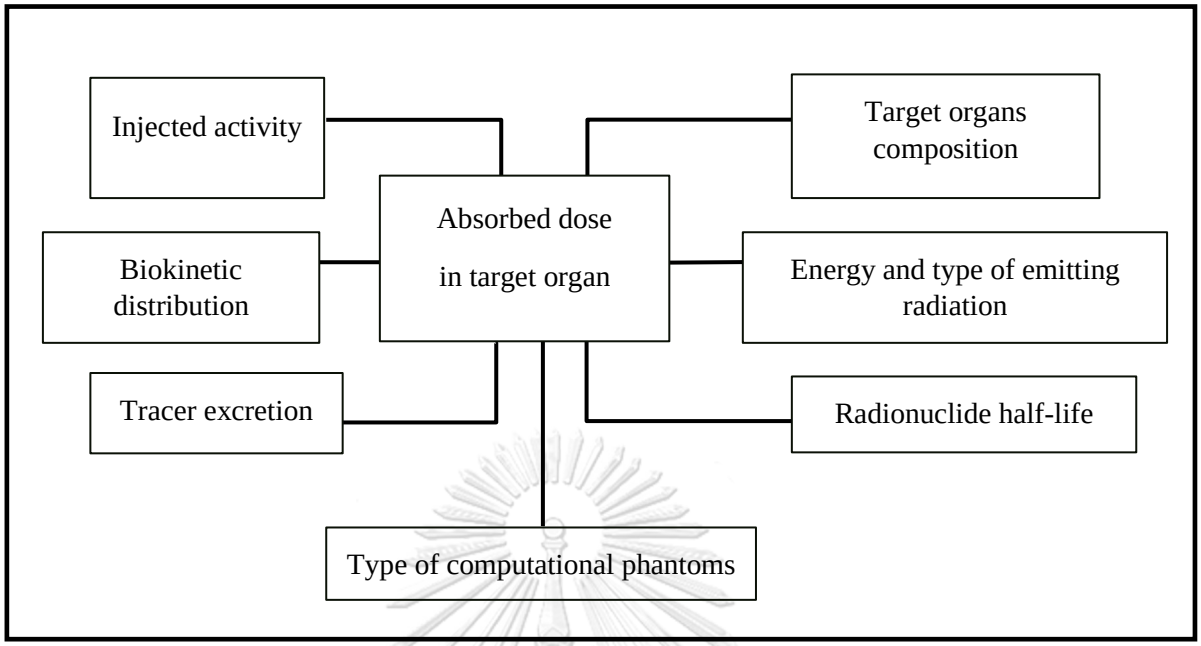

Figure 3.2 Conceptual framework.

3.4 Research question

What are the absorbed doses in the normal organs received from ^{177}Lu-PSMA for patients in metastasis prostate cancer treatment?

3.5 Keywords

- ^{177}Lu-PSMA I&T
- Theranostics
- MIRD scheme
- Radiopharmaceutical therapy

3.6 The sample

3.6.1 Target population

The patients who were diagnosed with metastasis prostate cancer and treated by ^{177}Lu-PSMA I&T at Division of Nuclear Medicine, King Chulalongkorn Memorial Hospital were collected.

3.6.2 Sample population

The patients who were treated by ^{177}Lu-PSMA I&T and underwent SPECT/CT examination at King Chulalongkorn Memorial Hospital from February 2018 to April 2019 and met the eligible criteria.

3.6.3 Eligible criteria

3.6.3.1 Inclusion criteria

The patients who treated by ^{177}Lu-PSMA I&T and underwent whole-body planar scintigraphy at least 3 time-point.

3.6.3.2 Exclusion criteria

The patient underwent planar scintigraphy less than 3 time-point.

3.6.4 Sample size determination

The sample size will be determined by formula as follows:

$$N = \frac{(Z_{\alpha/2})^2 . \sigma^2}{d^2}$$

Where

N = Sample size
$Z_{\alpha/2}$ = 95% Confidence Interval (1.96)
σ^2 = Variance of data
d = Acceptable error (0.5)

Solve equation

$$N = \frac{(1.96)^2 \text{ X } (0.76)^2}{(0.5)^2} = 8.87$$

- Variance of data (σ^2) obtained from ref. SD of lacrimal glands was taken from Hohberg et al. (24), Journal of Molecular Imaging and Biology 2016
- Acceptable error (d) obtained from Gwennaëlle Marina et al. (28), Journal of Physica Medica 2018)

Therefore: 9 patients were collected.

According to the results of sample size calculation in various target organs, the minimum number of 9 patients was collected for this study.

3.7 Materials

3.7.1 Single Photon Emission Computed Tomography/ Computed Tomography (SPECT/CT)

The SPECT/CT system model Discovery 670 manufactured by General Electric at Division of Nuclear Medicine, King Chulalongkorn Memorial Hospital (KCMH), Bangkok, Thailand was used for data acquisition. The SPECT detector system of NaI (Tl) crystal is 59.1x44.5 cm. The useful field of view (FOV) is 54x40 cm and the total number of photomultiplier tubes (PM tubes) is 59. The energy range of the detector is 40-620 keV.

Figure 3.3 The SPECT/CT system model by General Electric.

3.7.2 Image acquisition

During each treatment cycle, ^{177}Lu-PSMA I&T whole-body planar images were acquired at immediately, 4, and 24 h after injection using GE Discovery NM/CT 670 SPECT/CT system at Division of Nuclear Medicine, KCMH. Two patients were additionally acquired at 48 h after injection. The patients were not allowed for voiding at the first time-point scan in order to determine the conversion factor between the counts and injected activity. Planar whole-body imaging was performed using a dual-headed gamma camera coupled with medium-energy general purpose (MEGP) parallel-hole collimators, and the scan speed of 8 cm/min. The energy window was set at 208-keV and 113-keV photon peak ± 20% for imaging studies. A matrix size of 256 x 1024 pixels was used, and no scatter correction was applied.

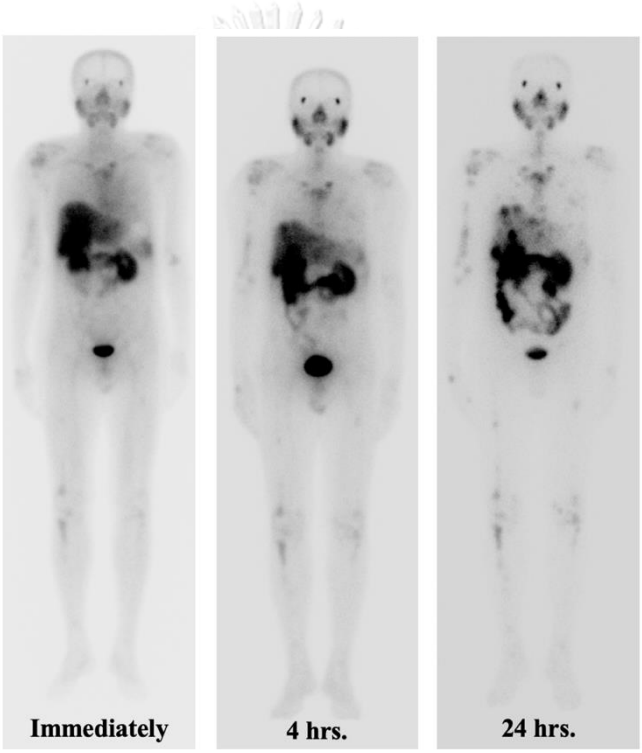

Figure 3.4 The example of the anterior whole-body planar images.

3.7.3 Software packages

- The region of interests (ROIs) were manually defined using the OsiriX MD program in order to measure the total counts for each time point in source organ.

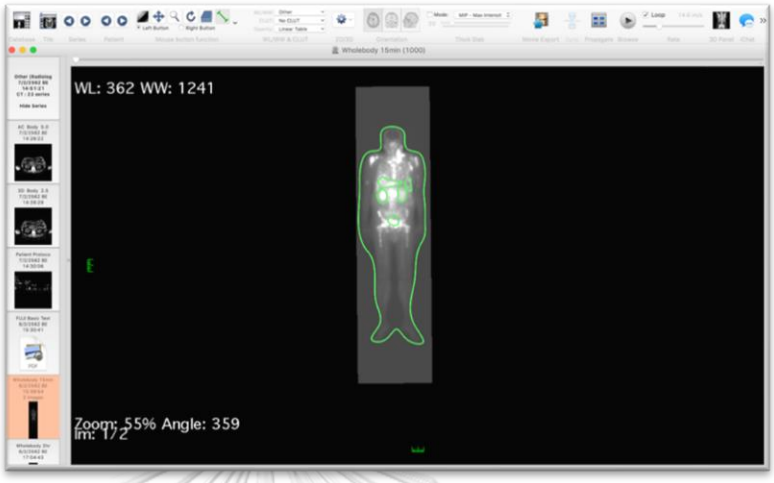

Figure 3.5 OsiriX MD program.

- The time-integrated activity coefficient (TIAC) was computed by fitting time activity curve (TAC) using MATLAB program as shown in Figure 3.6.

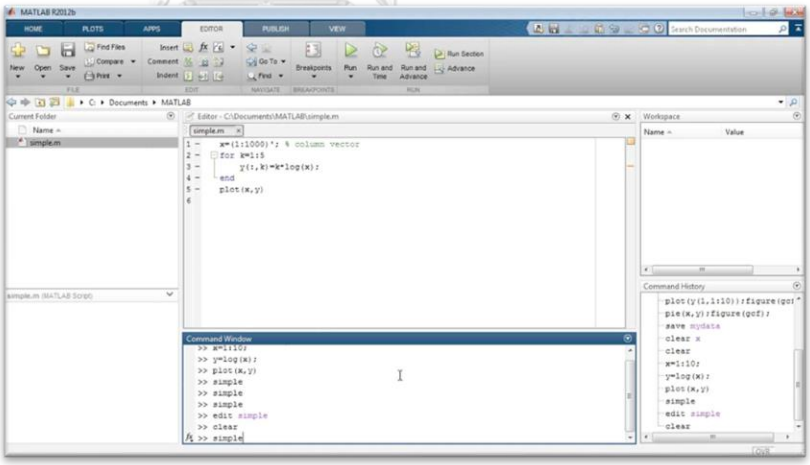

Figure 3.6 MATLAB program.

- Organ Level INternal Dose Assessment/EXponential Modeling® (OLINDA/EXM®) 2.0 dosimetry program:
  - The absorbed dose in lacrimal glands was calculated using the spheres model method derived from OLINDA/EXM version 2.0.

- The S-values based on the Non-uniform Rational B-Spline (NURBS) computational phantoms extracted from the OLINDA/EXM version 2.0 was used for calculation.

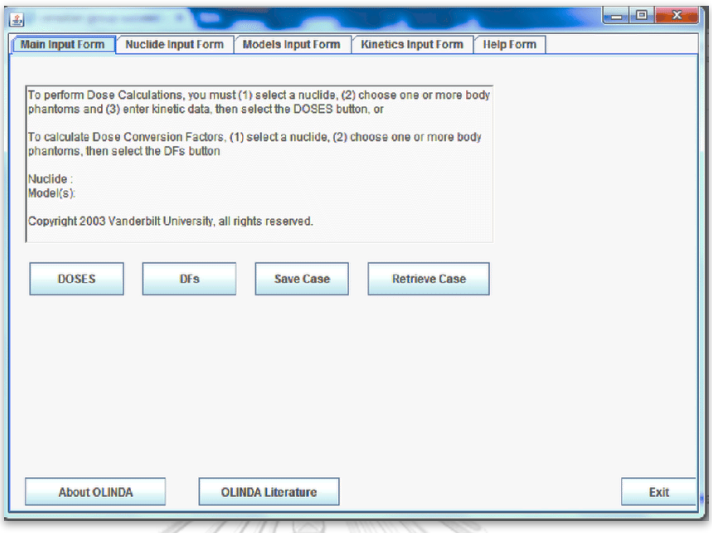

Figure 3.7 OLINDA/EXM® version 2.0 dosimetry program.

3.8 Methods

3.8.1 SPECT/CT Quality Control [APPENDIX D]

The research was begun with the quality control (QC) of the SPECT/CT scanner. For SPECT system, background count rate (kc/s), energy peak (keV), extrinsic energy resolution, and extrinsic uniformity were evaluated as daily QC tests. The weekly QC is center of rotation (COR) test which must be accurately aligned with the center of the acquisition matrix in the computer. The x-ray CT tube warm-up and fast calibration were performed daily.

3.8.2 Subjects

Data of patients diagnosed with metastasis prostate cancer and was treated using ^{177}Lu-PSMA I&T at King Chulalongkorn Memorial Hospital (KCMH) were collected.

3.8.3. Dose analysis

3.8.3.1 Calculation of the absolute activity in each source region

A series of whole-body conjugate-view (anterior and posterior) was collected for 3 time-point at immediately, 4, 24 hours after injection. At each patient data set, the data were analyzed by steps as followings: Region of interests (ROIs) were defined on whole-body scintigraphy images in both anterior and superior images at each time point using the OsiriX MD program in order to measure the total counts in

the source organs consisting of the whole body, red bone marrow, kidneys, liver, urinary bladder wall, spleen and lacrimal glands. For activity quantification, the conjugate view method was used and the absolute organ activity (MBq) was determined by geometrical mean calculation as the following equation:

$$A = \frac{1}{F}.\sqrt{N_A.N_P} \qquad \text{Eq.3.1}$$

where, N_A and N_P are the number of counts in ROI of anterior and posterior images. F is ratio between whole body count and the decay corrected injected activity in terms of counts per unit activity. It was used as the conversion factor from counts to activity.

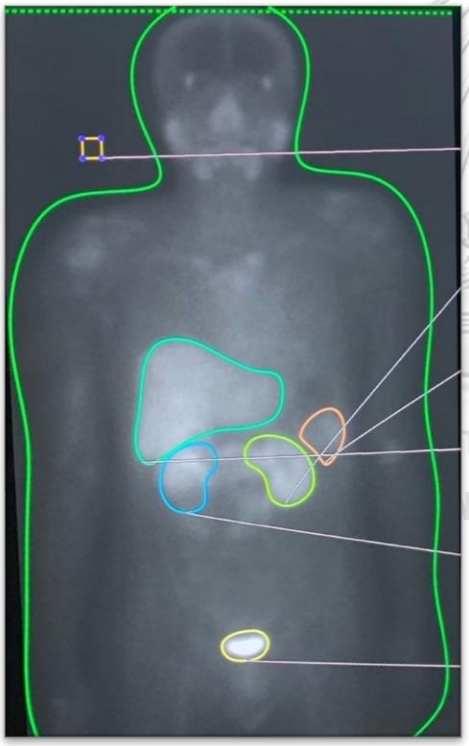

Figure 3.8 ROIs covering the source organs.

The first whole-body images at immediately scan before any excretion of activity were used to normalize the count-to-activity conversion factor assuming that the total number of counts in a ROI encompassing the whole body represents the total injected activity. Geometric mean of the counts in anterior and posterior images was divided by decay-corrected injected activity (counts per unit activity) represented the factor for conversion from count to absolute activity. For background correction, the separate ROIs were measured adjacent to the whole-body planar image and used to subtract the total counts, then injected activity was corrected for physical decay of ^{177}Lu. The ^{177}Lu radioactivity was extrapolated into 48 and 120 h after injection.

The overlay structures such as liver and right kidneys on planar images, the alteration was performed using the mean count concentration (mean count/pixel) in the overlay liver region multiplied by projected area of the liver. The image of the right kidney was treated in the same way.

3.8.3.2 Curve fitting and determination of time-integrated activity

After fitting the TAC generated by the MATLAB program, the area under the curve of TAC was integrated in order to obtain the time-integrated activity (TIA) in each source organ. Therefore, TIA is a total number of disintegration nuclear transformation in the source tissue. TIA depends on the amount of activity administered to patients and life-time of the radiotracer within the body. In this study, the TIA was generated using mono-exponential function to fit the data.

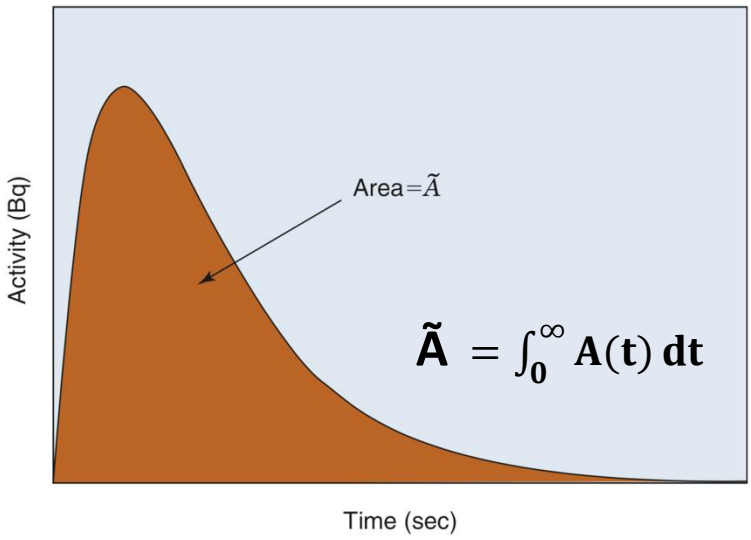

Figure 3.9 The time-integrated activity (TIA).

The time integrated activity coefficient (TIAC, ã), the former name was "residence time" in various source organs can be calculated as the following equation:

$$\tilde{a}(r_s) = \frac{\tilde{A}(r_s)}{A_0} \qquad \text{Eq.3.2}$$

where, $\tilde{a}(r_s)$ in the unit of time (e.g. second or hours) is the time integrated activity coefficient (TIAC), A_0 is the administered activity.

3.8.3.3 The effective half-time of ^{177}Lu-PSMA I&T in each source organ

The effective half-life (T_{eff}) is defined as the period of time required to reduce exactly one half of its initial activity level as a result of the combined action of radioactive decay and biological elimination. The effective half-life is corresponding to the physical half-life (T_p or $T_{1/2}$) and the biological half-life (T_b). The effective half-life is given by:

$$\frac{1}{T_{eff}} = \frac{1}{T_p} + \frac{1}{T_b} \qquad \text{Ep.3.3}$$

where, T_{eff} is the effective half-time, T_p is the physical half-time and T_b is the biological half-time.

The biological half-life is defined as the period of time required to reduce the amount of a tracer in an organ or the body to 50 percent its original value due solely to biological elimination.

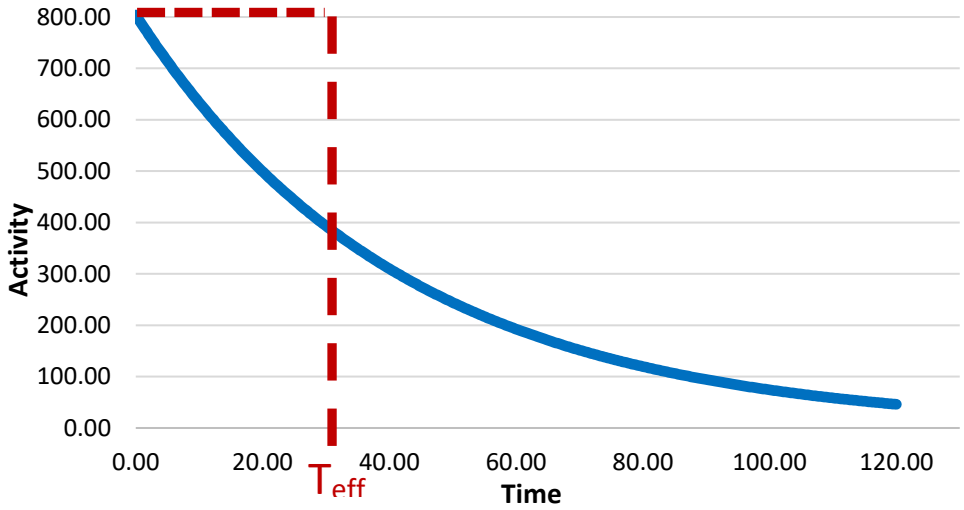

Figure 3.10 Show the TIC in the source organ. The time when the initial activity becomes half by metabolism is effective half-life (T_{eff}).

3.8.3.4 Internal Dosimetry

The absorbed dose, $D(r_T)$, to target region, r_T, was calculated in accordance with the methodology described by the Medical Internal Radiation Dose (MIRD) Committee Pamphlet No. 21. The MIRD formulation in Equation 3 is used to calculate radiation dose delivered to the target organ from the radionuclides that are deposited in source organ as follows

$$D(r_T) = \sum_{r_S} \tilde{A}(r_S) \cdot S(r_T \leftarrow r_S), \qquad \text{Eq.3.4}$$

where $D(r_T)$ is the mean absorbed dose to the target organ (mGy), $\tilde{A}(r_s)$ is the time-integrated activity; TIA (MBq.s) representing the total number of disintegration nuclear transformation in the source tissue r_s overdose-integration period, $S(r_T \leftarrow r_S)$ is the radionuclide-specific quantity representing the mean absorbed dose to target organ r_T per unit of time-integrated activity in a specified source organ r_s, (mGy/MBq.s). The S value is given by:

$$S(r_T \leftarrow r_S) = \frac{1}{M(r_T)} \sum_i E_i Y_i \phi(r_T \leftarrow r_S, E_i), \qquad \text{Eq.3.5}$$

where E_i is the mean energy of the i^{th} radiation, $\phi(r_T \leftarrow r_S, E_i)$ is the fraction of radiation energy E_i emitted by the source region (r_s) that is absorbed by a target region (r_T), Y_i is the yield for the i^{th} radiation per nuclear transformation, and $M(r_T)$ is the mass of the target region. With moderately weak beta-particle-emitting of ^{177}Lu, only the self-dose ($r_s = r_T$) was used to consider for the dosimetry calculation.

The S values in this study were derived from the OLINDA/EXM software version 2.0 that utilizes the non-uniform rational B-spline (NURBS) computational phantoms which combine the flexibility of mathematical organ geometry representation with the anatomical reality (26). The S value was scaled by relating the patient body weight with the International Commission on Radiological Protection (ICRP) 89 adult male reference phantom 73 kg in order to obtain the patient weight-specific S value (see Eq.5). The TIA was then divided by the injected activity in order to obtain the time-integrated activity coefficient (TIAC), former name residence time (τ), in a source tissue. The absorbed doses coefficient (mGy/MBq) from ^{177}Lu-PSMA I&T was obtained by normalizing the mean absorbed dose in target organ with the injected activity. The S values of ^{177}Lu used for dosimetry calculation will be shown in APPENDIX A

$$S_{patient} \approx S_{phantom} \cdot \frac{m_{phantom}}{m_{patient}} \qquad \text{Eq.3.6}$$

where, $S_{patient}$ is the S value take into account for individual patient.

$S_{phantom}$ is the S value derived from the standardized phantom.

$m_{phantom}$ is mass of adult male reference phantom 73 kg.

$m_{patient}$ is mass of the patient.

For the lacrimal glands, the absorbed dose was calculated using the spherical model method derived from OLINDA/EXM version 2.0. The organ mass of lacrimal glands at 1.4 g according to Hohberg et al. was assumed for this calculation (22). The prediction curve model to calculate the dosimetry in lacrimal glands as a function of organ mass is shown in Figure 3.9.

The absorbed dose in bone marrow was calculated using the planar image-based two-compartment method described by Svensson et al. (24) Starting from manually drawn of ROI to delineate the whole-body area, then used the 3D ROI isocontour to automatically segment the high uptake area from the low uptake area. The threshold level was gradually adjusted until the background shading disappeared in order to cut-off between the high uptake and low uptake compartments. The high uptake compartment includes the organs with physiologically high uptake comprising the liver, spleen, kidneys, urinary bladder, lacrimal glands, salivary glands, and tumors, while the low uptake compartment was taken into account rest of the body.

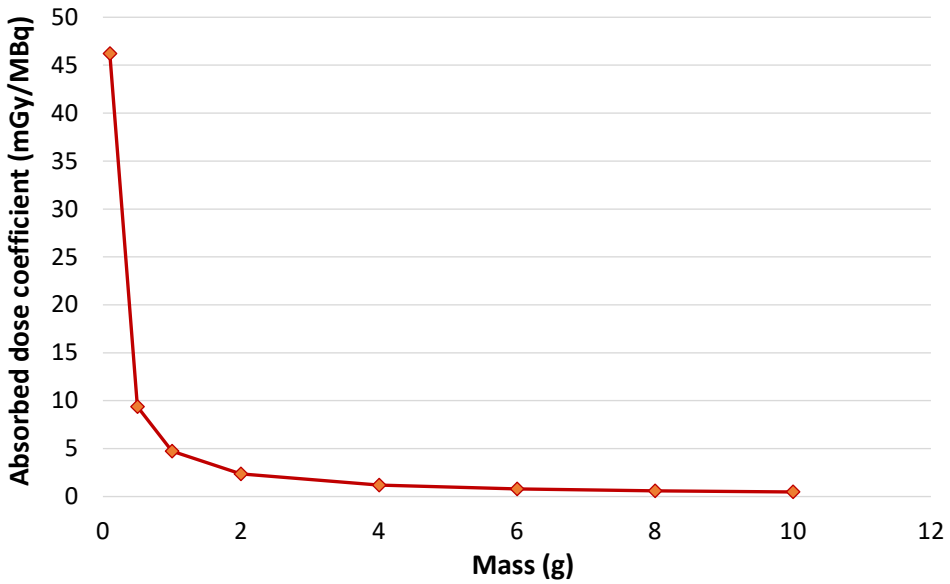

Figure 3.11 The relationship between absorbed dose and mass of organ in lacrimal gland calculated by the OLINDA/EXM® version 2.0.

The dose constraint for radiopharmaceutical therapy according to the joint MIRD pamphlet no.26 EANM/MIRD guidelines, the critical organs in radionuclide therapy with ^{177}Lu-PSMA I&T are bone marrow and kidneys with accumulative dose limit of 2 Gy and 23 Gy, respectively. The accumulative dose limit of 40 Gy in lacrimal glands was also determined in this study. The absorbed doses in theses organs-at-risk in each fraction of treatment were determined in order to avoid the toxicity.

3.8.4.5 Data analysis

The mean absorbed doses in kidneys, red bone marrow, lacrimal glands, liver, spleen, and salivary glands were analyzed and compared with literatures. The recommended organs at risk and tolerance absorbed dose in radionuclide therapy treated with ^{177}Lu-PSMA I&T (9, 22) are:

- Red bone marrow → cumulative dose limit of 2 Gy
- Kidneys → cumulative dose limit of 23 Gy
- Lacrimal glands → cumulative dose limit of 40 Gy
- Salivary glands → cumulative dose limit of 20 Gy

3.9 Statistical analysis

All continuous data obtained in this study were expressed using descriptive statistics as followings:

- Mean
- Standard Deviation (SD)
- Range (Maximum, Minimum)

3.10 Ethical Consideration

The research proposal was approved on August 1, 2020 by the Institutional Review Board of the Faculty of Medicine, Chulalongkorn University, Bangkok, Thailand

3.11 Expected benefits

- Obtain patient dose from ^{177}Lu-PSMA I&T in Thai metastasis prostate cancer patients.
- Obtain the absorbed doses in normal organs for preliminary results of theranostic in Thai patients.

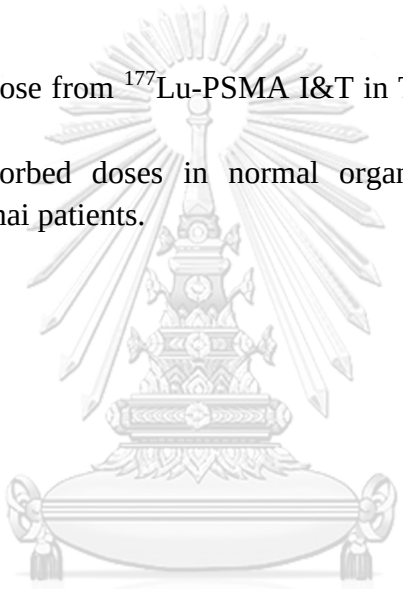

CHAPTER 4
RESULTS

4.1 Patient data selection

This study was investigated the internal dosimetry according to the MIRD scheme by analyzing of 8 metastases prostate cancer patients who was received 12 treatment fractions. Four patients received 2 treatment cycles and the other 4 patients received a single treatment cycle. The whole-body and 8 target organs consisting of the kidneys, urinary bladder, liver, spleen, lacrimal glands, bone marrow, and salivary glands (parotid and submandibular glands) were determined. The average patient age and body weight were 66.67±7.35 years, and 60.37±9.48 kg, respectively. The patient's demographics and injected activity of ^{177}Lu-PSMA I&T are shown in Table 4.1.

Table 4.1 The patient characteristic and injected activity.

Patient	Treatment cycle	Age at treatment (years)	Weight (kg.)	Height (cm.)	PSA	Injected activity of ^{177}Lu-PSMA I&T	
						mCi	GBq
P1	1	62	67.0	173	116.70	149	5.51
	2	62	67.0	173	87.80	150	5.55
P2	1	69	51.7	159	501.90	203	7.51
	2	69	51.7	159	1,681.70	159	5.58
P3	1	66	49.8	161	2.89	222	8.21
	2	66	49.8	161	12.68	184	6.81
P4	1	58	62.0	163	409.20	181	6.70
	2	58	62.0	163	521.80	205	7.59
P5	1	82	56.0	165	163.00	118	4.37
P6	1	73	56.0	165	77.00	152	5.62
P7	1	75	73.3	168	181.00	232	8.58
P8	1	60	78.2	165	814.00	210	7.77
Mean		66.67	60.37	164.58	380.81	180.42	6.68
SD		7.35	9.48	4.74	479.48	34.99	1.29

4.2 The dosimetry parameter results

4.2.1 Time-integrated activity (TIA)

Time-integrated activity (TIA) in each source organ was determined from ROIs that were manually drawn covering each source organs using the OsiriX MD program.

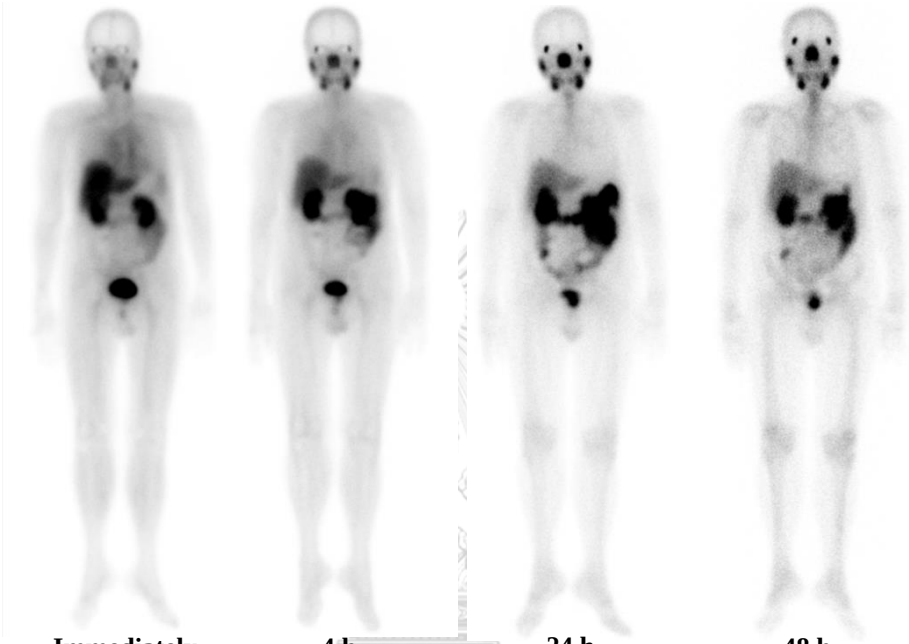

Figure 4.1 ^{177}Lu-PSMA I&T whole-body scintigraphy images at immediately, 4, 24, and 48 h post injection.

Table 4.2 The time-integrated activity (TIA) in unit of MBq-h of source organs in each treatment cycle.

Patient (cycle)	WB ($\times 10^4$)	Kidneys ($\times 10^3$)	Bladder ($\times 10^3$)	Liver ($\times 10^3$)	Spleen ($\times 10^2$)	Lacrimal glands ($\times 10^2$)	Bone Marrow ($\times 10^4$)	Parotid glands ($\times 10^2$)	Submandibular glands ($\times 10^2$)
P1 (1)	9.84	11.1	2.54	9.16	13.1	2.32	5.45	10.9	2.72
P1 (2)	8.71	12.5	3.28	9.51	8	3.15	6.91	9.54	2.11
P2 (1)	16.3	19	5.33	26.3	15.3	4.45	13	10.5	3.73
P2 (2)	12.5	11.6	6.35	34.8	10.6	2.2	8.07	3.19	1.45
P3 (1)	20.3	20.3	1.96	12.9	11.7	9.75	16.7	30.9	7.03
P3 (2)	9.79	19.9	1.36	15.1	8.94	2.81	8.05	4.36	6.05
P4 (1)	16.3	17	16.4	9.31	16.4	2.82	5.52	6.81	1.99
P4 (2)	30.6	12.7	72.1	15.2	29.6	5.38	18.7	23.3	5.56
P5	14.1	8.89	3.63	6.99	9.01	3.58	11.3	5.49	2.05
P6	11.7	17.3	2.83	7.46	23.1	3.31	7.71	11.1	5.34
P7	25.8	15.5	2.68	8.96	23.9	2.66	13.1	7.63	23.1
P8	22.9	26.5	33.2	10.1	15.7	1	18.5	20.4	4.01
Mean	16.6	16	12.6	13.8	15.4	4.37	11.1	12	5.43
SD	6.98	4.98	20.8	8.44	6.83	2.73	4.87	8.47	5.85

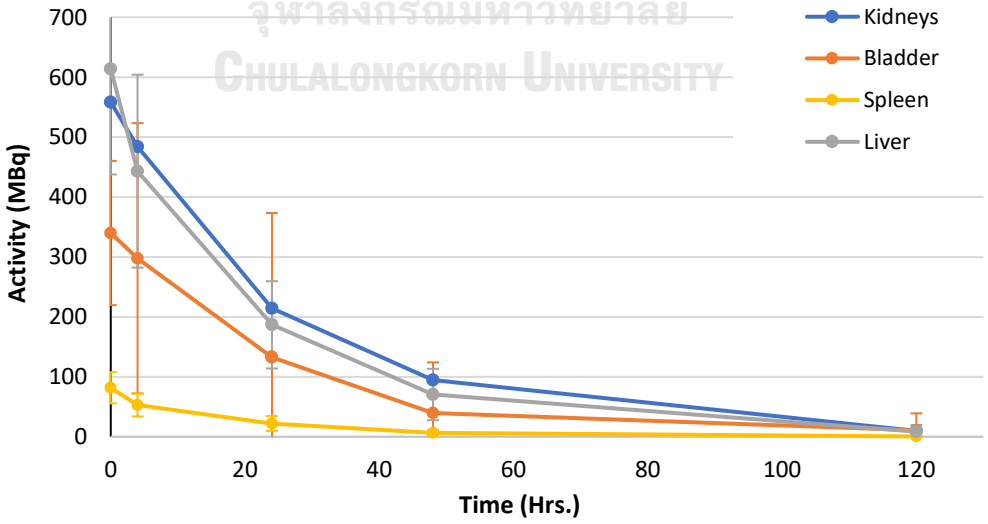

Figure 4.2 The example of time-activity curve in various source organs.

4.2.2 The time-integrated activity coefficient (TIAC)

The time-integrated activity coefficient or resident time, τ (former name), was calculated by fitting time-activity curve (TAC) using MATLAB program based on the mono-exponential function. The average TIAC (h) of whole-body, kidneys, bladder, liver, spleen, lacrimal gland, bone marrow, parotid, and submandibular glands were 24.50±7.50, 2.40±0.54, 1.76±2.71, 2.12±1.38, 0.23±0.09, 0.064±0.032, 16.47±5.93, 0.17±0.10, and 0.08±0.07 h, respectively. The TIAC in various source organs are shown in Table 4.3

Table 4.3 The time-integrated activity coefficient (TIAC) in unit hours of source organs in each treatment cycle.

Patient (cycle)	Kidneys	Bladder	Liver	Spleen	Lacrimal glands	Bone Marrow	Parotid glands	Submandibular glands
P1 (1)	17.91	2.02	0.46	1.67	0.24	0.042	9.93	0.2
P1 (2)	15.75	2.26	0.59	1.72	0.14	0.057	12.48	0.17
P2 (1)	22.05	2.57	0.72	3.55	0.21	0.06	17.53	0.14
P2 (2)	21.5	2	1.09	5.99	0.18	0.038	13.9	0.05
P3 (1)	24.73	2.48	0.24	1.57	0.14	0.119	20.32	0.38
P3 (2)	14.47	2.94	0.2	2.24	0.13	0.041	11.9	0.06
P4 (1)	24.38	2.54	2.44	1.39	0.25	0.042	8.26	0.1
P4 (2)	40.39	1.68	9.51	2.01	0.39	0.07	24.61	0.31
P5	32.3	2.04	0.83	1.6	0.21	0.082	25.88	0.13
P6	20.84	3.09	0.5	1.33	0.41	0.059	13.74	0.2
P7	30.14	1.81	0.31	1.05	0.28	0.031	15.32	0.09
P8	29.52	3.41	4.27	1.3	0.2	0.129	23.8	0.26
Mean	24.5	2.4	1.76	2.12	0.23	0.064	16.47	0.17
SD	7.5	0.54	2.71	1.38	0.09	0.032	5.93	0.1

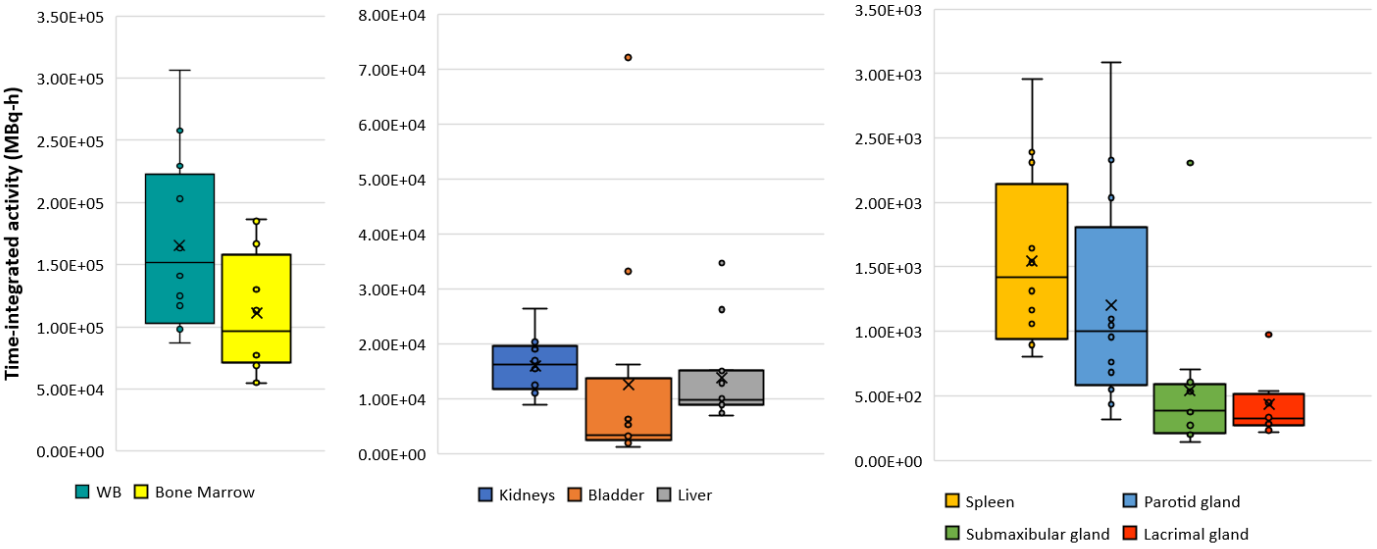

Figure 4.3 The time-integrated activity (TIA) in unit of MBq-h of source organs in each treatment cycle.

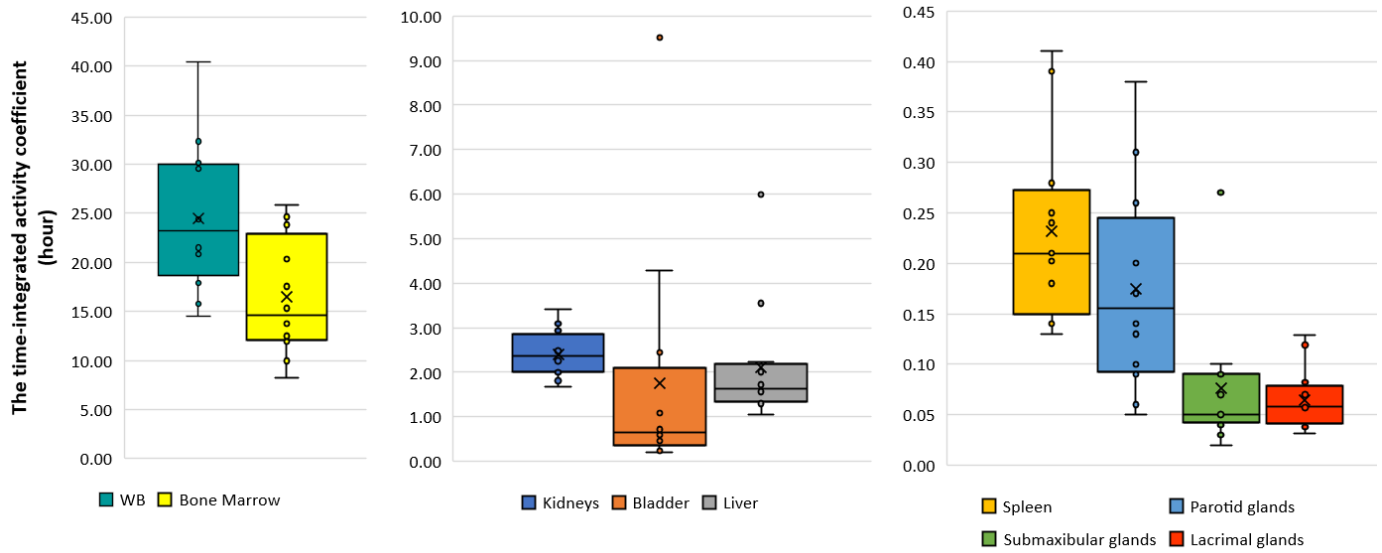

Figure 4.4 The time-integrated activity coefficient (TIAC) in unit hours of source organs in each treatment cycle.

4.3 The absorbed dose coefficient of target organs

Dosimetry in target organs in this study was calculated using MIRD scheme, while absorbed dose to lacrimal glands, the spherical model method was applied. The S values in this study were derived from the OLINDA/EXM software version 2.0. The absorbed dose to 8 target organs (kidneys, bladder, liver, spleen, lacrimal glands, bone marrow, parotid, and submandibular glands) were calculated. The results showed that lacrimal glands received the highest mean absorbed organ dose for the ^{177}Lu-PSMA I&T treatment. The mean absorbed dose for 8 organs were calculated by twelve treatment cycles, maximum absorbed dose was in lacrimal glands (3.62±1.78 Gy/GBq). The mean absorbed doses in target organs of 12 treatment cycles are shown in Table 4.4 in unit of Gy/GBq and Table 4.5 in unit of Gy/cycle.

To evaluate the difference of computational phantoms used for dosimetry calculation, the absorbed doses in lacrimal was calculated by the OLINDA/EXM version 2.0 and the OLINDA/EXM version 1.0. It was found that the difference of absorbed doses of 6.4% was obtained. The comparison of absorbed dose in lacrimal glands calculated by different version of OLINDA/EXM is shown in Table 4.8.

Table 4.4 The mean absorbed dose in unit of Gy/GBq of target organs in each treatment cycle.

Patient (cycle)	Kidneys	Bladder	Liver	Spleen	Lacrimal glands	Bone Marrow	Parotid glands	Submandibular glands
P1 (1)	0.517	0.088	0.075	0.126	2.370	0.009	0.182	0.045
P1 (2)	0.578	0.113	0.078	0.076	3.220	0.011	0.158	0.035
P2 (1)	1.000	0.209	0.224	0.166	3.380	0.023	0.197	0.070
P2 (2)	0.780	0.317	0.412	0.146	2.140	0.019	0.077	0.035
P3 (1)	1.014	0.073	0.113	0.120	6.710	0.029	0.552	0.126
P3 (2)	1.196	0.061	0.161	0.111	2.310	0.017	0.094	0.130
P4 (1)	0.834	0.598	0.081	0.166	2.370	0.009	0.120	0.035
P4 (2)	0.551	0.493	0.116	0.264	3.950	0.028	0.362	0.086
P5	0.742	0.226	0.103	0.155	4.630	0.032	0.164	0.061
P6	1.122	0.136	0.085	0.308	3.330	0.017	0.258	0.124
P7	0.502	0.065	0.051	0.160	1.750	0.015	0.089	0.268
P8	0.889	0.830	0.060	0.109	7.280	0.021	0.245	0.048
Mean	0.810	0.267	0.130	0.159	3.620	0.019	0.208	0.089
SD	0.241	0.248	0.101	0.066	1.781	0.008	0.136	0.067

Table 4.5 The absorbed dose in unit of Gy/Cycle of target organs in each treatment cycle.

Patient (cycle)	Kidneys	Bladder	Liver	Spleen	Lacrimal glands	Bone Marrow	Parotid glands	Submandibular glands
P1 (1)	2.851	0.485	0.415	0.694	12.129	0.048	1.006	0.294
P1 (2)	3.207	0.626	0.430	0.423	17.025	0.061	0.876	0.194
P2 (1)	7.512	1.567	1.830	1.247	25.012	0.176	1.481	0.527
P2 (2)	4.588	1.865	2.421	0.862	12.596	0.109	0.451	0.204
P3 (1)	8.329	0.599	0.930	0.984	27.353	0.235	4.534	1.032
P3 (2)	8.148	0.416	1.095	0.755	22.683	0.113	0.639	0.888
P4 (1)	5.584	4.006	0.541	1.114	14.733	0.062	0.803	0.234
P4 (2)	4.178	3.739	0.883	2.006	30.188	0.211	2.744	0.656
P5	3.239	0.986	0.449	0.676	16.765	0.141	0.716	0.268
P6	6.309	0.767	0.480	1.734	17.153	0.097	1.452	0.697
P7	4.313	0.557	0.440	1.373	14.507	0.126	0.761	2.300
P8	6.907	6.448	0.464	0.844	25.874	0.166	1.904	0.375
Mean	5.43	1.84	0.86	1.06	19.67	0.13	1.45	0.64
SD	1.98	1.91	0.64	0.46	6.22	0.06	1.17	0.59

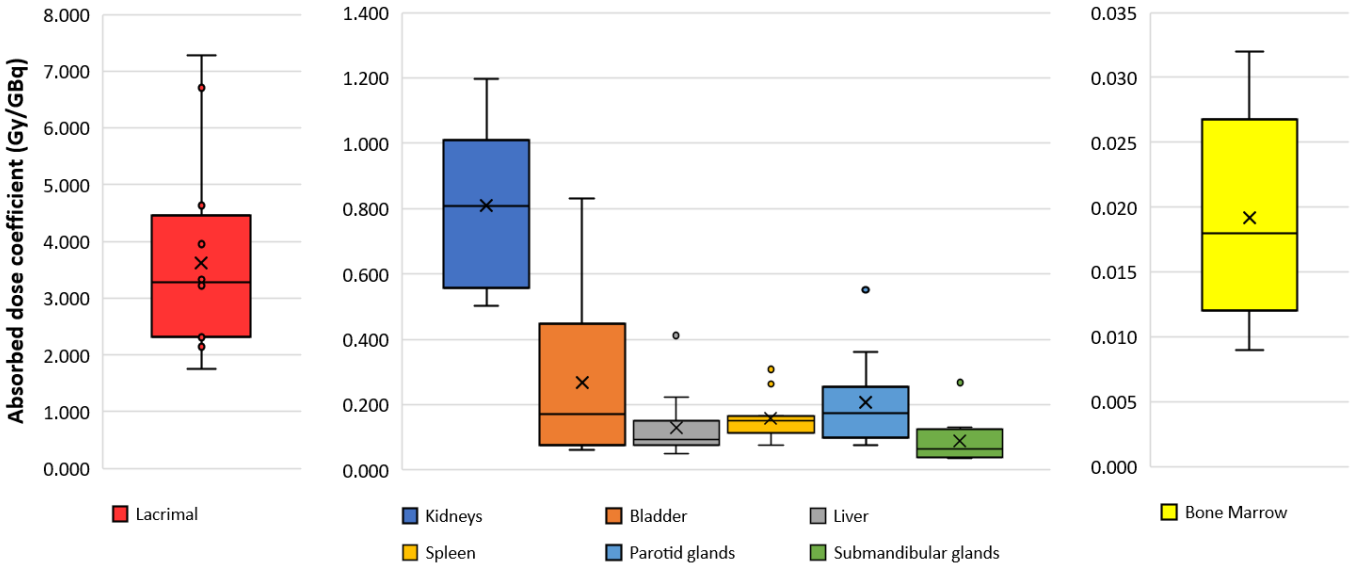

Figure 4.5 The mean absorbed dose in unit of Gy/GBq of target organs in each treatment cycle.

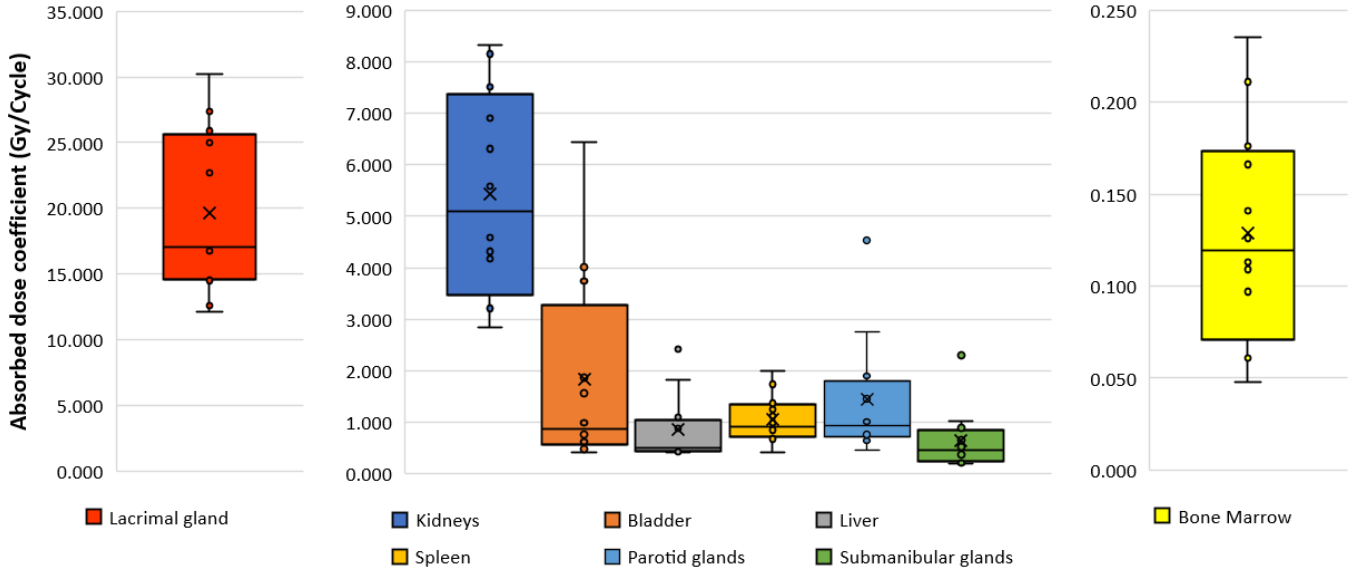

Figure 4.6 The mean absorbed dose in unit of Gy/Cycle of target organs in each treatment cycle.

Table 4.6 The individual absorbed dose in unit of Gy/GBq of target organs in 4 patients underwent 2 treatment cycle.

Patient (cycle)	Kidneys	Bladder	Liver	Spleen	Lacrimal glands	Bone Marrow	Parotid glands	Submandibular glands
P1 (1)	2.851	0.485	0.415	0.694	12.129	0.048	1.006	0.294
P1 (2)	3.207	0.626	0.430	0.423	17.025	0.061	0.876	0.194
Mean	3.03	0.56	0.42	0.56	14.58	0.05	0.94	0.24
SD	0.25	0.10	0.01	0.19	3.46	0.01	0.09	0.07
P2 (1)	7.512	1.567	1.830	1.247	25.012	0.176	1.481	0.527
P2 (2)	4.588	1.865	2.421	0.862	12.596	0.109	0.451	0.204
Mean	6.05	1.72	2.13	1.05	18.80	0.14	0.97	0.37
SD	2.07	0.21	0.42	0.27	8.78	0.05	0.73	0.23
P3 (1)	8.329	0.599	0.930	0.984	27.353	0.235	4.534	1.032
P3 (2)	8.148	0.416	1.095	0.755	22.683	0.113	0.639	0.888
Mean	8.24	0.51	1.01	0.87	25.02	0.17	2.59	0.96
SD	0.13	0.13	0.12	0.16	3.30	0.09	2.75	0.10
P4 (1)	5.584	4.006	0.541	1.114	14.733	0.062	0.803	0.234
P4 (2)	4.178	3.739	0.883	2.006	30.188	0.211	2.744	0.656
Mean	4.88	3.87	0.71	1.56	22.46	0.14	1.77	0.45
SD	0.99	0.19	0.24	0.63	10.93	0.11	1.37	0.30

Table 4.7 The mean absorbed dose / injected activity 7.4 GBq.

	Kidneys	Bladder	Liver	Spleen	Lacrimal glands	Bone Marrow	Parotid glands	Submandibular glands
Mean (Gy)	5.994	1.976	0.962	1.147	26.788	0.141	1.539	0.659

Table 4.8 Comparison of absorbed doses in lacrimal glands based on OLINDA/EXM version 2.0 and OLINDA/EXM version 1.0.

Patient (cycle)	Absorbed dose in lacrimal glands (Gy/GBq)		Percentage Different
	OLINDA/EXM v. 1.0	OLINDA/EXM v. 2.0	
P1 (1)	2.52	2.37	6.00%
P1 (2)	3.42	3.22	5.83%
P2 (1)	3.60	3.38	6.19%
P2 (2)	2.28	2.14	6.23%
P3 (1)	7.14	6.71	6.03%
P3 (2)	2.46	2.31	6.21%
P4 (1)	2.52	2.37	6.00%
P4 (2)	4.20	3.95	6.01%
P5	4.92	4.63	5.93%
P6	3.55	3.33	6.10%
P7	1.86	1.75	6.08%
P8	7.73	7.28	5.86%
Mean	3.85	3.62	6.01%
SD	1.89	1.78	--

*Percentage Different = $\frac{(2)-(1)}{(1)}$ x 100

Where (1) is Absorbed dose in lacrimal glands OLINDA/EXM version 1.0

(2) is Absorbed dose in lacrimal glands OLINDA/EXM version 2.0

4.4 Effective half-life of ^{177}Lu-PSMA

The effective half-life (T_{eff}) in each organ was determined at the time point that when the activity decreased to 50 percent from the beginning. The effective half-life of ^{177}Lu-PSMA I&T in each organ and patient are shown in Table 4.9.

Table 4.9 The effective half-life (h) of ^{177}Lu-PSMA I&T in each organ.

	WB	Kidneys	Bladder	Liver	Spleen	Lacrimal glands	Bone Marrow	Parotid glands	Submandibular glands
Mean	15.023	20.111	18.360	13.974	12.099	15.720	14.000	29.946	20.965
SD	5.584	7.241	17.863	9.246	3.291	7.092	4.345	26.287	18.371

CHAPTER 5
DISCUSSION AND CONCLUSIONS

5.1 Discussion

Theranostics in nuclear medicine has become of increasing interest as its benefits provide more precision in diagnosis and cancer treatment especially at the late stage with metastasis. As the patients underwent several treatment fractions, the radiation doses received should be concerned and the higher amount of administered activity for each fraction can be given while avoiding the toxicity to the critical organs. The present study aimed to provide the radiation dosimetry using ^{177}Lu-PSMA I&T radiopharmaceutical therapy at KCMH as the first report in Thailand. This study included 12 treatment fractions in 8 metastases prostate cancer patients to determine absorbed doses in the kidneys, urinary bladder, liver, spleen, lacrimal glands, red bone marrow, parotid, and submandibular glands. In this study, radiation dosimetry was calculated based on MIRD scheme.

5.1.1 Factors affecting S value in calculation of absorbed dose in target organ

Patient-specific internal dosimetry is used to determine the risks of deterministic tissue reactions and the probability of disease control for the individual patient and requires patient-specific estimates of S-values. Definition of S-values is the total amount of radiation energy emitted by the radioactivity in the source organ and the fraction of energy emitted by the source organ that is adsorbed by the target organ. The S values can be calculated by Monte Carlo radiation-energy transport calculations. The value depends on the radiation type, the energy emitted per transformation, the geometry of the mathematical phantoms and especially mass of the target organ as shown in Chapter III following Equation 3.5:

$$S(r_T \leftarrow r_S) = \frac{1}{M(r_T)} \sum_i E_i Y_i \phi(r_T \leftarrow r_S, E_i),$$

where E_i is mean (or individual) energy of the i^{th} nuclear transition, Y_i is the yield, i.e. the number of ith nuclear transitions per nuclear transformation (number of emitted particles or photons per decay).

Two factors as mentioned previously are different in case of using different radionuclide. In this study, the radionuclide ^{177}Lu was used for all treatments. Thus, the parameters of E_i and Y_i for the dosimetry calculation n this study were identical or very similar.

Another factor is the mass scaling of precompiled S values, between reference phantom mass and patient tissue mass. If patient's weight less than reference phantom body weight, this will affect by increasing of absorbed dose in target organ. Moreover, this study compared the dosimetry using different S-value from different computational phantoms. The S-values from OLINDA/EXM version 1.0 were calculated using Christy-Eckerman (CE) phantoms, whereas S-values from OLINDA/EXM version 2.0 was calculated using non-uniform rational B-spline (NURBS) computational phantoms. Thus, the absorbed dose in target organs of different phantom was also found to be different. Each model is specifically calculated by creating an ideal model of human anatomy. It is defined as a set of distinctly different organ volumes positioned appropriately with mass and composition chosen to reflect general or standard human anatomy. It can be seen that the use of different models directly affects the S value due to one factor being the absorbed fractions, which the spectrum of emission types will determine the fraction of energy emitted by a radionuclide that is absorbed by a particular target mass. For example, almost all β- particles are generally absorbed within the source organ as a non-penetrating radiation, where over 80% of ^{177}Lu emitted β- radiation, and this is a reason of considering only self-absorbed dose calculation. Moreover, model and design of phantom such as location of the organ, distancing of organs can lead to uncertainty of the S value affecting the amount absorbed in the target organ (27).

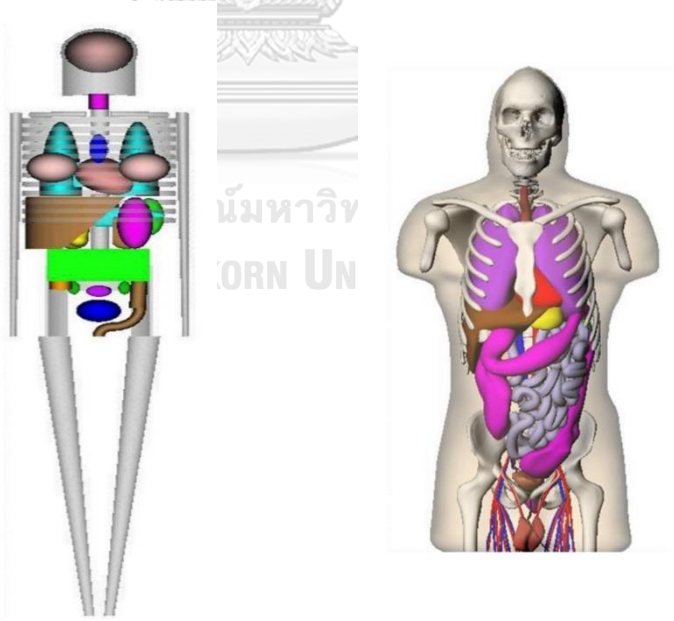

Figure 5.1 The Christy-Eckerman and NUEBS computational phantoms used for S values determination.

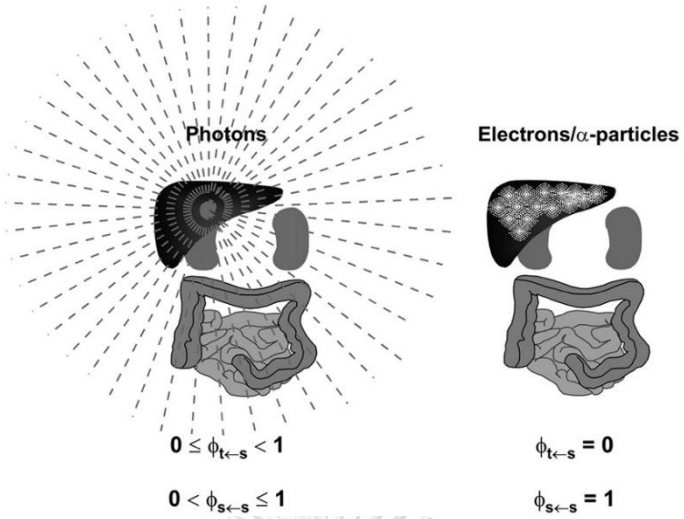

Figure 5.2 Absorbed fraction for photon, electron and alpha particles.

Different tissue absorption properties of photons versus electron or α-particle emissions of radionuclide for source to source and source to target tissues are illustrated in Figure 5.2. Photons originating in liver, for example, depending on energy, can irradiate distant organs. Correspondingly, not all of photon energy emitted within source organ will be absorbed by source organ, as reflected in possible range of absorbed fraction values for photons. In contrast, great majority of electrons (Auger and β-particles) or α-particle energy will be absorbed close to emission source and within source tissue. Correspondingly, energy absorption to other tissues is negligible (28).

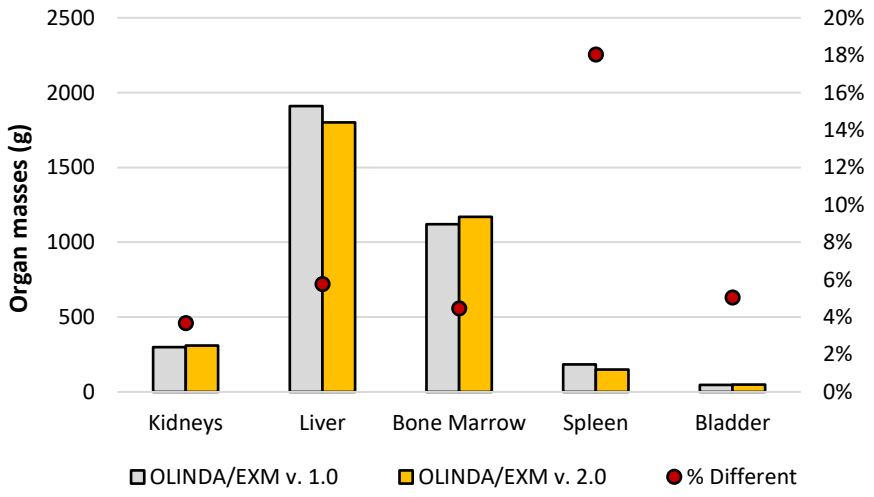

Figure 5.3 Comparison of organ masses for adult males from OLINDA/EXM version 1.0 and OLINDA/EXM version 2.0.

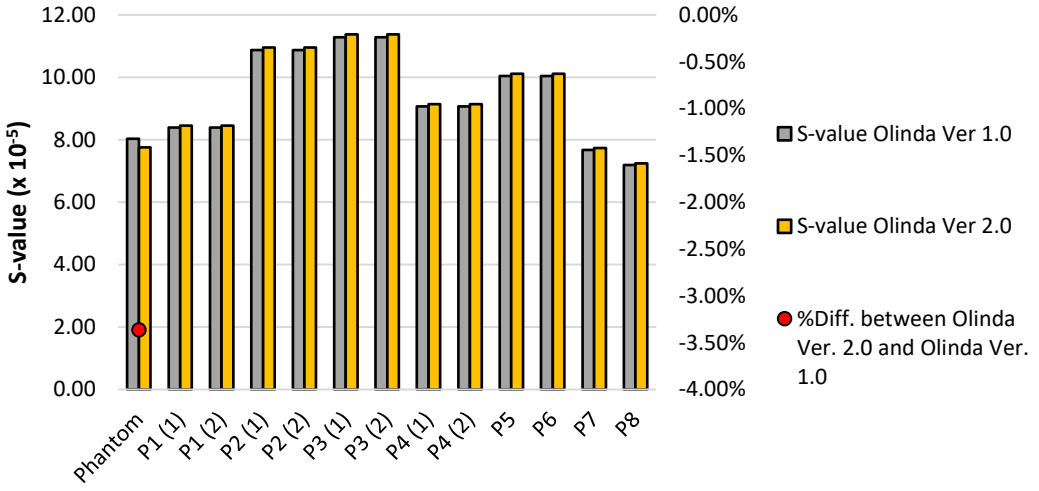

Figure 5.4 Comparison of S-value in kidneys between patient specific S-value and reference S-value in phantom of both OLINDA/EXM version 1.0 and OLINDA/EXM version 2.0.

Table 5.1 S-value of kidneys between patient specific S-value and reference S-value in phantom of both OLINDA/EXM version 1.0 and OLINDA/EXM version 2.0.

Patient	OLINDA/EXM v. 1.0		OLINDA/EXM v. 2.0	
	Mass (kg.)	S-value × (10^{-5})	Mass (kg.)	S-value × (10^{-5})
Phantom	70.00	8.03	62.00	7.76
1 (cycle 1)	67.00	8.39	67.00	8.45
1 (cycle 2)	67.00	8.39	67.00	8.45
2 (cycle 1)	51.70	10.87	51.70	10.96
2 (cycle 2)	51.70	10.87	51.70	10.96
3 (cycle 1)	49.80	11.29	49.80	11.38
3 (cycle 2)	49.80	11.29	49.80	11.38
4 (cycle 1)	62.00	9.07	62.00	9.14
4 (cycle 2)	62.00	9.07	62.00	9.14
5	56.00	10.04	56.00	10.12
6	56.00	10.04	56.00	10.12
7	73.25	7.67	73.25	7.73
8	78.20	7.19	78.20	7.24

5.1.2 Comparison of absorbed dose coefficient in kidneys with published data

Renal toxicity is one of the great limiting factors in ^{177}Lu-PSMA I&T therapy, with most of ^{177}Lu-PSMA I&T is mainly excreted via the kidneys but then reabsorbed and accumulated in the kidney cortex. Therefore, kidneys were also taken into account for critical organ for ^{177}Lu-PSMA I&T. In calculating the absorbed dose in kidney from planar images in this study, our results of absorbed dose were slightly higher than those values reported from previous studies (Figure 5.6) (21-23, 25). Due to overlapping organs inside peritoneum, this may be one reason for the overestimation of absorbed dose in kidneys. As shown in Figure 5.5, it was found that the planar images at 24 hours showed the renal region overlaps with other organs. However, this problem was solved by the mean count concentration (mean count/pixel) used to treat this phenomenon.

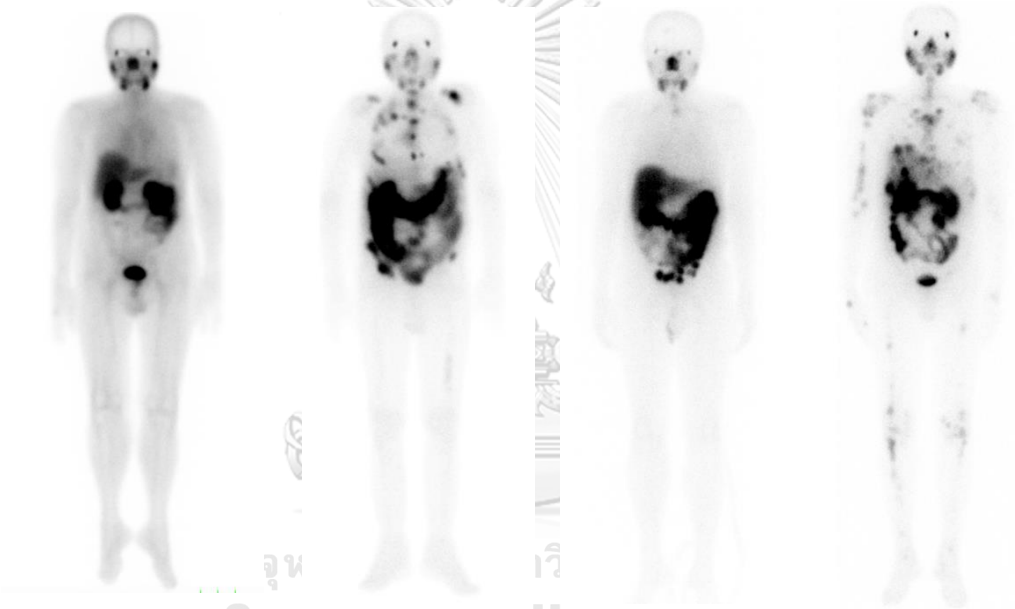

Figure 5.5 The example of WB planar images at 24 h of the location of kidneys overlie to other organs in patients treated by ^{177}Lu-PSMA I&T at KCMH.

However, this study indicated that the average absorbed dose for kidneys was within the dose limits at 23 Gy (9, 22), which was safe and no nephrotoxicity was found in any patients. The mean absorbed dose of kidneys determined in this study for ^{177}Lu-PSMA I&T was 0.81±0.24 Gy/GBq. It was comparable to the mean absorbed dose for kidneys of ^{177}Lu-DFKZ-PSMA-617. The mean absorbed dose of 0.53±0.17 Gy/GBq investigated in nine prostate cancer patients were reported by Hohberg et al. (22), as well as the absorbed dose of 0.60±0.18 Gy/GBq from five patients were studied by Delker et al. (23). Okamoto et al. found that the absorbed dose of 0.72±0.21 Gy/GBq weas obtained from total of 34 treatment cycles in 18 prostate cancer patients (21). The maximum absorbed dose of kidneys in this study was 8.33 Gy (patient 3, cycle 1). Therefore, this study confirmed that ^{177}Lu-PSMA I&T was safe, and no nephrotoxicity found in any patients who treated at KCMH. The comparison of the absorbed dose in kidneys obtained from this study and compared with previous published data are shown in Figure 5.6. Even though only eight prostate cancer patients with twelve treatment cycles were investigated in this study, these patient sample size were comparable with Hohberg et al and Delker et al (22, 23).

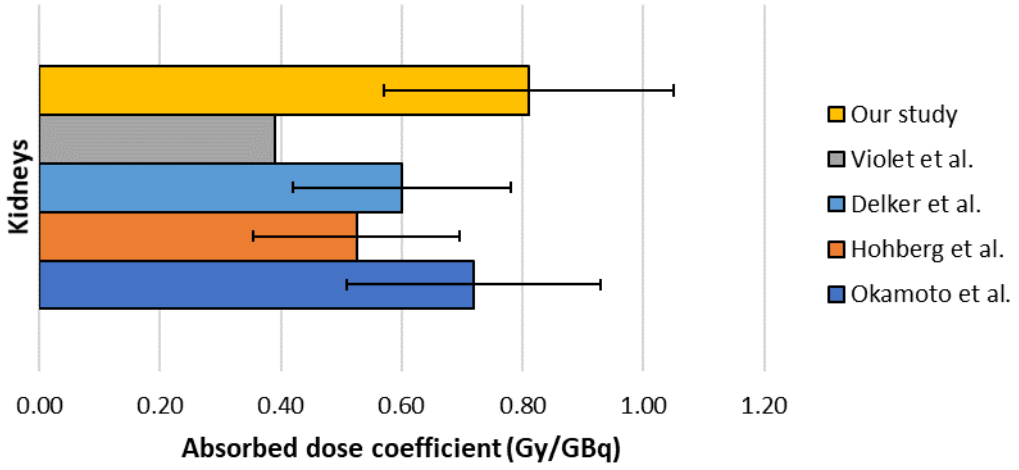

Figure 5.6 Comparison of absorbed dose in kidneys between this study and published data.

5.1.3 Comparison of absorbed dose of lacrimal gland with published data

The highest amount of the absorbed dose coefficient in this study was seen in the lacrimal glands of 3.62±1.78 Gy/GBq resulting the mean absorbed dose of 26.79 Gy for injected activity 7.4 GBq. At present, the source-to-target S value are not yet available for the lacrimal glands in both OLINDA/EXM version 1.0 and version 2.0 software packages. As the organ mass 1.4 g of the lacrimal glands taken from Hohberg et al. (22) was used as the reference, the calculation was performed using the spherical model-based instead similar to the dosimetry calculation in tumors. The calculation of the absorbed doses was mainly contributed from only self-dose,

meanwhile omitted the cross-dose from surrounding tissues. This study showed that mean absorbed dose in the lacrimal glands was slightly lower than previous published data. The mean absorbed dose of 3.80±1.40 Gy/GBq for ^{177}Lu-PSMA I&T were studied by Shozo et al. (21), 3.78 Gy/GBq for ^{177}Lu-PSMA-617 reported by Violet et al. (25), and higher than recent report for ^{177}Lu-DKFZ-PSMA-617 studied by Hohberg et al. (mean, 2.82±0.76 Gy/GBq) (22). The absorbed dose in the present study was comparable with the previous published data as shown in Figure 5.7. Although those studies mentioned that the lacrimal glands were not likely a critical organ for ^{177}Lu-PSMA, a cumulative dose from our study will likely be almost the dose limit and will perhaps exceed 40 Gy after second treatment cycles. So, the patients follow up should be performed for the patients who received the absorbed dose at lacrimal glands greater than 40 Gy after the treatment to observe the toxicity and deterministic effect in the lacrimal glands (22).

The difference of absorbed doses of 6.01% was found between the Non-uniform rational B-spline (NURBS) computational phantom calculated by the OLINDA/EXM version 2.0 (3.62±1.78 Gy/GBq), and the stylized Christy-Eckerman (C-E) phantom calculated by the OLINDA/EXM version 1.0 (3.85±1.89 Gy/GBq). This slightly difference in dosimetry calculation using spherical model for the lacrimal glands was most likely due to the better anatomical representation in NURBS phantom where tissues are in contact with each other. Recently, the mean absorbed dose in lacrimal glands of 3.78 Gy/GBq calculated with voxelized computational phantoms was determined by Violet J. (25), which was slightly higher than our study.

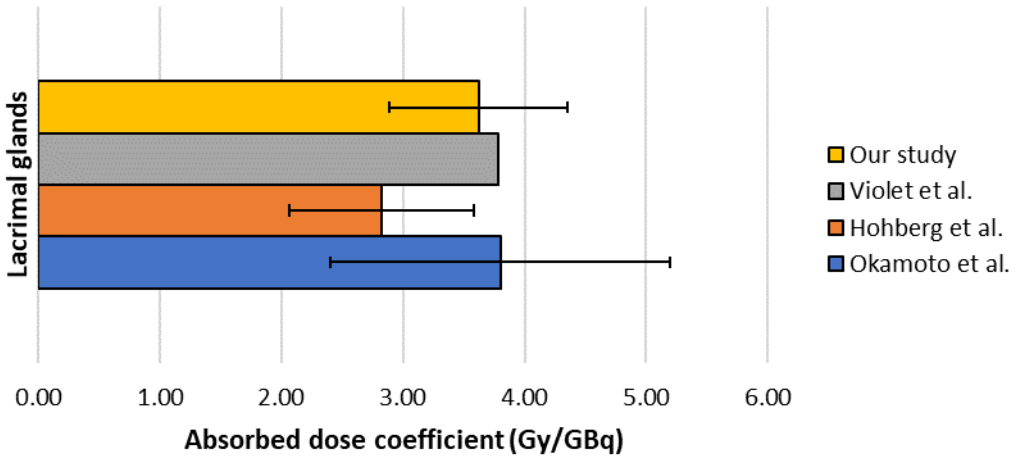

Figure 5.7 Comparison of absorbed dose in lacrimal glands between this study and published data.

5.1.4 Comparison of absorbed dose of bone marrow with published data

Bone marrow was considered as another critical organ, and the dose constraint to avoid the bone marrow suppression should be below 2-Gy (9). The self-dose dominated the contributions to the absorbed dose to the bone marrow similar to the study of SandstrÖm et al (29). Another issue that needs to be considered when comparing absorbed dose between studies is the S-values parameters used for calculation, from either the original MIRD Pamphlet No.11 (Christy-Eckerman) or newer computational phantoms. In this study, the use of S-value from OLINDA/EXM version 2.0 software and the planar image-based method yielded a mean bone marrow absorbed dose of 0.142±0.057 Gy/7.4 GBq for ^{177}Lu-PSMA I&T, which were comparable to previous published bone marrow dosimetry data as shown in Figure 5.10. The comparison of the absorbed doses for bone marrow using image-based two-compartment method for the patients underwent first and second cycle of treatment is shown in Figure 5.8. The large difference of absorbed dose was found in patient 4 as the first treatment did not show the bone metastases resulted the absorbed dose of 0.009 Gy/GBq, totally 0.062 Gy per fraction for the injected activity 4.37 GBq. For the second therapy, the skeletal metastases were progressing resulting the absorbed dose 3.5-fold higher than first therapy (0.028 Gy/GBq) for the injected activity 6.70 GBq. Thus, the absorbed dose in bone marrow was correlated to the level of skeletal metastases agreed with study of Delker, et al (23). Also, the image-based dosimetry methods can demonstrate that increased absorbed doses resulted in higher platelet toxicity (9). The underestimation or overestimation of the absorbed dose in bone marrow also depended on the accuracy of ratio between the bone marrow and the low compartment estimation. However, the blood-based methods have uncertainties, including the timing and handling of the blood samples and calibration of the instruments. Therefore, the image-based method would provide less invasive option to the patients for calculating the bone marrow absorbed doses for radiopharmaceutical dosimetry.

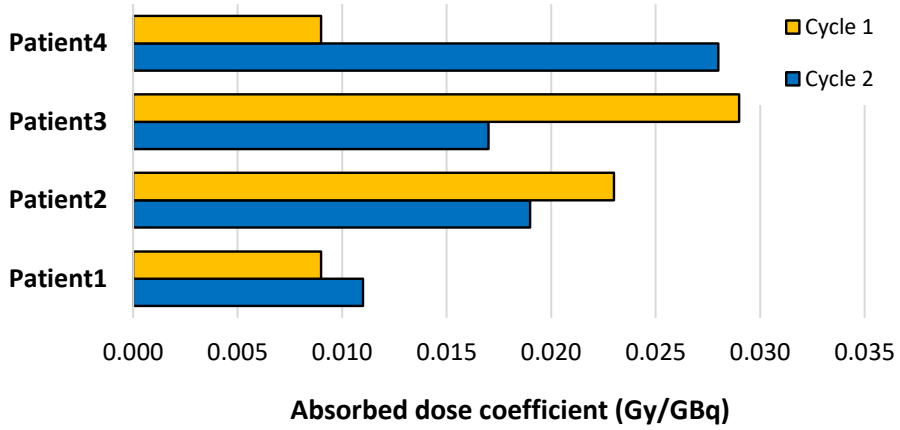

Figure 5.8 Comparison of absorbed dose in bone marrow between first cycle and second treatment cycle of four patients.

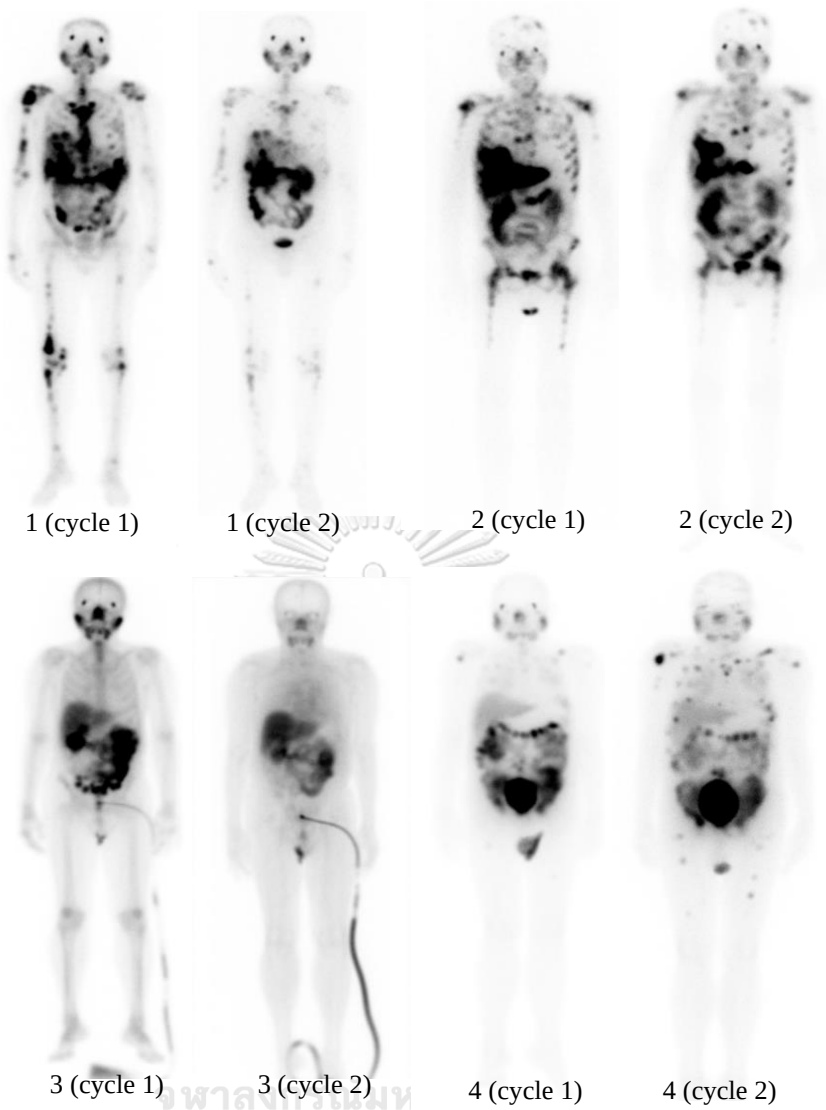

Figure 5.9 The example of WB planar images of 4 patients treated by ^{177}Lu-PSMA I&T for two cycles at KCMH.

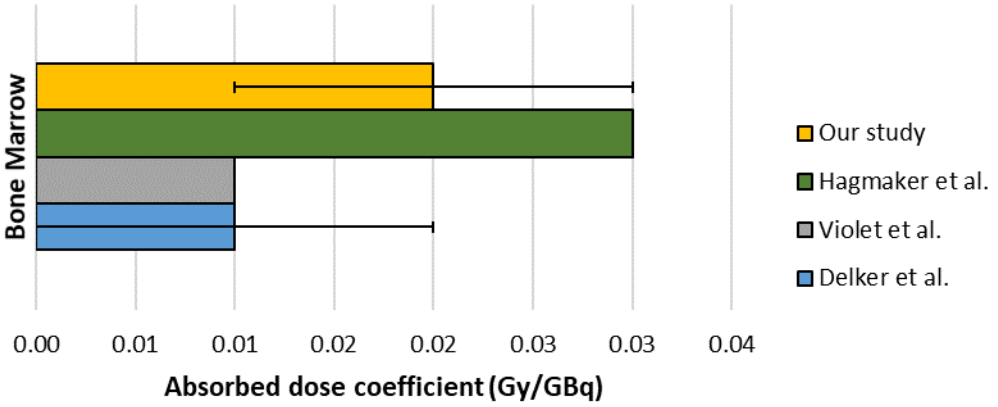

Figure 5.10 Comparison of absorbed dose in bone marrow between this study and published data.

5.1.5 Comparison of absorbed dose of salivary glands with published data

Both of parotid and the submandibular glands were also the concern areas for the treatment. Even though both organs were not critical organ, they were clearly uptake of ^{177}Lu-PSMA I&T from the planar scintigraphy images. Mean absorbed dose in parotid glands was 0.208±0.136 Gy/GBq, which was significantly lower than previous studies for ^{177}Lu-PSMA I&T as shown in Figure 5.11. Mean absorbed dose of 0.55±0.14 Gy/GBq, and 0.58 Gy/GBq for ^{177}Lu-PSMA-617 were reported by Okamoto et al. (21) and Violet et al. (25), respectively. Also, mean absorbed dose in submandibular of 0.089±0.067 Gy/GBq obtained in this study was significantly lower than both previous studies 0.64±0.40 Gy/GBq (21), and 0.44 Gy/GBq (25). Although the effect of cooling of salivary glands during the therapy is still unclear, at KCMH, the patients received cold-packs compression over the parotid and submandibular glands from 30 min prior to and up to 60 min after administration of ^{177}Lu-PSMA I&T in order to mitigate therapy-induced damage to the salivary glands.

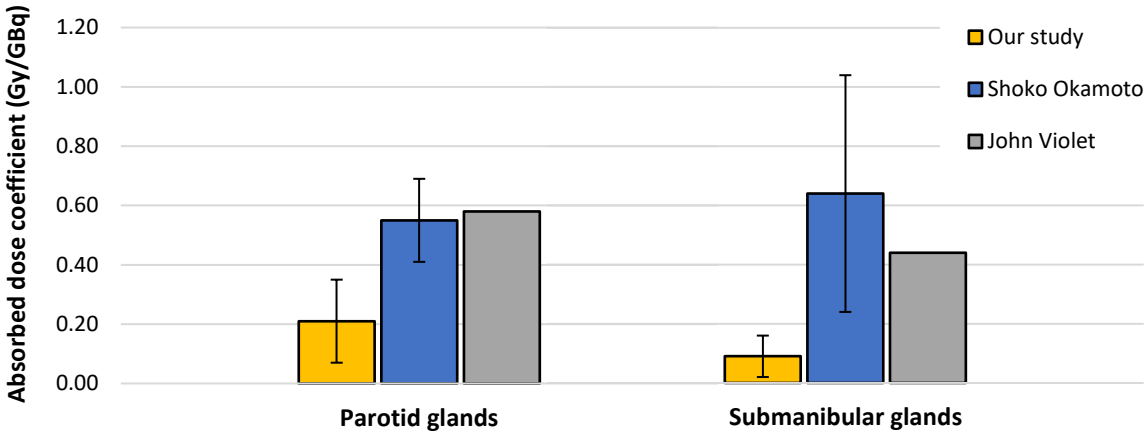

Figure 5.11 Comparison of absorbed dose in parotid and submandibular glands between this study and published data.

Table 5.2 Comparison of the absorbed doses between this study and literatures.

Organs	Absorbed dose coefficient (Gy/GBq)				
	Number of studies				
	12	5	9	18	30
	This study	Delker et al. (23)	Hohberg et al. (22)	Okamoto et al. (21)	Violet et al. (25)
Kidneys	0.810±0.241	0.60±0.18	0.53±0.17	0.72±0.21	0.39
Liver	0.130±0.101	0.10±0.06	--	0.12±0.06	0.10
Spleen	0.155±0.068	0.10±0.03	--	--	0.08
Lacrimal glands	3.62±1.78	--	2.82±0.76	3.80±1.40	3.78
Bone marrow	0.019±0.008	0.01±0.01	--	--	0.11
Parotid glands	0.208±0.136	--	--	0.55±0.14	0.58
Submandibular glands	0.089±0.067	--	--	0.64±0.40	0.44

5.2 Conclusions

According to 12 treatment cycles treated by ^{177}Lu-PSMA I&T radionuclide therapy at King Chulalongkorn Memorial Hospital, the mean absorbed dose in kidneys, urinary bladder, liver, spleen, lacrimal glands, bone marrow, parotid, and submandibular glands were 0.81±0.24, 0.27±0.25, 0.13±0.10, 0.16±0.07, 3.62±1.78, 0.02±0.01, 0.21±0.14, and 0.09±0.07 Gy/GBq, respectively. Kidneys were concerned as a critical organ. Location of kidneys that overlay on other organs may lead to overestimate absorbed dose. The absorbed dose in bone marrow was correlated to the level of bone metastases. However, the total absorbed doses in our results did not exceed the dose limit in kidneys and bone marrow in any patients. Lacrimal glands were not likely a critical organ for ^{177}Lu-PSMA I&T and our absorbed dose results were less than the dose limit.

The levels of absorbed doses in critical organs (kidneys, and bone marrow) were still lower than the recommended dose constraints. Therefore, the treatment with ^{177}Lu-PSMA I&T is safe for metastasis prostate cancer patients. From this study, it is likely to increase the number of treatment cycles or the amount of injected activity while sparing the toxicity to the normal tissues in order to achieve the most benefit concept for theranostics in nuclear medicine.

REFERENCES

1. Bray F, Ferlay J, Soerjomataram I, Siegel RL, Torre LA, A. J. GLOBOCAN estimates of incidence and mortality worldwide for 36 cancers in 185 countries https://www.wcrf.org/dietandcancer/cancer-trends/worldwide-cancer-data: International Agency for Research on Cancer (IARC); 2018 [
2. M.D. DCHW. Treatment & Management of Prostate Cancer https://news.cancerconnect.com/prostate-cancer/treatment-management-of-prostate-cancer-ZzAYTB_x-UKiFpbJqIBwkw?fbclid=IwAR2ilbeX0zdDz3pLKHxUhsEk7zKoz1CCasK-rKaJbiM4DIXJO8fVA0S1l9k2021 [
3. Radionuclide therapy [International Atomic Energy Agency:[Available from: https://www.iaea.org/topics/radionuclide-therapy.
4. Munjal A, Gupta. N. Radiopharmaceuticals. 2021.
5. Simpson BR, van Staden MJ, Lubbe J, van Wyngaardt WM. Accurate activity measurement of Lu-177 by the liquid scintillation 4pibeta-gamma coincidence counting technique. Appl Radiat Isot. 2012;70(9):2209-14.
6. Bouchelouche K, Turkbey B, Choyke PL. PSMA PET and Radionuclide Therapy in Prostate Cancer. Semin Nucl Med. 2016;46(6):522-35.
7. Ebrahimnejad Gorji K, Abedi Firouzjah R, Khanzadeh F, Abdi-Goushbolagh N, Banaei A, Ataei G. Estimating the Absorbed Dose of Organs in Pediatric Imaging of 99mTc-DTPATc-DTPA Radiopharmaceutical using MIRDOSE Software. J Biomed Phys Eng. 2019;3:285–94.
8. Ruigrok EAM, van Vliet N, Dalm SU, de Blois E, van Gent DC, Haeck J, et al. Extensive preclinical evaluation of lutetium-177-labeled PSMA-specific tracers for prostate cancer radionuclide therapy. Eur J Nucl Med Mol Imaging. 2020.
9. Hagmarker L, Svensson J, Ryden T, van Essen M, Sundlov A, Gleisner KS, et al. Bone Marrow Absorbed Doses and Correlations with Hematologic Response During (177)Lu-DOTATATE Treatments Are Influenced by Image-Based Dosimetry Method and Presence of Skeletal Metastases. J Nucl Med. 2019;60(10):1406-13.
10. IAEA SAFETY GLOSSARY TERMINOLOGY USED IN NUCLEAR SAFETY AND RADIATION PROTECTIO2018.
11. Guinn VP. Radioactivity. Third, editor: Academic Press; 2003.
12. Cherry SR, Sorenson JA, Phelps ME. PHYSICS in NUCLEAR MEDICINE. 4th, editor: Saunders; 2012.
13. Sgouros G, Bodei L, McDevitt MR, Nedrow JR. Radiopharmaceutical therapy in cancer: clinical advances and challenges. Nat Rev Drug Discov. 2020;19(9):589-608.
14. Velikyan I. Radionuclides for Imaging and Therapy in Oncology2014.
15. Canedo-Antelo M, Baleato-Gonzalez S, Mosqueira AJ, Casas-Martinez J, Oleaga L, Vilanova JC, et al. Radiologic Clues to Cerebral Venous Thrombosis. Radiographics. 2019;39(6):1611-28.
16. Hosono M. Perspectives for Concepts of Individualized Radionuclide Therapy, Molecular Radiotherapy, and Theranostic Approaches. Nucl Med Mol Imaging. 2019;53(3):167-71.
17. Stringer RE. RADIOCHEMICAL METHODS | Pharmaceutical Applications. Second ed2005.
18. Tateishi U. Prostate-specific membrane antigen (PSMA)-ligand positron

emission tomography and radioligand therapy (RLT) of prostate cancer. Jpn J Clin Oncol. 2020;50(4):349-56.
19. Kramer V, Fernandez R, Lehnert W, Jimenez-Franco LD, Soza-Ried C, Eppard E, et al. Biodistribution and dosimetry of a single dose of albumin-binding ligand [(177)Lu]Lu-PSMA-ALB-56 in patients with mCRPC. Eur J Nucl Med Mol Imaging. 2021;48(3):893-903.
20. Susie Medeiros Oliveira Ramos, Sylvia Thomas, Monica Araujo Pinheiro, Francisco de Assis Romeiro Figueiroa Benicio Coelho, Marta de Souza Albernaz CLGdS, Mirta Bárbara Torres Berdeguez, et al. Internal radiation dose and modeling codes in nuclear medicine: a fresh look at old problems. Int J Radiol Radiat Ther. 2017;4(5):439-43.
21. Okamoto S, Thieme A, Allmann J, D'Alessandria C, Maurer T, Retz M, et al. Radiation Dosimetry for (177)Lu-PSMA I&T in Metastatic Castration-Resistant Prostate Cancer: Absorbed Dose in Normal Organs and Tumor Lesions. J Nucl Med. 2017;58(3):445-50.
22. Hohberg M, Eschner W, Schmidt M, Dietlein M, Kobe C, Fischer T, et al. Lacrimal Glands May Represent Organs at Risk for Radionuclide Therapy of Prostate Cancer with [(177)Lu]DKFZ-PSMA-617. Mol Imaging Biol. 2016;18(3):437-45.
23. Delker A, Fendler WP, Kratochwil C, Brunegraf A, Gosewisch A, Gildehaus FJ, et al. Dosimetry for (177)Lu-DKFZ-PSMA-617: a new radiopharmaceutical for the treatment of metastatic prostate cancer. Eur J Nucl Med Mol Imaging. 2016;43(1):42-51.
24. Svensson J, Ryden T, Hagmarker L, Hemmingsson J, Wangberg B, Bernhardt P. A novel planar image-based method for bone marrow dosimetry in (177)Lu-DOTATATE treatment correlates with haematological toxicity. EJNMMI Phys. 2016;3(1):21.
25. Violet J, Jackson P, Ferdinandus J, Sandhu S, Akhurst T, Iravani A, et al. Dosimetry of (177)Lu-PSMA-617 in Metastatic Castration-Resistant Prostate Cancer: Correlations Between Pretherapeutic Imaging and Whole-Body Tumor Dosimetry with Treatment Outcomes. J Nucl Med. 2019;60(4):517-23.
26. Lee C, Lodwick D, Hurtado J, Pafundi D, Williams JL, Bolch WE. The UF family of reference hybrid phantoms for computational radiation dosimetry. Phys Med Biol. 2010;55(2):339-63.
27. Madsen MT, Sunderland JJ. The Phantoms of Medical and Health Physics. G. E, editor: Springer Science+Business Media; 2014.
28. Sgouros G. Dosimetry of internal emitters. J Nucl Med. 2005;46 Suppl 1:18S-27S.
29. Sandstrom M, Garske-Roman U, Granberg D, Johansson S, Widstrom C, Eriksson B, et al. Individualized dosimetry of kidney and bone marrow in patients undergoing 177Lu-DOTA-octreotate treatment. J Nucl Med. 2013;54(1):33-41.

APPENNDIX

APPENDIX A

Table A.1 S-values for calculation of absorbed doses to target organs based on organ masses of Asian reference man.

Target organs	Source organs						
	Kidneys	Liver	Salivary glands	Red marrow	Spleen	UB Cont	Total Body
Kidneys	7.76E-05	1.20E-07	6.39E-10	4.71E-08	2.65E-07	1.18E-08	3.58E-07
Liver	1.18E-07	1.37E-05	2.16E-09	2.44E-08	3.12E-08	3.78E-09	3.58E-07
Salivary Glands	6.39E-10	2.16E-09	2.78E-04	2.07E-08	1.80E-09	3.17E-11	3.56E-07
Red Marrow	3.35E-08	3.09E-08	2.23E-08	1.15E-05	3.67E-08	3.96E-08	2.74E-07
Spleen	2.58E-07	3.03E-08	1.53E-09	2.48E-08	1.60E-04	3.47E-09	3.58E-07
Urinary Bladder Wall	1.18E-08	3.78E-09	3.17E-11	2.44E-08	3.47E-09	5.78E-05	3.62E-07
Total Body	3.49E-07	3.40E-07	3.38E-07	3.57E-07	3.46E-07	3.52E-07	3.54E-07

APPENDIX B

Steps to define calculation absorbed dose in target organ, for example kidneys.

1. ROI covering the kidneys (red box) were manually drawn using the Osirix MD program. Then value of total count of kidney will appear in yellow box.

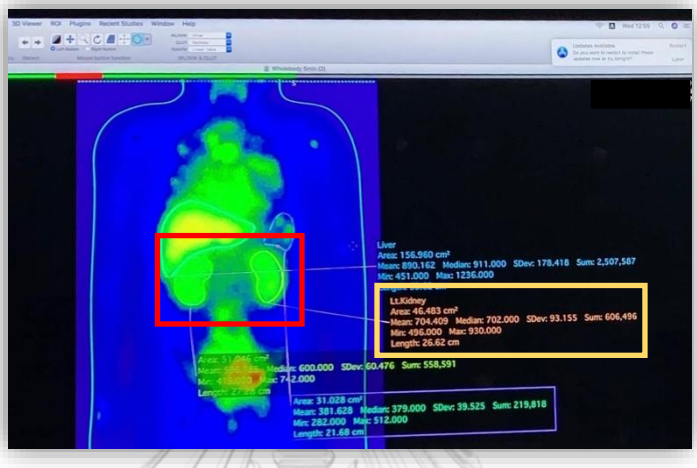

In this example will show the solution to define absorbed dose of kidneys.

Net counts of WB and kidneys from Osirix MD program are following below.

Anteroposterior (AP) image

Background counts value	= 6.42 kc.
Total counts of WB	= 22,154 kc.
Total counts of right kidney	= 1,004 kc.
Total counts of left kidney	= 614 kc.

Posteroanterior (PA) image

Background counts value	= 8.03 kc.
Total counts of WB	= 21,751 kc.
Total counts of right kidney	= 376 kc.
Total counts of left kidney	= 1,159 kc.

2. For background correction, net total counts of kidneys are difference between count of kidneys and background count. Thus,

Anteroposterior (AP) image

Net counts of right kidney = Total counts of right kidney – Background count
= 1,004 – 6.42
= 997.58 kc.

Net counts of left kidney = Total counts of left kidney – Background count
= 614 – 6.42
= 607.58 kc.

Net counts of kidneys (N_A) = Net counts of right kidney + Net counts of left kidney
= 997.58 + 607.58
= 1,605.16 kc

Posteroanterior (PA) image

Net counts of right kidney = Total counts of right kidney – Background count
= 376 – 8.03
= 367.97 kc.

Net counts of left kidney = Total counts of left kidney – Background count
= 1,159 – 8.03
= 1,150.97 kc.

Net counts of kidneys (N_P) = Net counts of right kidney + Net counts of left kidney
= 367.97 + 1,150.97
= 1,518.94 kc

3. Geometrical mean of the counts in anterior and posterior images, substitute net total counts of kidneys of AP and PA image in following below equation.

$$A = \frac{1}{\mathrm{F}} . \sqrt{\mathrm{N_A} . \mathrm{N_P}} \text{ where F =1}$$

$$A = \sqrt{1{,}605.16 \times 1{,}518.94}$$

$$A = 1{,}561.46\ kc.$$

4. Find ratio of total net counts of kidneys to total net counts of WB at initial time point, due to at immediately after injection total net count of WB is equal to total injected activity. To define net counts of whole-body is repeat step 2 and step 3.

$$Ratio_{Kidneys/WB} = \frac{Net\ counts\ of\ kidney}{Net\ counts\ of\ whole-body}$$

$$= \frac{1{,}561.46}{21{,}944.35}$$

$$= 0.0712\ kc.$$

5. For physical decay of ^{177}Lu correction, the injected activity was corrected from following equation for physical decay of ^{177}Lu.

$$\mathrm{A(t)} = \mathrm{A(0)}\ e^{-\lambda t} \qquad \text{where } \lambda = \frac{ln2}{T_{1/2}}$$

To define activity in whole-body at 15 minutes after injection.

$$A_{15} = 181e^{-\frac{(0.693)(0.25)}{(159.52)}}$$

$$= 180.80\ mCi$$

$$= 180.80 \times 37 = 6{,}689.73\ MBq$$

6. Activity in kidneys is equal to injected activity from step 5 multiply by ratio of total net counts of kidneys to total net counts of WB from step 4.

$$A_{Kidney\ at\ 15\ min.} = 0.0712 \times 6{,}689.73$$

$$= 476.02\ MBq$$

7. Repeat step 6 at each time point.

$$A_{Kidney\ at\ 236\ min.} = 404.50\ MBq$$

$$A_{Kidney\ at\ 1414\ min.} = 239.18\ MBq$$

8. Extrapolated time-activity curve to 48 h and 120 h by fitting time-activity curve 3 time points (immediately, 2h, 24h) from step 7 then using mono-exponential function to fit the data.

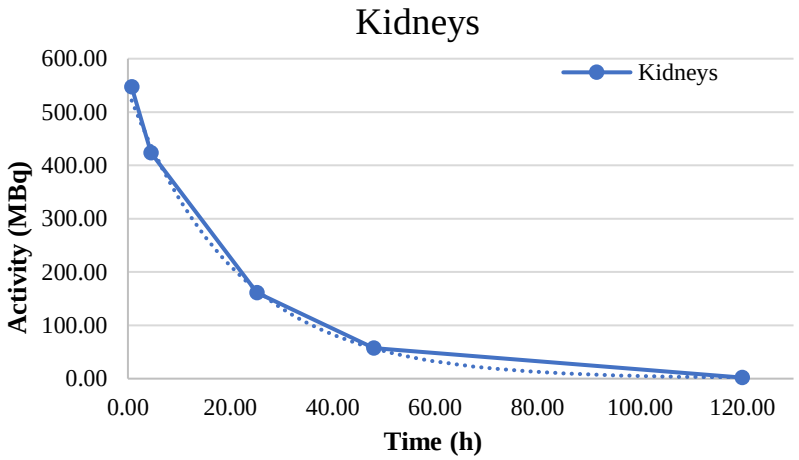

The mono exponential equation of above TAC is $y = 468.43e^{-0.029x}$

$$y = 468.43e^{-0.029t}$$ where t is time in hour.

Thus, activity in kidneys at 48 and 120 hours are

$$A_{Kidneys\ at\ 48h} = 4.68.43e^{-(0.029)(48)} = 116.09\ MBq$$

$$A_{Kidneys\ at\ 120h} = 4.68.43e^{-(0.029)(120)} = 14.39\ MBq$$

9. The time-integrated activity (TIA or $\tilde{A}$) in unit MBq-h was generated using MATLAB program. Result from MATLAB is TIA $(\tilde{A}) = 1.70 \times 10^4\ MBqh$

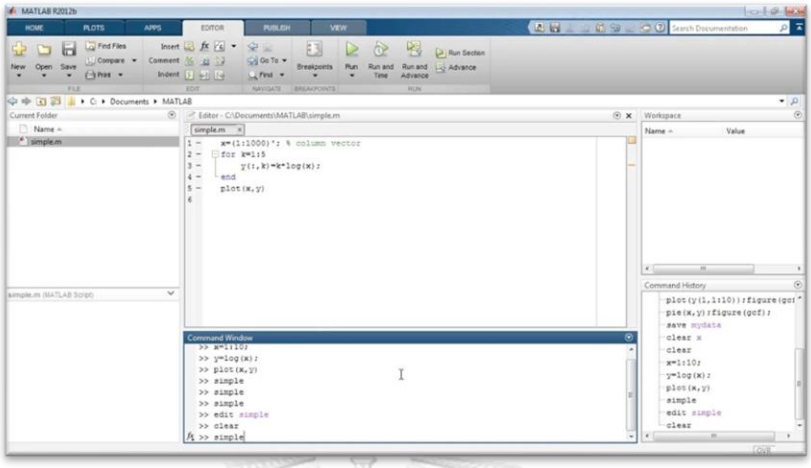

10. The time integrated activity coefficient (TIAC, $\tilde{a}$) or residence time in unit h, can be calculated as the following equation (see Eq.3.2).

$$\tilde{a}(r_s) = \frac{\tilde{A}(r_s)}{A_0}$$

$$= \frac{1.70 \times 10^4}{6.70 \times 10^3}$$

$$= 2.54\ h$$

11. The S value was scaled by relating the patient body weight with the International Commission on Radiological Protection (ICRP) 89 adult male reference phantom 73 kg in order to obtain the patient weight-specific S value (see Eq.5).

$$S_{patient} \approx S_{phantom_{(r_{Kidneys} \leftarrow r_{Kidneys})}} \cdot \frac{m_{phantom}}{m_{patient}}$$

$$= (7.76 \times 10^{-5}) \times \frac{73}{62}$$

$$= 9.14 \times 10^{-5}$$

12. Absorbed dose of kidney was calculated in accordance with the methodology described by the Medical Internal Radiation Dose (MIRD) Committee Pamphlet No. 21 as follows equation (see Eq.3.4).

$$D_{(r_{Kidneys})} = \tilde{A}_{(r_{Kidneys})} \cdot S_{(r_{Kidneys} \leftarrow r_{Kidneys})}$$

$$= (1.70 \times 10^4 \times 3{,}600) \cdot (9.14 \times 10^{-5})$$

$$= 5.59\ Gy$$

$$Absorbed\ dose\ coefficient = \frac{Absorbed\ dose}{Injected\ activity}$$

$$= \frac{5.59}{6{,}697}\ \frac{Gy}{MBq}$$

$$= 0.83\ \text{Gy/GBq}$$

APPENDIX C

Step to define count Whole-body and Background

1. Select whole-body planar image which we need to drawn ROI

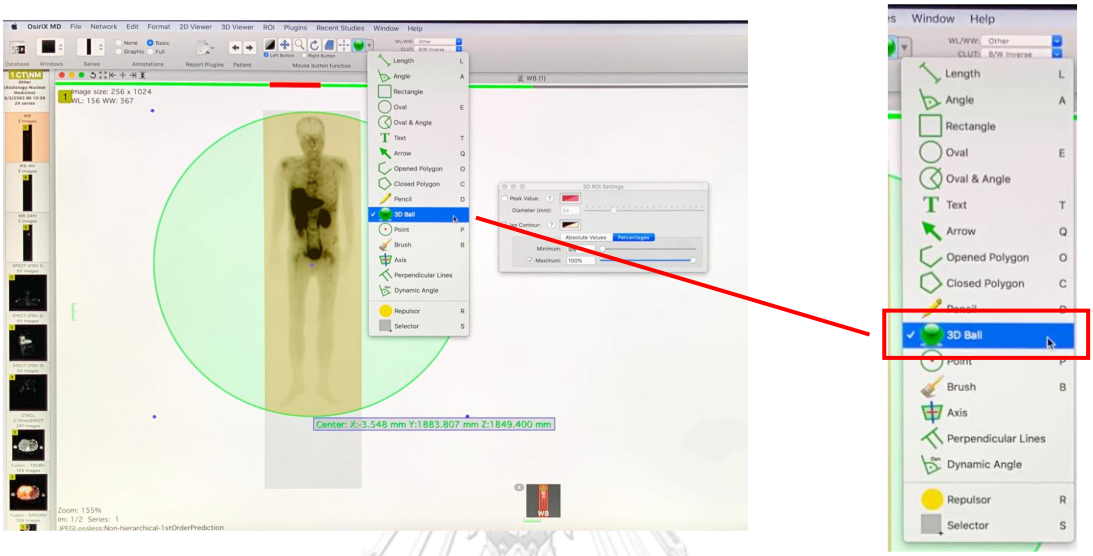

2. Select tool for drawn ROI, click “3D Ball”
3. Select area that need to known count value
    a. Press right click at ROI ball (green cirlcle)
    b. Select ROI setting
    c. Adjust maximum to 100% and minimum to 0%
    d. Press right click at ROI ball

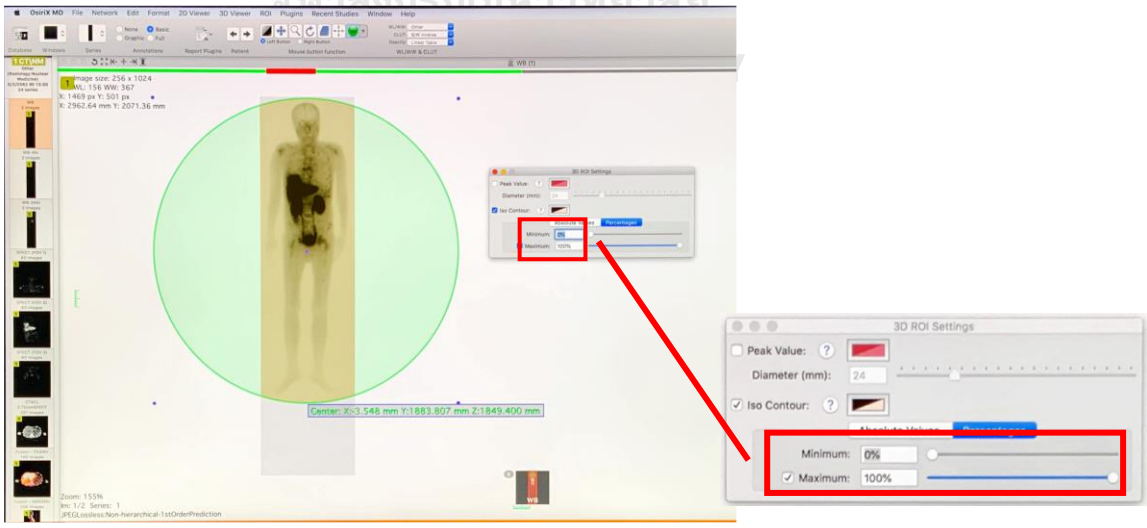

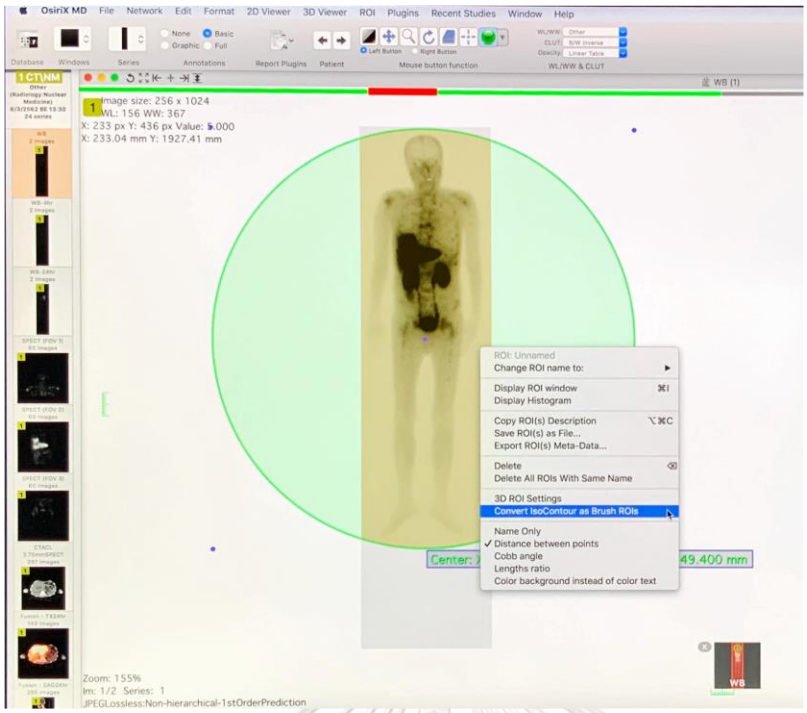

f. Select “Convert IsoContour as Brush ROIs”

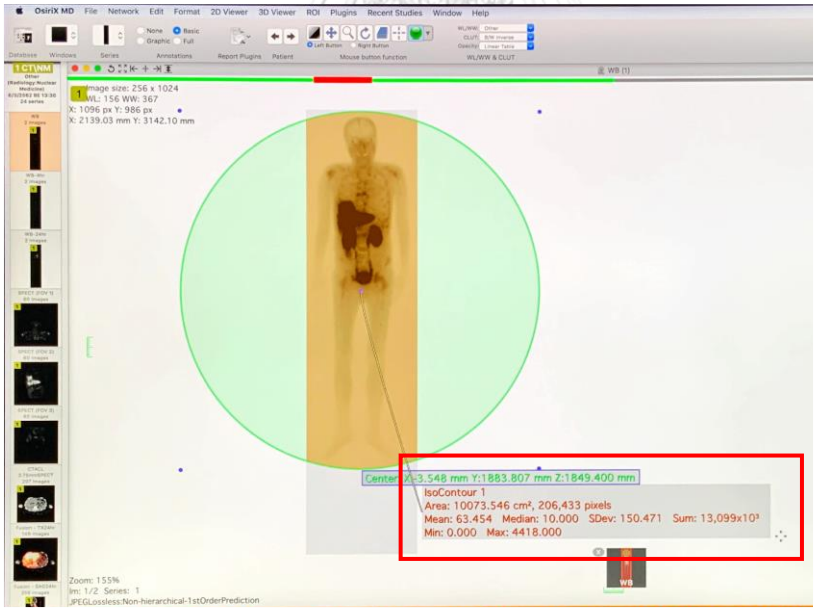

g. IsoCountour will appear in rectangular box

4. To define count of background
    a. Press “Tool” then select “rectangle”
    b. Drawn rectangular nearly whole-body
    c. Count of background was appearing

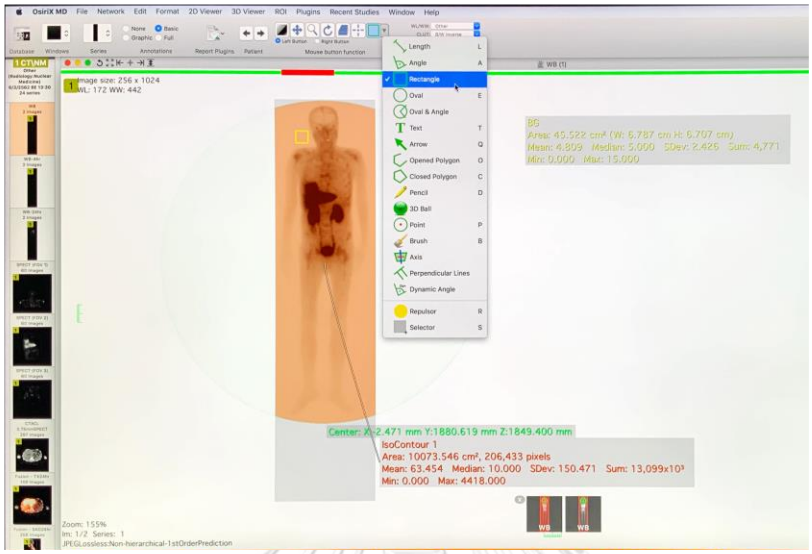

APPENDIX D

Step to define hot uptake

1. Repeat step 1 to 3b
    a. Adjust maximum to 100%
    b. Adjust minimum until noise is disappear

    c. Press right click at ROI ball
    d. Select “Convert IsoContour as Brush ROIs”

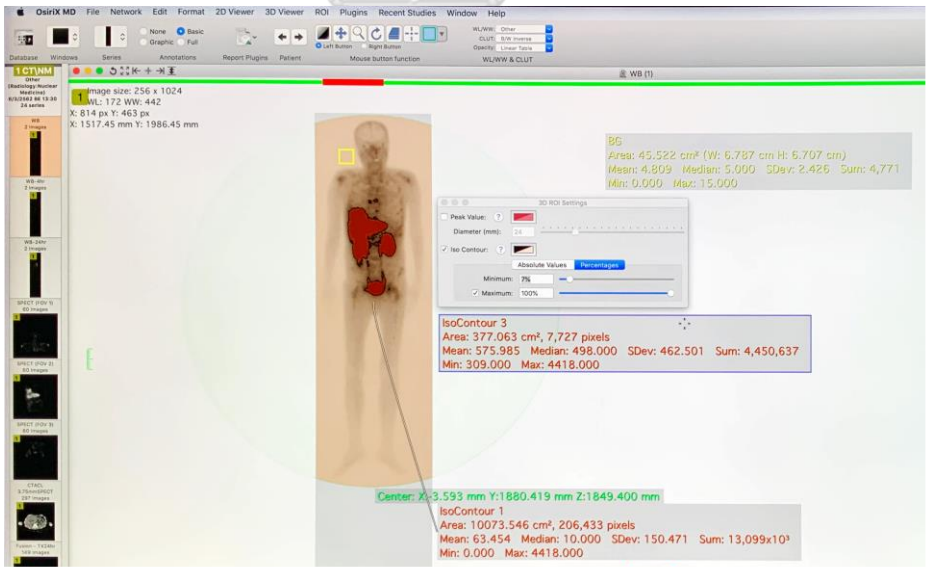

To located hot uptake by adjust planar image

e. Adjust WL/WW, CLUT and Opacity

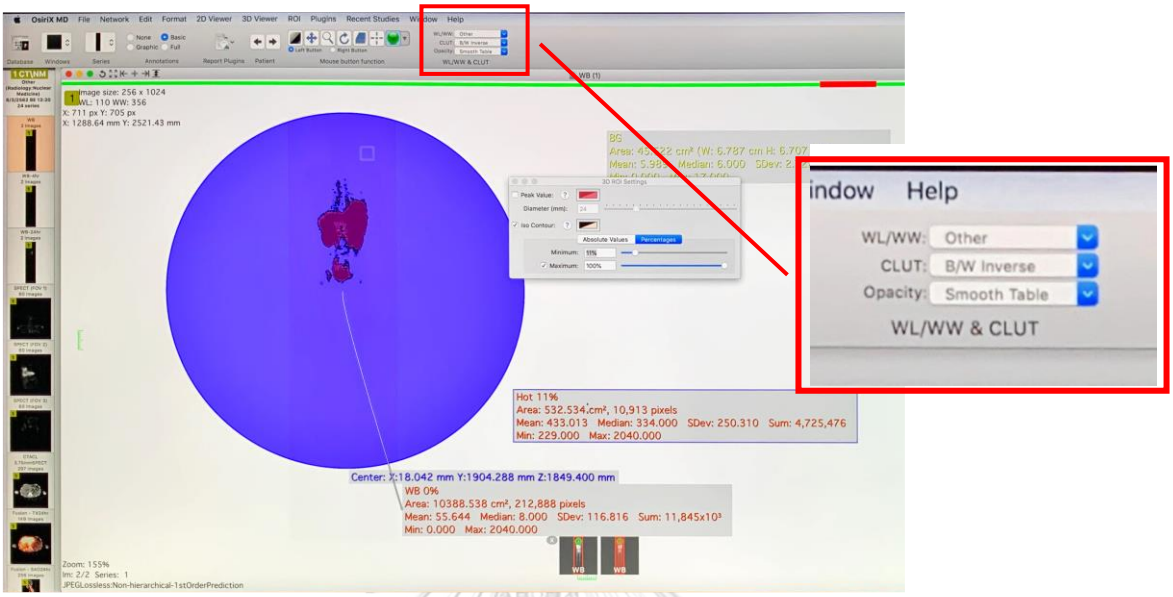

Table D.1 The results of quality control on January, 2019

Date	CT		Background (kc/s)		Energy Peak (keV)		Energy Res. (FWHM %)		Uniformity Det 1 (%)		Uniformity Det 2 (%)		Temp (C)	Humd (%)
	Warm up	Fast cal	Det 1	Det 2	Det 1	Det 2	Det 1	Det 2	CFOV	UFOV	CFOV	UFOV		
3/1/19	P	P	0.29	0.33	122.86	122.38	10.11	10.13	2.16	2.64	2.93	3.62	16.5	70.0
4/1/19	P	P	0.29	0.33	122.85	122.36	10.12	10.09	2.43	2.60	2.80	3.55	16.3	67.0
7/1/19	P	P	0.24	0.27	122.27	122.73	10.73	10.78	2.94	2.94	2.97	2.97	15.8	70.0
8/1/19	P	P	0.28	0.32	122.83	122.32	10.14	10.09	2.36	2.83	2.77	3.65	16.0	70.0
9/1/19	P	P	0.29	0.33	122.84	122.38	10.16	10.11	1.77	2.81	3.07	3.88	16.0	70.0
10/1/19	P	P	0.29	0.32	122.98	122.39	10.05	10.06	1.96	3.10	0.0	0.0	16.4	69.0
11/1/19	P	P	0.29	0.32	122.89	122.34	10.11	10.11	2.85	3.38	3.09	3.51	16.7	67.0
14/1/19	P	P	0.29	0.33	122.94	122.41	10.12	10.10	3.02	3.42	3.29	4.00	0.0	0.0
15/1/19	P	P	0.29	0.32	122.96	122.42	10.12	10.10	2.05	2.69	3.46	3.56	0.0	0.0
16/1/19	P	P	0.29	0.32	122.99	122.49	10.09	10.07	2.37	2.84	3.00	3.64	0.0	0.0
17/1/19	P	P	0.29	0.33	122.90	122.40	10.12	10.08	2.75	3.04	3.11	3.67	16.7	64.0
18/1/19	P	P	0.28	0.32	122.90	122.42	10.10	10.12	2.97	3.78	3.01	3.61	0.0	0.0
21/1/19	P	P	0.29	0.32	123.04	122.52	10.10	10.07	2.34	3.10	2.94	2.69	0.0	0.0
22/1/19	P	P	0.29	0.33	123.00	122.45	10.13	10.09	0.0	0.0	0.0	0.0	16.7	65.0
23/1/19	P	P	0.28	0.32	122.90	122.17	10.41	10.47	2.68	2.68	2.86	2.86	22.9	50.0
24/1/19	P	P	0.28	0.32	123.09	122.06	9.93	10.01	3.33	4.10	3.29	4.04	23.6	46.0
25/1/19	P	P	0.30	0.34	123.01	121.99	9.91	9.99	3.11	3.94	3.09	3.42	23.9	45.0
28/1/19	P	P	0.29	0.32	123.17	122.04	9.9	10.00	3.22	4.12	3.10	3.32	24.0	44.0
29/1/19	P	P	0.29	0.33	123.21	123.59	10.09	10.04	3.30	3.83	3.33	3.45	17.3	64.0
30/1/19	P	P	0.29	0.33	123.14	122.61	10.10	10.04	1.07	2.85	2.85	3.72	17.3	64.0

Table D.2 The results of quality control on February, 2019

Date	CT		Background (kc/s)		Energy Peak (keV)		Energy Res. (FWHM %)		Uniformity Det 1 (%)		Uniformity Det 2 (%)		Temp (C)	Humd (%)
	Warm up	Fast cal	Det 1	Det 2	Det 1	Det 2	Det 1	Det 2	CFOV	UFOV	CFOV	UFOV		
1/2/19	P	P	0.30	0.34	123.14	122.65	10.09	10.02	2.79	3.83	3.25	3.70	16.0	69.0
4/2/19	P	P	0.28	0.32	123.14	122.67	10.15	10.06	3.15	4.24	3.53	3.93	16.0	69.0
5/2/19	P	P	0.29	0.32	123.16	122.61	10.13	10.06	3.39	3.73	3.09	3.78	16.0	69.0
6/2/19	P	P	0.31	0.34	123.15	122.64	10.11	10.04	2.40	2.81	3.36	3.47	16.0	69.0
7/2/19	P	P	0.30	0.34	123.1	122.58	10.14	10.06	3.40	3.95	2.85	4.07	17.0	68.0
8/2/19	P	P	0.31	0.34	123.1	122.57	10.14	10.06	3.08	3.48	3.04	3.28	17.1	67.0
11/2/19	P	P	0.31	0.34	123.06	122.95	10.16	10.11	3.04	3.68	2.69	3.00	17.0	68.0
12/2/19	P	P	0.31	0.34	123.10	123.61	10.06	10.09	2.13	3.08	2.88	3.67	16.9	68.0
13/2/19	P	P	0.31	0.34	123.10	122.61	10.14	10.06	3.55	3.91	2.60	2.96	16.8	68.0
14/2/19	P	P	0.31	0.34	123.10	122.59	10.14	10.07	2.52	2.89	2.98	3.83	16.8	68.0
15/2/19	P	P	0.31	0.34	123.14	122.61	10.12	10.06	2.95	3.52	2.65	3.08	16.8	68.0
18/2/19	P	P	0.31	0.34	123.16	122.67	10.14	10.05	3.22	3.69	2.71	3.89	17.0	70.0
20/2/19	P	P	0.30	0.33	123.16	122.66	10.16	10.06	3.16	3.73	3.53	4.01	17.0	71.0
21/2/19	P	P	0.30	0.34	123.15	122.66	10.12	10.04	2.86	3.38	3.19	3.65	17.0	68.0
22/2/19	P	P	0.29	0.32	123.19	122.68	10.10	9.99	2.38	3.27	3.03	3.72	17.0	68.0
25/2/19	P	P	0.28	0.32	123.20	122.65	10.16	10.00	2.29	3.04	3.10	3.48	17.0	67.0
26/2/19	P	P	0.01	0.03	123.18	122.00	10.01	10.00	3.17	3.99	3.02	3.64	17.0	67.0
27/2/19	P	P	0.30	0.34	123.19	122.71	10.16	10.07	2.70	3.41	2.70	2.78	17.0	67.0
28/2/19	P	P	0.27	0.30	122.93	122.00	10.10	1.08	2.39	3.21	3.54	3.79	17.0	67.0

Table D.3 The results of quality control on March, 2019

Date	CT		Background (kc/s)		Energy Peak (keV)		Energy Res. (FWHM %)		Uniformity Det 1 (%)		Uniformity Det 2 (%)		Temp (C)	Hu69.0md (%)
	Warm up	Fast cal	Det 1	Det 2	Det 1	Det 2	Det 1	Det 2	CFOV	UFOV	CFOV	UFOV		
1/3/19	P	P	0.29	0.33	123.20	123.64	10.13	10.03	2.61	2.98	3.03	3.57	17.4	67.0
4/3/19	P	P	0.29	0.32	123.22	122.78	10.17	10.02	2.37	2.87	4.03	4.07	17.2	67.0
5/3/19	P	P	0.29	0.32	123.18	122.77	10.15	10.01	1.94	2.99	3.35	3.82	17.2	67.0
6/3/19	P	P	0.29	0.33	123.22	122.74	10.16	10.01	2.08	2.90	2.82	3.59	17.2	67.0
7/3/19	P	P	0.27	0.20	122.97	122.58	10.08	10.04	2.56	2.47	4.47	3.39	17.1	67.0
8/3/19	P	P	0.28	0.32	123.20	122.60	10.11	10.06	1.90	2.54	3.26	3.81	17.0	67.0
11/3/19	P	P	0.29	0.32	123.15	122.74	10.13	10.01	2.47	2.71	3.33	3.86	17.2	68.0
12/3/19	P	P	0.24	0.27	123.21	122.74	10.14	10.00	2.04	2.44	3.51	4.03	17.0	66.0
18/3/19	P	P	0.28	0.32	122.96	122.41	10.04	10.06	2.80	3.03	3.18	3.57	18.0	67.0
19/3/19	P	P	0.29	0.32	122.94	122.35	10.08	10.07	2.90	3.62	2.93	3.21	18.0	67.0
20/3/19	P	P	0.28	0.32	122.97	122.42	10.03	10.03	1.83	2.61	2.75	3.34	18.0	66.0
21/3/19	P	P	0.28	0.32	122.97	122.42	10.03	10.03	1.83	2.61	2.75	3.34	18.0	67.0
22/3/19	P	P	0.28	0.32	123.06	122.45	10.02	10.07	2.23	2.68	2.59	3.81	18.0	66.0
25/3/19	P	P	0.28	0.32	123.05	122.43	10.08	10.06	1.95	2.07	3.36	4.06	18.0	64.0
26/3/19	P	P	0.29	0.32	123.00	122.37	10.11	10.07	2.31	2.72	3.34	3.64	17.9	65.0
27/3/19	P	P	0.28	0.32	123.04	122.39	10.08	10.11	2.46	3.48	2.67	3.09	18.3	64.0
28/3/19	P	P	0.28	0.33	123.05	122.46	10.01	10.07	2.49	3.12	3.34	3.70	18.0	65.0

Table D.4 The results of quality control on Apirl, 2019

Date	CT		Background (kc/s)		Energy Peak (keV)		Energy Res. (FWHM %)		Uniformity Det 1 (%)		Uniformity Det 2 (%)		Temp (C)	Hu69.0md (%)
	Warm up	Fast cal	Det 1	Det 2	Det 1	Det 2	Det 1	Det 2	CFOV	UFOV	CFOV	UFOV		
1/4/19	P	P	0.28	0.32	123.08	122.50	10.03	10.07	3.05	3.21	2.93	3.26	18.0	65.0
2/4/19	P	P	0.29	0.32	123.10	122.46	10.06	10.06	2.17	2.70	3.14	3.14	17.0	67.0
3/4/19	P	P	0.29	0.33	123.10	122.44	10.05	10.06	1.90	2.86	2.34	2.76	18.4	65.0
4/4/19	P	P	0.29	0.32	123.12	122.54	10.04	10.01	2.48	2.76	2.71	3.13	17.9	65.0
5/4/19	P	P	0.28	0.33	123.12	122.56	10.03	10.02	2.96	3.55	3.72	4.51	18.0	67.0
9/4/19	P	P	0.29	0.33	123.18	122.54	10.08	10.05	2.23	2.99	2.82	3.16	18.0	66.0
10/4/19	P	P	0.29	0.32	123.16	122.52	10.08	10.06	2.33	2.76	2.57	3.46	18.0	68.0
11/4/19	P	P	0.28	0.32	123.15	122.51	10.07	10.07	2.01	2.88	2.92	3.86	17.8	66.0
17/4/19	P	P	0.28	0.32	123.28	122.58	10.07	10.07	1.97	2.36	3.24	3.47	18.0	65.0
18/4/19	P	P	0.29	0.33	123.28	122.60	10.09	10.02	3.19	3.34	3.24	3.28	18.0	64.0
19/4/19	P	P	0.28	0.32	123.34	122.63	10.06	9.98	2.78	3.46	2.77	2.83	18.0	65.0
22/4/19	P	P	0.29	0.33	123.25	122.62	10.09	10.02	3.30	3.85	2.75	2.91	18.0	65.0
23/4/19	P	P	0.28	0.33	123.30	122.63	10.09	9.96	2.28	2.49	2.94	4.19	17.0	62.0
24/4/19	P	P	0.29	0.33	123.28	122.62	10.08	9.99	2.06	2.33	3.01	3.69	18.0	64.0
25/4/19	P	P	0.29	0.32	123.29	122.63	10.07	9.98	3.22	3.55	2.90	3.32	18.0	65.0
26/4/19	P	P	0.29	0.32	123.21	122.62	10.09	10.01	2.39	3.15	3.08	3.50	17.0	63.0
29/4/19	P	P	0.29	0.33	123.33	122.71	10.08	9.95	2.08	2.76	2.72	3.19	18.0	65.0
30/4/19	P	P	0.29	0.33	123.32	122.69	10.09	9.96	2.86	3.20	2.36	3.22	18.0	64.0

Table D.5 The results of quality control on May, 2019

Date	CT		Background (kc/s)		Energy Peak (keV)		Energy Res. (FWHM %)		Uniformity Det 1 (%)		Uniformity Det 2 (%)		Temp (C)	Hu69.0md (%)
	Warm up	Fast cal	Det 1	Det 2	Det 1	Det 2	Det 1	Det 2	CFOV	UFOV	CFOV	UFOV		
1/5/19	P	P	0.31	0.34	123.38	122.60	10.11	10.03	2.83	3.30	3.66	4.11	18.4	65.0
2/5/19	P	P	0.30	0.34	123.28	122.61	10.08	10.03	2.25	3.23	2.72	3.13	18.1	65.0
3/5/19	P	P	0.30	0.34	123.32	122.63	10.07	10.02	2.79	3.23	2.79	3.18	18.0	64.0
7/5/19	P	P	0.31	0.34	123.35	122.67	10.10	9.99	3.08	4.02	3.10	3.33	17.8	65.0
8/5/19	P	P	0.31	0.34	123.32	122.59	10.06	10.02	3.11	3.65	2.89	3.26	18.0	63.0
10/5/19	P	P	0.28	0.32	123.38	122.70	10.11	10.00	3.21	3.50	2.95	3.31	18.0	63.0
13/5/19	P	P	0.31	0.34	123.30	122.59	10.08	10.05	3.51	3.86	3.03	3.03	17.7	64.0
14/5/19	P	P	0.31	0.34	123.30	122.62	10.13	10.06	2.98	3.52	3.24	3.24	18.0	66.0
15/5/19	P	P	0.30	0.35	123.30	122.60	10.13	10.04	2.15	2.93	3.00	3.18	18.0	63.0
16/5/19	P	P	0.31	0.34	123.35	122.69	10.07	9.99	3.45	4.18	3.08	3.30	18.0	63.0
21/5/19	P	P	0.31	0.34	123.44	122.73	10.16	10.01	2.90	3.76	2.96	4.04	18.1	64.0
22/5/19	P	P	0.31	0.34	123.40	122.70	10.11	9.99	2.66	3.40	2.99	3.18	18.0	64.0
23/5/19	P	P	0.31	0.34	123.35	122.74	10.17	9.98	2.70	3.22	3.08	3.84	18.0	64.0
27/5/19	P	P	0.31	0.34	123.44	122.75	10.16	10.01	2.28	3.27	2.96	3.39	18.0	63.0
28/5/19	P	P	0.31	0.34	123.41	122.76	10.14	9.97	2.15	2.73	3.15	3.76	18.0	63.0
29/5/19	P	P	0.31	0.34	123.33	122.75	10.11	10.00	2.88	3.95	2.81	3.27	17.8	63.0
30/5/19	P	P	0.30	0.34	123.42	122.81	10.15	9.98	3.01	3.92	3.05	3.51	17.8	63.0
31/5/19	P	P	0.28	0.33	123.42	122.72	10.13	9.99	2.90	3.36	2.66	3.10	17.9	62.0

Table D.6 The results of quality control on June, 2019

Date	CT		Background (kc/s)		Energy Peak (keV)		Energy Res. (FWHM %)		Uniformity Det 1 (%)		Uniformity Det 2 (%)		Temp (C)	Hu69.0md (%)
	Warm up	Fast cal	Det 1	Det 2	Det 1	Det 2	Det 1	Det 2	CFOV	UFOV	CFOV	UFOV		
4/6/19	P	P	0.28	0.32	123.46	122.79	10.16	9.96	2.86	4.09	2.94	3.18	18.7	63.0
5/6/19	P	P	0.27	0.32	123.48	122.80	10.13	9.93	3.16	3.72	2.55	3.12	18.7	63.0
6/6/19	P	P	0.28	0.32	123.48	122.79	10.17	9.92	1.93	2.54	2.83	3.33	18.0	64.0
7/6/19	P	P	0.27	0.30	123.68	122.68	10.03	9.98	2.64	2.88	2.93	3.85	18.2	61.0
10/6/19	P	P	0.28	0.32	123.48	122.81	10.13	9.98	2.66	3.89	2.56	2.83	18.0	64.0
11/6/19	P	P	0.28	0.32	123.47	122.78	10.15	9.96	3.03	3.33	2.70	3.76	18.6	62.0
12/6/19	P	P	0.28	0.32	123.55	122.80	10.06	9.98	2.33	2.83	2.68	3.31	18.0	62.0
14/6/19	P	P	0.28	0.33	123.46	122.75	10.09	10.03	2.07	2.44	0.00	0.00	18.3	62.0
17/6/19	P	P	0.28	0.32	123.28	122.94	10.47	10.45	3.08	3.22	2.57	2.57	18.9	62.0
18/6/19	P	P	0.27	0.30	123.21	122.79	9.98	9.95	2.57	3.94	2.32	3.44	18.6	62.0
19/6/19	P	P	0.27	0.30	123.21	122.73	9.98	9.96	2.83	3.88	2.26	3.44	19.2	63.0
20/6/19	P	P	0.28	0.32	123.36	122.82	10.06	9.96	1.98	2.37	3.12	3.13	18.0	64.0
21/6/19	P	P	0.28	0.33	123.15	122.72	9.98	9.96	2.95	3.29	3.77	3.12	18.2	62.0
24/6/19	P	P	0.28	0.32	123.20	122.81	10.01	9.95	2.575	2.71	3.13	4.43	18.2	62.0
25/6/19	P	P	0.27	0.30	123.00	122.70	9.91	9.94	2.23	3.18	3.21	3.66	18.0	65.0
26/6/19	P	P	0.28	0.33	123.13	122.65	9.99	9.99	3.04	3.23	3.05	3.20	19.1	63.0
27/6/19	P	P	0.30	0.34	123.23	122.74	9.96	9.99	2.72	3.93	2.72	3.19	19.1	63.0
28/6/19	P	P	0.27	0.30	122.92	122.64	9.89	9.96	2.68	3.45	2.68	3.06	18.6	64.0

Table D.7 Center of rotation check from January 2019 to June 2019

Date	COR Det 1 (mm)		COR Det 2 (mm)		Comment
	Δx	Δy	Δx	Δy	
7/1/19	0.05	0.00	-0.17	0.18	P
28/1/19	0.02	0.00	-0.14	0.15	P
4/2/19	0.09	0.00	0.05	0.19	P
11/2/19	0.13	0.00	-0.16	0.16	P
18/2/19	0.13	0.00	-0.17	0.16	P
25/2/19	0.04	0.00	0.10	0.21	P
4/3/19	0.08	0.00	0.16	0.49	P
11/3/19	0.16	0.00	-0.17	0.34	P
25/3/19	0.09	0.00	-0.16	-0.10	P
1/4/19	0.07	0.00	0.15	0.01	P
9/4/19	0.15	0.00	0.17	0.04	P
17/4/19	0.10	0.00	0.15	0.01	P
22/4/19	0.13	0.00	0.16	0.03	P
29/4/19	0.10	0.00	0.17	0.07	P
7/5/19	0.13	0.00	-0.17	0.02	P
13/5/19	0.16	0.01	-0.15	0.00	P
21/5/19	0.11	0.00	0.11	0.07	P
27/5/19	0.17	0.00	-0.18	0.07	P
4/6/19	0.10	0.00	-0.11	0.03	P
10/6/19	8487.00	0.00	0.13	0.02	P
17/6/19	0.17	0.00	0.13	0.16	P
24/6/19	0.07	0.00	0.06	0.27	P

APPENDIX F

COA No. 958/2020

IRB No. 502/63

INSTITUTIONAL REVIEW BOARD

Faculty of Medicine, Chulalongkorn University

1873 Rama 4 Road, Patumwan, Bangkok 10330, Thailand, Tel 662-256-4493

Certificate of Approval

The Institutional Review Board of the Faculty of Medicine, Chulalongkorn University, Bangkok, Thailand, has approved the following study which is to be carried out in compliance with the International guidelines for human research protection as Declaration of Helsinki, The Belmont Report, CIOMS Guideline and International Conference on Harmonization in Good Clinical Practice (ICH-GCP)

Study Title	: Evaluation of patient doses from 177Lu-PSMA in metastases prostate cancer treatment at King Chulalongkorn Memorial Hospital
Study Code	: -
Principal Investigator	: Miss Kotchakorn Chatachot
Affiliation of PI	: Department of Radiology, Faculty of Medicine, Chulalongkorn University.
Review Method	: Expedited
Continuing Report	: At least once annually or submit the final report if finished.

Document Reviewed :

1. Research Proposal Version 2 Date 20 July 2020
2. Protocol Synopsis Version 2 Date 20 July 2020
3. Case record form Version 2 Date 20 July 2020
4. Curriculum Vitae and GCP Training
   - Miss Kotchakorn Chatachot
   - Assist.Prof. Kitiwat Khamwan, Ph.D.

Signature .....

(Emeritus Professor Tada Sueblinvong MD)

Chairperson

The Institutional Review Board

Signature .....

(Associate Professor Supeecha Wittayalertpanya)

Member and Assistant Secretary, Acting Secretary

The Institutional Review Board

Date of Approval : August 1, 2020

Approval Expire Date : July 31, 2021

Approval granted is subject to the following conditions: (see back of this Certificate)

APPENDIX G

Table F.1 Data collection sheet for patient information.

PATIENT INFORMATION	
Patient Number	
Age (years)	
Gender	
Body Weight (kg.)	
Height (cm.)	
No. of exam	
Date of exam	
Injected Activity (MBq)	
Injected time	
Start scan time	

Table F.2 Data collection sheet for data from ROIs contouring**.**

COLLECTED DATA							
Injected time	Scan time	Net Count AP	Net Count PA	Geometric mean count	Decay corrected	TIA (MBq.h)	TIAC (h)

VITA

NAME	KOTCHAKORN CHATAHKOT
DATE OF BIRTH	13 OCTOBER 1990
PLACE OF BIRTH	Lampang
INSTITUTIONS ATTENDED	2009 – 2012 Bachelor of Science, Radiological Technology program, Faculty of Medical Technology, Mahidol University, Bangkok, Thailand.
HOME ADDRESS	427 Village No.3, Thasao Sub-district, Muang District, Uttaradit, 53000
PUBLICATION	Chatachot K., Khamwan K., EVALUATION OF PATIENT DOSES FROM 177Lu-PSMA IN METASTASES PROSTATE CANCER TREATMENT AT KING CHULALONGKORN MEMORIAL HOSPITAL. In Proceeding of the 20th AOCMP & 18th SEACOMP, Phuket, Thailand, 2020